PEV Charging Infrastructure Integration into Smart Grid

by

Ahmed Abdalrahman Ahmed Abdalrazek

A thesis
presented to the University of Waterloo
in fulfillment of the
thesis requirement for the degree of
Doctor of Philosophy
in
Electrical and Computer Engineering

Waterloo, Ontario, Canada, 2020

Examining Committee Membership

The following served on the Examining Committee for this thesis. The decision of the Examining Committee is by majority vote.

External Examiner:	Min Dong Professor, Dept. of Electrical, Computer and Software Engineering, University of Ontario Institute of Technology
Supervisor:	Weihua Zhuang Professor, Dept. of Electrical and Computer Engineering, University of Waterloo
Internal Member:	Kankar Bhattacharya Professor, Dept. of Electrical and Computer Engineering, University of Waterloo
Internal Member:	Oleg Michailovich Professor, Dept. of Electrical and Computer Engineering, University of Waterloo
Internal-External Member:	Ruodu Wang Associate Professor, Dept. of Statistics and Actuarial Science, University of Waterloo

I hereby declare that I am the sole author of this thesis. This is a true copy of the thesis, including any required final revisions, as accepted by my examiners.

I understand that my thesis may be made electronically available to the public.

Abstract

Plug-in electric vehicles (PEVs) represent a huge step forward in a green transportation system, contribute to the reduction of greenhouse gas emission, and reduce the dependence on fossil fuel. With the increasing popularity of PEVs, public electric-vehicle charging infrastructure (EVCI) becomes indispensable to meet the PEV user requirements. EVCI can consist of various types of charging technologies, offering multiple charging services for PEV users. Proper integration of the charging infrastructure into smart grid is key to promote widespread adoption of PEVs. Planning and operation of EVCI are technically challenging, since PEVs are characterized by their limited driving range, long charging duration, and high charging power, in addition to the randomness in driving patterns and charging decisions of PEV users. EVCI planning involves both the siting and capacity planning of charging facilities. Charging facility siting must ensure not only a satisfactory charging service for PEV users but also a high utilization and profitability for the chosen facility locations. Thus, the various types of charging facilities should be located based on an accurate location estimation of the potential PEV charging demand. Capacity planning of charging facilities must ensure a satisfactory charging service for PEV users in addition to a reliable operation of the power grid. During the operation of EVCI, price-based coordination mechanisms can be leveraged to dynamically preserve the quality-of-service (QoS) requirements of charging facilities and ensure the profitability of the charging service. This research is to investigate and develop solutions for integrating the EVCI into the smart grid. It consists of three research topics:

First, we investigate PEV charging infrastructure siting. We propose a spatial-temporal flow capturing location model. This model determines the locations of various types of charging facilities based on the spatial-temporal distribution of traffic flows. In the proposed model, we consider transportation network dynamics and congestion, in addition to different characteristics and usage patterns of each charging facility type.

Second, we propose a QoS aware capacity planning of EVCI. The proposed framework accounts for the link between the charging QoS and the power distribution network (PDN) capability. Towards this end, we firstly optimize charging facility sizes to achieve a targeted QoS level. Then, we minimize the integration cost for the PDN by attaining the most cost-

effective allocation of the energy storage systems and/or upgrading the PDN substation and feeders. Additionally, we capture the correlation between the occupation levels of neighboring charging facilities and the blocked PEV user behaviors.

Lastly, we investigate the coordination of PEV charging demands. We develop a differentiated pricing mechanism for a multiservice EVCI using deep reinforcement learning (RL). The proposed framework enhances the performance of charging facilities by motivating PEV users to avoid over-usage of particular service classes. Since customer-side information is stochastic, non-stationary, and expensive to collect at scale, the proposed pricing mechanism utilizes the model-free deep RL approach. In the proposed RL approach, deep neural networks are trained to determine a pricing policy while interacting with the dynamically changing environment. The neural networks take the current EVCI state as input and generate pricing signals that coordinate the anticipated PEV charging demand.

Acknowledgements

First of all, I shall praise and thank Allah almighty for providing me with the ideas and patience necessary for the successful completion of this thesis.

Then, I would like to express my sincere gratitude and appreciation to my supervisor, Professor Weihua Zhuang, for her invaluable guidance, continuous support, and encouragement throughout my PhD program. I am deeply grateful for all the time and effort she gave me. Professor Zhuang's insightful thoughts and valuable instructions always inspire me to pursue excellence and success not only in academic endeavors but also in every other aspect of life. Professor Zhuang is and will always be a role model of mine.

Furthermore, I wish to thank my PhD committee members: Professor Kankar Bhattacharya, Professor Oleg Michailovich, Professor Ruodu Wang, and Professor Min Dong for their valuable comments and suggestions. Their precious time and efforts devoted to this thesis are highly appreciated.

I would like to offer my special thanks to Professor Xuemin (Sherman) Shen for the great insights he shared with us in the broadband communication research (BBCR) group meetings. The weekly group meetings coordinated by Professor Shen provided me an excellent opportunity to broaden my knowledge and improve my presentation skills.

No words on earth can express my love and gratitude to my beloved parents, Abdalrahman and Eman, my brothers, Mahmoud and Mohanad, and my lovely sister, Menna, for their endless support, encouragement, and prayers.

I cannot express enough gratitude to my wife, Aliaa, for her deep love and constant support during my PhD adventure. For sure, our beautiful daughters, Rokaya, and Karmah have made this adventure enjoyable and helped me overcome the tough times that one faces at some points during the PhD program.

Finally, I would like to thank all my friends at the University of Waterloo for the great time we had together. I shall always remember you and value your friendship as you have been there for me when I needed you most.

Thank you all!

This PhD thesis is dedicated to, my father, Abdalrahman, my mother, Eman, and my wife, Aliaa.

Table of Contents

List of Tables

List of Figures

List of Abbreviations

AC-PC FRLM	Arc-cover Path-cover Flow Refueling Location Model
BIC	Bayesian Information Criterion
CSP	Charging Service Provider
DA	Disaggregation-aggregation
DTA	Dynamic Traffic Assignment
EM	Expectation-maximization
ESS	Energy Storage System
EVCI	Electric Vehicle Charging Infrastructure
FCLM	Flow-capturing Location Model
FCS	Fast Charging Station
GMM	Gaussian Mixture Model
IEA	International Energy Agency
MDP	Markov Decision Process
MILP	Mixed Integer Linear Programming
MNL	Multinomial Logit Model
NHPP	Non-homogeneous Poisson Process
OD	Origin Destination
OWC	On-road Wireless Chargers
PDN	Power Distribution Network
PEV	Plug-in Electric Vehicle
PL	Parking Lots With Slow Chargers
QoS	Quality-of-Service

RL	Reinforcement Learning
RTN	Road Transportation Network
SAE	Society-of-Automotive Engineers
SoC	State-of-Charge
ST-FCLM	Spatial-temporal Flow Capturing Location Model
TD3	Twin-delayed Deep Deterministic Policy Gradient
WPT	Wireless Power Transfer

List of Symbols

$\mathcal{A}$	Set of all RL agent's actions
$\mathcal{B}$	Set of all PDN buses, indexed by j
$\mathcal{D}$	Set of destinations of the daily PEV users trips
$\mathbf{F}$	Set of all FCSs in the EVCI, $\mathbf{F} \subseteq \mathbf{N}$
$\mathbf{L}^T$	Set of all directed links on RTN
$\mathcal{L}$	Set of all PDN branches, indexed by ij
$\mathbf{M}$	Set of service classes in the EVCI, indexed by m
$\mathbf{N}^T$	Set of all nodes on RTN
$\mathbf{N}$	Set of all facilities in EVCI, indexed by n
$\mathcal{O}$	Set of origins of the daily PEV users trips
$\mathbf{O}$	Set of all OWCs in the EVCI, $\mathbf{O} \subseteq \mathbf{N}$
$\mathbf{P}$	Set of all PLs in the EVCI, $\mathbf{P} \subseteq \mathbf{N}$
$\mathbf{Q}$	Set of all OD pair on the RTN, indexed by q
$\mathbf{R}_q$	Set of routs between OD pair q, indexed by r
$\mathbf{S}$	Set of all load scenarios, indexed by s
$\mathcal{S}$	Set of all system states
$\mathbf{T}$	Set of time segments over a day, indexed by t
B_n	Number of waiting positions allocated in facility n
C^P	Cost of ESS power rating
C^E	Cost of ESS energy rating
C^{Sb}	Cost of substation expanding
C^F	Cost of feeder upgrading

$C^e_{s,t}$	Day-ahead hourly energy cost at load scenario s time t
c_n	Number of chargers allocated in facility n
$E_{s,t,n}$	Stored energy in ESS at facility n at load scenario s at time t
e_n	Variable controls ESS energy capacity at facility n
$f_{q,r}(t)$	Time-varying traffic flow over the route r between OD pair q at time t
$\mathcal{F}$	Traffic flow dataset generated by DTA
f_{ij}	Variable controls the capacity upgrade of feeder connecting buses i and j
G^R_j	Rated expansion power of substation connected to bus j
g_j	Variable controls the expansion of substation connected to bus j
$\mathcal{I}$	Annual interest rate
k	Number of clusters in the GMM
K_n	Maximum number of PEVs in facility n including charging and waiting
$\mathcal{L}$	Log-likelihood function
L	ESS life time
$L_{s,t,ij}$	Squared current magnitude of branch connecting buses i and j at load scenario s at time t
$\mathcal{N}$	Number of flow vectors
O^C_l	Annual ESS operational cost at year l
$\mathbb{P}^R$	Vector contains membership probability for data points with respect to the peak traffic flow cluster
$\mathbb{P}^N$	Vector contains membership probability for data points with respect to the non-peak traffic flow cluster
$p_{i_{t,n}}$	Probability of having i PEVs in facility n at time t
P^R_n, E^R_n	Rated power/energy capacity of ESS at facility n
$P^{ES,c}_{s,t,n}$,$P^{ES,d}_{s,t,n}$	ESS charging/discharging power at facility n at load scenario s at time t
$P^{EV}_{t,n}$	Power demand of charging facility n at time t
$P^G_{s,t,j}, Q^G_{s,t,j}$	Active/reactive power provided by substation at bus j at load scenario s at time t

$P^D_{s,t,j}, Q^D_{s,t,j}$	Active/reactive load demand at bus j at load scenario s at time t
$P_{s,t,ij}$, $Q_{s,t,ij}$	Active/reactive power flow at branch connecting buses i and j at load scenario s at time t
p_n	Variable controls ESS power rating at facility n (chapter 3)
$p_{n,t}$	Normalized charging price at facility n at time t (chapter 4)
$\mathcal{P}$	PEV penetration rate
q_m	Minimum QoS level of service class m
$\mathcal{Q}_{n,t}$	Service performance metric at charging facility n at time t
Q^π	Action-value function for each state-action pair following policy π
S^R_{ij}	Rated upgrade power of the feeder connecting buses i and j
$v_{\min}$, $v_{\max}$	Minimum and maximum bus voltage
$V_{s,t,j}$	Squared voltage magnitude of bus j at load scenario s at time t
W^τ	Targeted expected waiting time
$\mathcal{X}_{t,n}$	Number of admitted PEVs to charging facility n at time t
β_n	Self-elasticity parameter with respect to the service price at facility n
$\beta_{n,\hat{n}}$	Cross-elasticity parameter with respect to the service price at facility $\hat{n}$
δ	Threshold value indicates the convergence of EM algorithm
$\triangle t$	Time segment duration
$\delta^c_{s,t,n}$, $\delta^d_{s,t,n}$	Charge/discharge binary indicators of ESS at facility n at load scenario s at time t
$\eta^{ES,c}$, $\eta^{ES,d}$	ESS charging/discharging efficiency
ℓ_{ij}	RTN link length (chapter 2) and PDN feeder length (chapter 3)
γ_m	Self-elasticity parameter with respect to the service QoS at class m
$\gamma_{m,\hat{m}}$	Cross-elasticity parameter with respect to the service QoS at class $\hat{m}$
π	Pricing policy
γ	Discount factor
λ	Parameters collection of the GMM clustering algorithm
$\lambda^*_{t,n}$	Modified offered load arrival rate to facility n at time t

μ^F, μ^O, μ^P	service rates of FCS, OWC, and PL, respectively
ν	Average charging frequency of a PEV
ω_i	Weight of the ith Gaussian component in the GMM algorithm (chapter 2), and weight reflects the relative cost of a charger versus that of a waiting position for each charging facility (chapter 3)
Φ^R	Cumulative traffic flows during the peak traffic periods
Φ^N	Cumulative traffic flows during the non-peak traffic periods
Φ^S	Cumulative traffic flows at destination nodes
τ	Soft target update factor
θ^i	Cluster i of the traffic flow dataset
Θ^τ	Targeted throughput

Chapter 1

Introduction

The smart grid is the modernized electrical power grid that uses two-way flows of electricity and information to enhance the effectiveness and efficiency of electric power delivery [1]. One of the main anticipated benefits and requirements of the smart grid is to enable the transition to an electrified transportation system. The introduction of plug-in electric vehicles (PEVs) is considered a viable solution to reduce carbon emissions and decrease the dependence on fossil fuel, for an economical and environmentally friendly transportation system. According to the International Energy Agency (IEA) forecast, the number of PEVs around the globe exceeded 5.1 million in 2018, with an approximately 60% year-on-year growth rate [2]. This number is expected to rapidly increase in the near future due to the narrowing in the cost gap between conventional vehicles and electric vehicles. Thus, the number of electric vehicles is expected to exceed 130 million by 2030 [2]. To achieve this ambitious goal, there are some barriers hindering the mass adoption of PEVs that should be overcome. These barriers include PEV cost, negative impacts on the power system, and availability of charging infrastructure [3].

Although the operating cost of PEVs is lower than the conventional vehicles, the PEV and associated battery costs are still higher than that of conventional vehicles. Moreover, the PEV charging demand of electricity is not only high but also dynamically and randomly appears at any node on the distribution system at any time due to PEV mobility [4]. The deployment of electric-vehicle charging infrastructure (EVCI) leads to an increase in sys-

tem electricity demand, and a large-scale penetration of PEVs is expected to significantly influence peak demand, feeder loss, and voltage fluctuations in power distribution network (PDN) [5]. EVCI availability is another concern to the PEV users. At the moment, charging facilities is not widely deployed as ordinary gas stations, because establishing charging facilities requires a huge investment. Another challenge is caused by the long charging duration of PEVs at charging facilities. As users spend a long time charging their PEV batteries at a charging facility, other PEV users need to wait for a longer time before getting a charging service at that facility. Also, PEV users can be blocked from a charging facility if the facility is at its full capacity. Long waiting times and high blocking rate degrade PEV user satisfaction and hence charging quality-of-service (QoS).

1.1 PEV Charging Infrastructure

There are various types of charging technologies available in the market and standardized internationally by the Society of Automotive Engineers (SAE). According to the standard SAE J1772, charging levels for PEVs include the alternating current (AC) level 1, AC level 2, AC level 3, and direct current (DC) fast charging, as summarized in Table 1.1 [2,6]. AC level-1 chargers have the lowest power level, and hence take the longest charging duration to charge a PEV battery. This charging level uses the conventional home outlets, which are not typically used for PEV charging. Almost every popular PEV around the globe utilizes AC Level 2 on-board charges in the 6.6 kW–7.4 kW range. Slow charging facilities with AC level 2 chargers can fully charge a PEV battery in an overnight session (7-10hrs) [6]. Usually, slow charging facilities are deployed in homes, parking lots in workplaces and shopping malls. AC level 3 on-board chargers use three-phase AC plugs and provide power levels between 22 kW and 43.5 kW. DC level 3 chargers are the fastest charging option, which provide power up to 400kW. Fast charging stations with DC level 3 chargers can charge a PEV battery up to 80% state-of-charge (SoC) in approximately 20 minutes [6].

In addition to the plug-in charging facilities, PEVs can be charged without cables through the relatively new wireless power transfer (WPT) technology [7]. Dynamic wireless charging (or on-road wireless charging) can charge PEVs while they move on roads, which

Table 1.1: Standard charging level classification

	Level	Current	Power
Conventional plugs	Level 1	AC	$\leq$ 3.7 kW
Slow chargers	Level 2	AC	3.7 - 22 kW
Fast chargers	Level 3	AC, three phase	22 - 43.5 kW
		DC	<400 kW

can significantly reduce the on-board battery pack, hence PEVs become lighter in weight and may be less expensive [8]. Currently, several studies and test sites are underway to develop the dynamic chargers [9]. For example, the fifth-generation of the on-line electric vehicles (OLEVs) project can obtain WPT with 22 kW maximum pick-up power and maximum efficiency 91% at 9.5 kW with 20 cm air gap [10].

1.2 Motivation and Research Contributions

This research is to develop solutions for integrating the EVCI into the smart grid. We focus on EVCI planning and operation. In the EVCI planning, we investigate two problems, namely, the siting and capacity planning of charging facilities. In the operation of EVCI, we investigate the coordination of PEV charging demand using dynamic pricing of charging services. Planning and operation of EVCI are technically challenging, since PEVs are characterized by their limited driving range, long charging duration, and high charging power, in addition to the randomness in driving patterns and charging decisions of PEV users. Several factors should be considered during the integration of EVCI into the smart grid, including PEV characteristics, PEV owner driving behaviors, in addition to operational constraints of the power system. The research motivations and contributions are discussed in the following.

1.2.1 Charging Infrastructure Siting

PEV charging infrastructure siting is a problem of strategically locating various types of charging facilities in a network, while considering unique characteristics and usage patterns of each facility type. PEV charging infrastructure siting must account for the limited driving range of PEVs, in addition to the randomness in driving patterns and charging decisions of PEV users. Furthermore, each type of charging facility must be sited in locations that conform to the requirements of the PEV users in order to maximize their satisfaction. Due to the high capital cost associated with charging facility construction, the planning body must ensure high utilization and profitability of the chosen facility locations [11]. Charging facility utilization will be maximized if they are close to demand locations. However, PEV charging demand is closely related to driving behavior, which varies from one customer to another. Thus, charging infrastructure siting should be based on an accurate location estimation of the potential PEV charging demand [12].

In existing studies, traffic flows are estimated based on the assumption that travelers choose a single route (i.e., the shortest distance route) in traveling between each origin-destination (OD) pair. Then, a flow capturing model sites a given number of charging facilities to intercept with the maximum amount of traffic flow. The traffic flow is said to be captured if at least one charging facility is sited on the shortest distance route between OD pair. The assumption that drivers always choose the shortest distance routes simplifies the estimation of driver route choices. However, traffic flows can be over-estimated for some roads if driver route choices are governed only by the distance between OD pair. Moreover, the assumption neglects the impact of time-dependent dynamics of traffic flows. In reality, drivers use various routes between the same OD pair to avoid traffic congestion. Temporal traffic distribution contributes to accurately estimating the spatial traffic distribution. Some traffic phenomena, such as road congestion, dynamic routing and peak spreading, can only be described using the temporal dimensions of traffic flows. It is more practical that drivers choose the routes with minimum travel times to their destinations, considering various user departure times and network congestion. Thus, both the spatial and temporal distributions of traffic flows should be used in estimating the PEV charging demand. Furthermore, existing siting models locate a single type of charging facility without

considering the unique characteristics and usage patterns of each charging technology.

Considering the aforementioned challenges, in Chapter 2, we investigate and develop the spatial-temporal flow capturing location model (ST-FCLM) for siting various types of PEV charging facilities on the transportation network. The ST-FCLM accounts not only the transportation network dynamics and congestion, but also the different characteristics and usage patterns of each charging facility type. The major contributions of this study are as follows:

1. The new siting model extends the existing flow capturing models by addressing the dynamic traffic flows rather than static flows. We consider all the feasible routes that travelers may choose for each OD pair to minimize their travel time in this formulation. Moreover, travelers' departure times and congestion levels on the road network are inherently accounted in the time-varying traffic flows, which we extract from a simulation-based dynamic traffic assignment (DTA) model;

2. The proposed ST-FCLM model locates multiple types of charging facilities, taking advantage of the unique characteristics and usage patterns of each charging technology. Towards this end, we partition the traffic flow dataset into distinct categories by using the Gaussian mixture model-based clustering (GMM). Then, we site each type of charging facility to capture a specific traffic pattern.

1.2.2 Capacity Planning of PEV Charging Infrastructure

Capacity planning of EVCI is a problem of determining appropriate sizes for charging facilities that quantify the number of chargers and waiting positions. Charging facilities must be sized to satisfy the PEV user requirements while complying with power grid constraints. PEV user satisfaction can be achieved by fulfilling the stochastic and time-varying charging service requirements. Charging QoS is a measure of PEV user satisfaction. Although increasing the facility sizes enhances the charging QoS, it presents a substantial load to the power grid that may exceed the capability of PDN. To accommodate the expected power demand of charging facilities, PDN components (i.e., feeders and substations) may

need upgrade, which in turn requires huge investments. Utilizing an energy storage system (ESS) in charging facilities can be a solution to alleviate the required PDN upgrades if the ESS cost is less than the reinforcements cost [13–15]. Consequently, there are inter-relationships among the QoS level of EVCI, the required PDN upgrades, and the ESS allocation in charging facilities. These inter-relationships offer guidance to size the charging facilities in a cost-effective manner, in addition to provide insights into how to make a trade-off between the PEV user satisfaction and the required investment in PDN.

There exist several studies on sizing of charging infrastructure. One approach is to optimize the size of charging facilities based on the expected charging demand of users. This approach maximizes the PEV user satisfaction and the profit of system operator, without considering the operational constraints of the power system. Another approach compromises between the charging service requirements and the power system operational constraints. It focuses on minimizing the negative impacts on the power system without ensuring PEV user satisfaction. This is because planning models usually re-locate and/or re-size the charging facilities to fulfill the requirements of the power system. Consequently, existing sizing models either ignore the power system constraints or degrade the charging QoS.

Different from the existing studies, in Chapter 3, we present a QoS-aware capacity planning framework of networked EVCI. The major contributions of this study are as follows:

1. The new capacity planning framework takes account of the inter-relationships among the targeted QoS, ESS allocation, and PDN upgrade. The proposed framework consists of two models that are solved sequentially: Firstly, the capacity planning of EVCI model is used to optimize the numbers of chargers and waiting positions allocated at each charging facility to realize the targeted QoS level for the entire networked EVCI. After that, PEV charging demand at each facility is estimated for inclusion in the PDN load demand. Finally, the integration with the PDN model is used to minimize the integration cost of EVCI with PDN by attaining the most cost-effective ESS allocation and/or PDN reinforcement;

2. The proposed EVCI model captures the correlation among the occupation levels of

neighboring charging facilities, in addition to blocked PEV user behaviors. Towards this end, we model the EVCI as an open queuing network with finite capacity and blocking;

3. The proposed approach accounts for the temporal variability of the charging demand by modeling the charging facilities as non-stationary queue systems. Then, a modified arrival rate function is derived to approximate the steady state performance of the systems.

1.2.3 Coordinate of PEV Charging Demand

Coordination of PEV charging demands has become indispensable to meet the PEV user requirements, while minimizing the negative impacts on the power grid. PEV charging demand management is classified into two main categories: centralized and decentralized (distributed) coordinations [16]. In the centralized coordination, a central controller directly controls the charging process of the participated PEVs. This approach can optimize the PEV charging process. However, it requires sophisticated communication and control systems to monitor and coordinate the charging process of a large number of PEVs. In the decentralized coordination, a dynamic pricing mechanism can be leveraged to coordinate the PEVs charging process and influence the behaviors of PEV users. The price-setting should simultaneously achieve the following objectives [17]: 1) to preserve the QoS of charging facilities to maximize users' satisfaction; 2) to alleviate the negative impacts on the power system; and 3) to maximize the utilization of charging facilities.

Recently, significant progress has been made in developing pricing schemes that account for the uncertainty of PEV charging demand, while considering the fluctuations in electricity price and power grid conditions. The preliminary pricing schemes do not deal with the multiple services offered by the EVCI and the multiple QoS classes associated with these services. In a multiservice EVCI, a set of charging services is offered, and each service is provided by a type of charging facility with a certain QoS class. Different service classes vary in the PEV charging rate, average waiting time, and charging method (i.e., either with a plug-in cable or wireless charging). Thereby, users' dwelling time during the PEV

charging depends on the charging service class. Each service class has a minimum level of QoS that must be preserved during the operation to ensure the PEV user satisfaction and the profitability of charging service.

In addition to the mentioned challenges, two issues remain to be addressed in the contemporary modeling approach of dynamic pricing for PEV charging demand. First, existing dynamic pricing models rely on simplified assumptions and can be unrealistic, such as full knowledge of the customer-side information including the current charging demand and the influence of pricing decisions on future user behaviors. Even if the demand is modeled as a random variable, the assumption of complete information about the expected demand is unrealistic. Second, PEV charging demand coordination is a complex non-stationary and stochastic process. Typically, PEV charging demand can change over time-of-day, day-of-the-week, seasons, or due to an increased or decreased desirability of particular charging technology. Applying abstract dynamic pricing models in this environment cannot ensure optimality, as any change of variables can lead to model misspecification, resulting in unreliable estimation of the system operation and/or revenue loss. To overcome the limitations, reinforcement learning (RL) is becoming one of the most promising tools for the decision-making problem in an unknown environment. RL is capable of learning from the interactions with the dynamically changing environment and optimizing the decision in the absence of complete information.

In Chapter 4, we propose a new way to use deep RL algorithms in the context of the dynamic pricing of charging services. The proposed pricing mechanism preserves different QoS classes at a multiservice EVCI. Additionally, the proposed approach is able to learn a pricing policy, while the complete customer-side information is not available. The major contributions of this study are as follows:

1. We propose a differentiated pricing mechanism that discourages over-allocation of a charging service, in addition to enhancing the performance of charging facilities in meeting the expectation of PEV users. Towards this end, the problem is formulated as a social welfare maximization problem, where the objective is to maximize the demand for charging services while maintaining the targeted QoS in all service classes;

2. The proposed framework is based on the twin-delayed deep deterministic policy gra-

dient (TD3) algorithm, which is a model-free RL approach using actor-critic methods. In the proposed approach, deep neural networks are trained to determine a pricing policy while interacting with the unknown environment. The neural networks take the current EVCI state as input and generate pricing signals that coordinate the anticipated PEV charging demand.

1.3 Research Objectives and Thesis Outline

The objective of this PhD research is to develop solutions for integrating the EVCI into smart grid, which can achieve high utilization and profitability for the chosen facility locations, satisfy PEV user requirements, and ensure that PEV load demand complies with power grid constraints. To attain the overall objective, the following objectives are tackled sequentially:

1. To introduce an EVCI siting model based on an accurate location estimation of the potential PEV charging demand, which considers the unique characteristics and usage patterns of each charging facility type;

2. To develop a capacity planning framework for the networked EVCI, which optimizes charging facility sizes to achieve a targeted QoS level, in addition to minimize the integration cost for the PDN by attaining the most cost-effective allocation of the ESSs and/or upgrading the PDN substation and feeders;

3. To present a differentiated dynamic pricing mechanism for multiservice EVCI, which motivates PEV users to avoid over-allocation of particular service classes, and learns and improves automatically without an explicit model of the environment.

The rest of the thesis is organized as follows. Chapter 2 introduces a novel EVCI siting model, called the ST-FCLM. The potential PEV charging demand is firstly estimated based on the dynamic traffic assignment model. Then, the ST-FCLM is formulated as an optimization problem. The performance of the proposed siting model is evaluated on two benchmark transportation networks. Chapter 3 investigates the capacity planning of

EVCI. We model the EVCI as a queuing network to capture the correlation among the occupation levels of neighboring charging facilities. Then, we describe the proposed sizing model for charging facilities and present the integration model with PDN. In Chapter 4, we present a differentiated pricing mechanism for a multiservice EVCI. We discuss the PEV charging demand in the presence of a price-based coordination mechanism. Then, we formulate the dynamic pricing problem and present an RL approach that decide the pricing policy. We conclude the research and give future research directions in Chapter 5.

Chapter 2

EVCI Siting Based on Spatial-Temporal Traffic Flow Distribution

In this chapter, we propose a spatial-temporal flow capturing location model. This model determines the locations of various types of charging facilities based on the spatial-temporal distribution of traffic flows. We utilize the dynamic traffic assignment model to estimate the time-varying traffic flows on the road transportation network. Then, we cluster the traffic flow dataset into distinct categories using the Gaussian mixture model and site each type of charging facilities to capture a specific traffic pattern. We formulate our siting model as an mixed integer linear programming (MILP) optimization problem. The model is evaluated based on two benchmark transportation networks, and the simulation results demonstrate effectiveness of the proposed model.

2.1 Related Work

PEV charging demand distribution plays a key role in optimizing the charging facility locations. The utilization of charging facility can be maximized if they are close to demand

locations. Hence, charging infrastructure siting should be based on an accurate location estimation of the potential PEV charging demand. There are two basic categories of charging facility siting models based on demand estimation methods: nodal PEV density-based models and traffic flow-based models [18].

In the nodal PEV density based models, a PEV is assumed to request a charging service at a particular location, such as shopping center or residential district. PEV users need to travel from their locations (demand point) to charging facility locations to charge their PEVs [11]. In these models, charging facilities are planned by dividing a given area into small unit areas (cells). The potential charging demand in each cell is proportional to the average number of PEVs parked in that cell [19]. Then, siting models locate charging facilities to maximize the number of covered nodal demand [20]. This method accounts for the differences in nodal demand. However, it does not capture PEV mobility, since it treats PEV demand as static and fixed in each node [21].

In the traffic flow-based models, PEV users are assumed to prefer charging their vehicles during trips to destination locations [21]. Thereby, the traffic flow conditions on the road system can be used to estimate potential PEV charging demand. When the traffic volume on a particular road is high, there is a high probability that the charging demand on that road will be high, and vice versa [22]. Traffic flow is defined as the number of vehicles which travel along the links that connect different transportation network nodes from an origin to a destination along a pre-determined travel route [21]. Flow capturing models are used to locate the charging facilities on the traveling routes to maximize the captured traffic flows. Note that the traffic flows are OD flows, not link flows. Although link flows are easier to obtain from vehicles count data than OD flows, flow capturing models utilize OD flows in locating the facilities [23]. This is because flow capturing models prevent flow double counting, which is the capture of a flow more than once at the expenses of other flows in the network that have not been captured at all. When link flows are used in these models, traffic flows that passes over many links can be captured more than once.

Several flow capturing models are proposed in the literature to site a single type of the charging facilities [24]. Flow-capturing location model (FCLM) is one of the early models, which sites charging facilities to maximize the captured passing flows. Traffic flow is considered captured if there is a charging facility located on the flow path [25]. An

extended version of FCLM has been developed to consider the limited driving range of PEVs [23, 26], which allows PEV users to have long-distance trips via multi-stop charging. The FCLM is further developed to minimize the number of required charging facilities by considering the deviation paths under an assumption that PEV users may accept slightly longer trips to charge their vehicles [27,28]. Additionally, the uncertainty of the traffic flows can be addressed to account for the future adoption of PEV charging demand [29, 30].

Existing traffic flow-based models locate the charging facilities based on the spatial distribution of PEVs with diversified traveling patterns. In order to estimate the spatial distribution of PEVs, these models assume that all the traffic between each OD pair is traveling through a single route, which is the shortest distance route. This assumption simplifies the estimation process of the traffic flows. However, the assumption neglects the impact of time-dependent dynamics of traffic flows. In reality, travelers usually choose the routes with minimum traveling time in traversing to their trip destinations, while considering the congestion level on roads. Thus, a new siting model based on an accurate estimation of the PEV charging demand is needed for siting the charging facilities. This model should account the transportation network dynamics and roads congestion.

Deployment of multiple types of charging facilities is studied in [31, 32], which adopt the tour-based approach in siting multiple types of charging facilities. In this approach, PEVs are assumed to travel through a tour of several sequential series of destinations, and the dwelling time at each destination is known. Then, the siting model deploys suitable types of charging facilities at destination nodes to utilize the dwelling time of the users. It is assumed that the trajectory and usage patterns of all PEVs in the system are known. This information may not be available in a system with a large fleet of PEVs.

The economic aspects in the placement of multiple-types of charging technologies are studied in [33–35]. The objectives of these studies are to minimize either the personal charging cost or the social cost of the charging infrastructure. From the perspective of the system planner, integrated planning frameworks with multiple-types of charging facilities are presented in [33, 35]. In [33], each charging service provider offers a charging service with a particular charging technology. The service providers compete with each other in choosing service locations and prices. The social cost of the entire charging infrastructure can be minimized by considering the substitution effect among different types of charging

facilities [35]. From the perspective of PEV users, an agent-based model can be used to characterize the interaction between PEV drivers and charging infrastructure. Multiple-types of charging facilities can then be sited in locations that minimize the charging cost of each PEV, including the opportunity cost of driver's time [34]. This approach is important in the high-level planning context; however, it does not account for the traffic conditions and congestion in identifying areas where it is more likely to use a certain type of charging facilities. A summary of main features of the charging infrastructure siting approaches is given in Table 2.1. A more comprehensive survey can be found in [18, 24].

Table 2.1: Summary of PEV charging infrastructure siting models

Function	Study	Main feature
Siting a single type of facilities	[25]	Maximize the captured traffic flows
	[23, 26]	Consider the limited PEV driving range
	[27, 28]	Consider the deviation paths of drivers
	[29, 30]	Consider the uncertainty of traffic flows
Siting multiple types of facilities	[31, 32]	Consider the multiple charging rates of charging facilities
	[33, 35]	Minimize the social cost of charging infrastructure
	[34]	Minimize the charging cost of PEVs

2.2 System Model

Consider a typical urban area with a road transportation network (RTN) consists of a set of nodes $\mathbf{N}^T$ and a set of directed links $\mathbf{L}^T$ connecting the network nodes. As shown in Figure 2.1, the RTN nodes can represent road intersections, highway exits, or locations with high traffic. The RTN links represent streets, roads, traffic lanes, etc. Vehicles are assumed to start daily trips from a set of origins represented by $\mathcal{O}$ ($\mathcal{O} \subseteq \mathbf{N}^T$) to a set of destinations represented by $\mathcal{D}$ ($\mathcal{D} \subseteq \mathbf{N}^T$). Traffic demand at the origin nodes is considered to be deterministic and independent of the traffic conditions in the network.

Let a ($a \in \mathbf{L}^T$) denotes a link, and r a route. A route is represented by a list of connected links $\{a_1, a_2, \ldots, a_m\}$ connect origin o ($o \in \mathcal{O}$) and destination d ($d \in \mathcal{D}$). In order to denote each OD pair, the single subscript q is replaced the double subscript od, where $\mathbf{Q}$ represents the set of all OD pairs in the RTN. Let $\mathbf{R}_q$ denote the set of all feasible routes that a driver may choose to travel between an OD pair q. Let $f_{q,r}(t)$ represents the time-varying traffic flow (i.e., vehicles volume per unit time) over the route r ($r \in \mathbf{R}_q$) between OD pair q at time t. Time is partitioned into T time slots with equal duration Δt, where $\mathbf{T} = \{0, 1, 2, \ldots, T\}$ denotes the set of all time slots over a day. The RTN is assumed empty at $t = 0$. Individual drivers are assumed seeking routes that minimize their traveling times, which is known as user equilibrium.

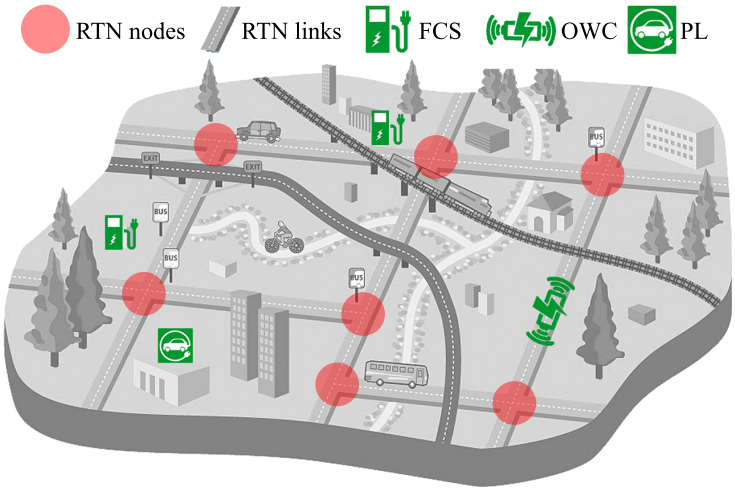

Figure 2.1: Road transportation network.

2.2.1 PEV Charging Infrastructure

The EVCI consists of a set charging facilities denoted by $\mathbf{N} = \{1, 2, \ldots, N\}$, which is composed of three subsets: subset $\mathbf{P}$ for parking lots (PLs) with AC chargers, subset $\mathbf{F}$ for DC fast-charging stations (FCSs), and subset $\mathbf{O}$ for on-road wireless chargers (OWCs). PEV users can choose any of these technologies to charge their PEV batteries. Each PEV in the system starts its daily trips with at least half full battery charge. Due to the PEV

limited driving range, the initial PEV battery charge assumption is used to determine the number of required charging facilities between an OD pair if the traveling distance between them is longer than the maximum PEV driving range. A PEV can be charged by plugging a cable into a charger in a PL or an FCS. The charging time in PLs is relatively longer than that with FCSs. Thereby, PLs are deployed on the destination nodes of the daily trips, such as workplaces and shopping centers. FCSs are deployed on the transportation system nodes, such as road intersections. Additionally, some PEVs in the system capable of charging through wireless power transfer technology in OWCs, which are deployed on the surface of dedicated road lanes, represented by transportation system links. Hence, a PEV may step into this charging lane to get a charging service, then return back to the normal traffic after charging.

2.2.2 Dynamic Traffic Assignment

The dynamic traffic assignment model forecasts traffic load in time-varying traffic patterns among transportation system roads [36]. Different from the static traffic estimation models, the DTA model describes effects such as network congestion and queuing, due to vehicles accumulation on the transportation network links if link inflows exceed link outflows [37,38]. In DTA, travelers are assumed to choose routes that minimize their experienced travel time between an OD pair, considering congestion levels in the whole network [39]. Travelers then choose time-dependent shortest routes instead of the shortest distance route, which are likely to differ significantly. Since link travel times change dynamically, depending on the time departure from the route origin and the traffic conditions encountered along the route. The traffic flows on roads at a particular time are then affected by the flows that may depart previously as well as the flows that will depart subsequently. The traffic flow history on the network has a direct impact on the traffic flows on roads [36]. To approximate traveler route choices, Wardrop's user-equilibrium principle is used. This principle states that the routes used by all travelers between the same OD pair at the same departure time have equal and lowest experienced travel time, and no user can lower his experienced travel time through unilateral actions [36]. Thereby, the DTA model excludes impractical routes such as routes including loops or routes with a high traveling time. In

simulation-based DTA, time-varying flows that satisfy the dynamic user equilibrium are determined through iterative procedures [36].

The DTA model requires time-dependent OD matrices, which specify individuals' traveling demands. OD matrices are generated by dividing the given area into zones. Then, the number of trips that begin or end in each zone, as well as when these trips will occur, are aggregated. Most urban planning and transportation agencies have OD matrices extracted from travel surveys conducted every 5-10 years [36]. These surveys contain information about trips made by individuals on a typical weekday such as origin, destination, start time, purpose, etc. OD matrices can also be estimated via other techniques such as mobile phone data [40]. Usually, OD matrices change slowly over a long time period, influenced by human factors such as socio-economic and environmental status [41]. Additionally, the DTA model requires the RTN characteristics dataset, which contains data about transportation network nodes and links attributes, such as network geometric, length of road segments, number of lanes in each road, and speed limits.

2.3 Spatial-temporal Flow Capturing Location Model

EVCI siting is a problem of strategically locating various types of charging facilities in a network. The ST-FCLM presented in the following is to site a given number of charging facilities in locations that maximize the captured traffic flows. EVCI contains three types of facilities, including OWCs, FCSs, and PLs. These facilities are to meet varying demands or preferences of PEV users, which can be either *en route* during the traveling from origins to destinations or *static* at the trip destinations. Practically, a PEV driver tends to charge a PEV at the trip destination if the PEV has enough SoC to complete the trip and there is a charging facility at the destination, to avoid waiting time at charging facilities. On the other hand, *en route* PEV charging will be limited to the situations where the SoC of PEV battery falls below a certain threshold or for a long distance trip [42]. Planning of PEV charging infrastructure should satisfy both types of charging demand (*en route* and *static*) to meet critical service requirements.

Both OWCs and FCSs are suitable for meeting the *en route* charging demand, as users

in general would prefer spending less time in charging facilities during the trips. The traffic flows during peak traffic periods are captured by the OWCs. The chosen OWC locations should intercept the maximum amount of traffic flow during the peak traffic periods. These locations are likely to be congested, which is more appropriate for the usage of OWCs. This is because vehicles speed will be lower and PEVs will be on top of the charging lanes for a longer time, thus allowing PEVs batteries to be charged by a larger amount of energy. Additionally, during the peak traffic hours, drivers will be highly motivated to use OWCs to charge their PEVs while driving, instead of waiting for charging service at a plug-in charging facility. The traffic flows during non-peak traffic periods are captured by the FCSs, since a PEV user is more likely to stay for some time at FCS for battery charging, including the battery charging time and the waiting time for charging service.

In addition to the *en route* PEV charging demand, users may need to charge their PEVs at trip destinations. This type of charging demand is considered *static*, as users utilize their dwelling time at destination nodes, in which PEVs are parked for several hours, such as working hours or overnight parking. The *static* PEV charging demand can be captured by PLs at the destination nodes of traffic flows. In this way, *en route* PEV charging demand will be covered during traveling between OD pairs by either OWCs or FCSs, and during parking at destination nodes by PLs. Consequently, the unique characteristics and usage patterns of the three types of charging facilities are considered in our proposed siting model.

To develop the ST-FCLM, we make some assumptions: 1) Drivers always choose the route that minimizes their personal travel time between each OD pair, considering departure time and congestion levels in the transportation network; 2) PEVs are assumed to be uniformly distributed across the given area and the PEV penetration rate is known. Currently, this assumption may not be accurate in many cities because PEV users have a certain income level and reside in some city regions. Our model and analysis can be extended to account for a non-uniform PEV distribution, provided such a distribution is available; 3) PEV driving range and energy consumption per unit distance are similar in all PEVs in the system, equal to the average of various PEV classes.

As shown in Figure 2.2, our approach for developing the ST-FCLM is comprised of the following steps: 1) To estimate the spatial-temporal traffic flows within the given study area using a simulation basted DTA model; 2) To distinguish between siting locations of

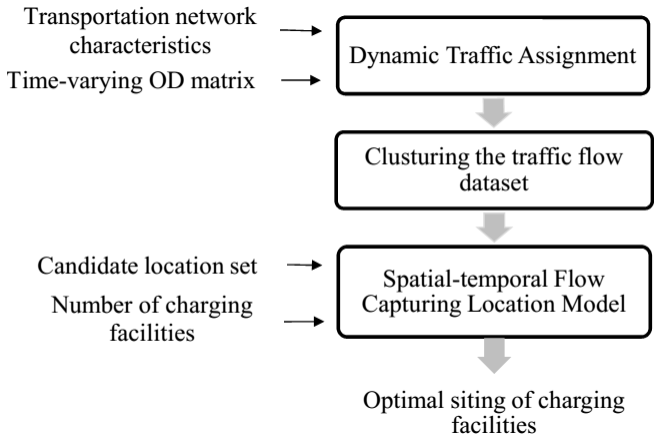

Figure 2.2: The ST-FCLM framework.

various charging facility types. To accomplish this task, the traffic flow dataset is clustered according to the temporal characteristics based on the GMM algorithm. Then, we site each type of charging facilities to capture a distinct traffic pattern; 3) To generate a set of candidate sites in order to consider the PEV limited driving range. Hence, more than one charging facility may be allocated between an OD pair in the network if the traveling distance between them is longer than the maximum PEV driving range.

2.3.1 Clustering the Traffic Flow Dataset

Recall that the exogenously generated traffic flow dataset, $\mathcal{F} = \{f_{q,r}(t)\}, \forall q, r, t$, represents the traffic volume on route $r \in \mathbf{R}_q$ between OD pairs $q \in \mathbf{Q}$ at time slot $t \in \mathbf{T}$ of a typical weekday. Thus, $\mathcal{F} \in \mathbb{R}^{\mathcal{N} \times T}$ is a matrix, where $\mathcal{N}$ denotes the number of flow vectors and T denotes the time periods. Each flow vector $f_{q,r} = [f_{q,r}^1, f_{q,r}^2, \cdots, f_{q,r}^T]$ represents the discretized time-varying flow volumes between on corresponding route and between the corresponding OD pair. For $\mathcal{N}$ flow vectors in the transportation network, the traffic flow

dataset is denoted as follows:

$$\mathcal{F} = \begin{bmatrix} f_{1,1}^1 & f_{1,1}^2 & f_{1,1}^3 & \cdots & f_{1,1}^T \\ \vdots & \vdots & \vdots & \ddots & \vdots \\ f_{q,r}^1 & f_{q,r}^2 & f_{q,r}^3 & \cdots & f_{q,r}^T \\ \vdots & \vdots & \vdots & \ddots & \vdots \\ f_{Q,R_q}^1 & f_{Q,R_q}^2 & f_{Q,R_q} & \cdots & f_{Q,R_q}^T \end{bmatrix}.$$

In order to site each type of charging facilities in locations that capture distinct traffic patterns, the time-varying traffic flows are clustered according to their similarities.

Definition 1. The clustering process is to partition $\mathcal{F}$ into k clusters $\{\theta^1, \theta^2, ..., \theta^k\}$ according to a similarity measure, where each cluster $\theta^i \subseteq \mathcal{F},\ (i = 1, 2, .., k)$ has a common characteristic.

Traffic flow dataset is clustered according to the temporal characteristics. The goal of clustering is to categorize the time periods in which the traffic flows are either high or low. More precisely, the clustering objective is to develop two heat maps that reflect the relative need for each type of charging facilities: 1) The first heat map is for the aggregated traffic flow during the peak traffic period, which is used to site OWCs; 2) The second heat map is for the aggregated traffic flow during the non-peak traffic period, which is used in siting FCSs. Additionally, PEV numbers are aggregated over time at the destination nodes to reflect the relative need for PLs at these nodes. All types of charging facilities in the system can be used by PEV users at anytime of day and those heat maps are only used for selecting appropriate locations for each charging facility type. Towards this end, the Gaussian mixture model-based clustering can be used, which is characterized by its speed of convergence and adaptability to sparse data [43–45]. Another key feature of the GMM algorithm is its soft assignments of data points to clusters. In the soft assignment, data points can be assigned to multiple clusters with certain probabilities [43]. The soft assignment feature facilitates accurate clustering of the traffic flow dataset.

The GMM is a probabilistic model that assumes all data points are generated by a mixture of a finite number of Gaussian distributions, in which each Gaussian component represents a unique cluster [46]. To cluster the traffic flow dataset according to the temporal

characteristic, the spatial dimension of the data is ignored, and temporal distance function is used to determine the dissimilarity between clusters. The traffic flow dataset is then represented as $\mathcal{F} = \{f_1, \ldots, f_T\}$, and the tth entry of a T-dimensional discrete-valued data vectors represents a vector of traffic flows via all routes and OD pairs on time t. For the GMM with k components, the density of f_t is a sum of weighted Gaussian densities $\{\theta(\mu_i, \Sigma_i)\}_{i=1}^{k}$ as given by the following equation [43, 46]:

$$p(f_t \mid \lambda) = \sum_{i=1}^{k} \omega_i \; \theta(f_t \mid \mu_i, \Sigma_i) \tag{2.1a}$$

$$= \sum_{i=1}^{k} \omega_i \; \frac{\exp(-\frac{1}{2} \; (f_t - \mu_i)^\intercal \; \Sigma_i^{-1} \; (f_t - \mu_i))}{(2\pi)^{T/2} \; |\Sigma_i|^{1/2}} \tag{2.1b}$$

where ω_i represents the weight of the ith Gaussian component with $\sum_{i=1}^{k} \omega_i = 1$. The mean vector and the covariance matrix are denoted by μ_i and Σ_i, respectively. The complete GMM parameters are represented by the mean vectors, covariance matrices and mixture weights of all the Gaussian component densities. These parameters are collectively denoted by $\lambda = \{\omega_i, \mu_i, \Sigma_i\}, i = 1, \cdots, k$.

Ideally, one should use the maximum likelihood (ML) estimation method in order to estimate the GMM parameters that best fit the distribution of the data vector. By assuming the independence among the data points, the log-likelihood function ($\mathcal{L}$) is given by the following equation [46]:

$$\mathcal{L} = \ln \; p(\mathcal{F} \mid \lambda) = \sum_{t=1}^{T} \; \ln \; \Big\{ \sum_{i=1}^{k} \omega_i \; \theta(f_t \mid \mu_i, \Sigma_i) \Big\}. \tag{2.2}$$

However, this equation is a nonlinear function of λ, making it difficult to maximize its expression [43, 46]. Instead, the expectation-maximization (EM) algorithm can be used to estimate the GMM parameters. The EM algorithm performs two iterative steps, which are the expectation step ($\mathbb{E}$-step) and the maximization step ($\mathbb{M}$-step) [43, 46]. The algorithm starts with the $\mathbb{E}$-step by picking an initial guess about the GMM parameters, then computes the posterior probabilities (or membership probabilities) of the given data,

which maximize the expected log-likelihood function. Using the current GMM parameters values, the posterior probability of data at time t belongs to component j is denoted by (p_{tj}), and is given by

$$p_{tj} = \frac{\omega_j \ \theta(f_t \mid \mu_j, \Sigma_j)}{\sum_{i=1}^{k} \omega_i \ \theta(f_t \mid \mu_i, \Sigma_i)}. \tag{2.3}$$

Afterwords, the $\mathbb{M}$-step updates the GMM parameters based on the current posterior probabilities, as given by

$$\omega_j^{new} = \frac{1}{T} \sum_{t=1}^{T} p_{tj}, \quad j = 1, \cdots, k \tag{2.4a}$$

$$\mu_j^{new} = \frac{1}{T\omega_j^{new}} \sum_{t=1}^{T} p_{tj} f_t, \quad j = 1, \cdots, k \tag{2.4b}$$

$$\Sigma_j^{new} = \frac{1}{T\omega_j^{new}} \sum_{t=1}^{T} p_{tj} (f_t - \mu_j^{new})(f_t - \mu_j^{new})^{\intercal}, \quad j = 1, \cdots, k. \tag{2.4c}$$

The EM algorithm converges when the changes in the log-likelihood function or alternatively in the GMM parameters are less than a given threshold value (δ). The termination condition of the EM algorithm is when $\mid \mathcal{L}^{new} - \mathcal{L} \mid < \delta$. Thus, the EM algorithm evaluates the log-likelihood function, as given by Equation (2.2).

The number of components in GMM can be efficiently selected based on the Bayesian information criterion (BIC) [43, 47, 48]. The basic idea of the BIC is that adding more components or clusters to the GMM will increase the value of the likelihood function, although the complexity of the model will increase as the GMM parameters increase. The BIC resolves this issue by penalizing the GMM complexity by the addition of more components. The formula of the BIC is given by

$$BIC = -2\mathcal{L} + k \ln T \tag{2.5}$$

where $\mathcal{L}$ is the maximized value of the likelihood function; k denotes the number of components or clusters in the GMM; T denotes the number of data points in the clustered dataset. The optimal number of components of the GMM is k^* that minimizes the BIC

score, as given by the following equation:

$$k^* = \arg\min_{k \in \mathbb{N}} BIC. \tag{2.6}$$

2.3.2 Optimization Problem

Based on the clustered traffic flow dataset, the GMM computes the membership probability for each time slot to the corresponding output label. The cluster that is parameterized with the highest mean value is labeled as the peak traffic flow cluster. Vector $\mathbb{P}^R = \begin{bmatrix} p_1^R & p_2^R & \dots & p_T^R \end{bmatrix}^\intercal$ contains the membership probability for data points with respect to the peak traffic flow cluster. Each element in that vector, p_t^R, represents the probability of the observed flows at time slot t belongs to the peak traffic flow cluster.

The ST-FCLM model captures the cumulative traffic flows over peak traffic periods by the OWCs, and the cumulative traffic flows over non-peak traffic periods by the FCSs. The cumulative traffic flows during the peak ($\Phi^R \in \mathbb{R}^{\mathcal{N}}$) and non-peak ($\Phi^N \in \mathbb{R}^{\mathcal{N}}$) traffic periods are defined as

$$\Phi^R = \mathcal{F} \cdot \mathbb{P}^R = \sum_{t=1}^{T} f_{q,r}(t) p_t^R \qquad \forall\ q \in \mathbf{Q},\ r \in \mathbf{R}_q \tag{2.7a}$$

$$\Phi^N = \mathcal{F} \cdot \mathbb{P}^N = \sum_{t=1}^{T} f_{q,r}(t) p_t^N \qquad \forall\ q \in \mathbf{Q},\ r \in \mathbf{R}_q \tag{2.7b}$$

where $\mathbb{P}^N$ is a vector that contains the membership probability for data points with respect to the non-peak traffic flow cluster. If the GMM partitions the traffic flow dataset with more than two components, we can then set $\mathbb{P}^N = 1 - \mathbb{P}^R$. The probability vectors act as weights to the traffic flow dataset that facilitates the evaluation of the cumulative traffic volumes on roads during various time windows.

The static charging demand of PEVs at the trip destinations can be reflected by the number of PEVs at destination nodes. The PEVs static charging demand can be estimated based on the cumulative traffic flows over time via all routes between each OD pair q.

Hence, PEVs static charging demand ($\Phi^S \in \mathbb{R}^Q$) is defined as

$$\Phi^S = \sum_{\forall t \in \mathbf{T}} \sum_{\forall r \in \mathbf{R}_q} f_{q,r}(t) \qquad \forall q \in \mathbf{Q}. \tag{2.8}$$

The objective of the ST-FCLM is to choose the best locations, which maximize the captured traffic flows, for each type of charging facilities. In the ST-FCLM, decision variables are partitioned into two sets: 1) A set of control variables (independent decision variables) $\mathbf{X} = (X_a^1, X_k^2, X_k^3)$ that control the siting of charging facilities on RTN nodes and links; 2) A set of state variables (dependent decision variables) $\mathbf{Y} = (Y_{q,r}^R, Y_{q,r}^N, Y_q^S)$ that indicate the covered *en route* and *static* PEV charging demand. The ST-FCLM is formulated as follows:

$$\max_{\mathbf{X},\mathbf{Y}} \left\{ \sum_{\forall q \in \mathbf{Q}} \sum_{\forall r \in \mathbf{R}_q} (\Phi_{q,r}^R Y_{q,r}^R + \Phi_{q,r}^N Y_{q,r}^N) + \sum_{\forall q \in \mathbf{Q}} \Phi_q^S Y_q^S \right\} \tag{2.9a}$$

$$s.t.\ X_a^1 \geq Y_{q,r}^R, \qquad \forall a \in \mathbf{W}_{q,r},\ q \in \mathbf{Q},\ r \in \mathbf{R}_q \tag{2.9b}$$

$$X_k^2 \geq Y_{q,r}^N, \qquad \forall k \in \mathbf{K}_{q,r},\ q \in \mathbf{Q},\ r \in \mathbf{R}_q \tag{2.9c}$$

$$X_k^3 \geq Y_q^S, \qquad \forall k \in N_q,\ q \in \mathbf{Q} \tag{2.9d}$$

$$Y_q^S \leq \sum_{\forall r \in \mathbf{R}_q} (Y_{q,r}^R + Y_{q,r}^N) \leq 1, \qquad \forall q \in \mathbf{Q} \tag{2.9e}$$

$$\sum_{\forall a \in \mathbf{W}} X_a^1 \leq N^1, \tag{2.9f}$$

$$\sum_{\forall k \in \mathbf{K}} X_k^j \leq N^j, \qquad \forall j \in \{2,3\} \tag{2.9g}$$

$$X_k^2 + X_k^3 \leq 1, \qquad \forall\ k \in \mathbf{K} \tag{2.9h}$$

$$X_a^1, X_k^2, X_k^3 \in \{0,1\}, \qquad \forall a \in \mathbf{W},\ k \in \mathbf{K} \tag{2.9i}$$

$$0 \leq Y_{q,r}^R, Y_{q,r}^N, Y_q^S \leq 1 \qquad \forall q \in \mathbf{Q}, r \in \mathbf{R}_q. \tag{2.9j}$$

The parameters and variables in this formulation are presented in Table 2.2. The objective function (2.9a) selects the siting plan $\mathbf{X} = (X_a^1, X_k^2, X_k^3)$ that maximizes the captured cumulative traffic flows via all routes that travelers may choose to travel between

Table 2.2: Nomenclature of ST-FCLM

$\mathbf{Q}$, q	the set and index of OD pairs
$\mathbf{R}_q$, r	the set and index of routes that used in traveling between an OD pair q
$\mathbf{K}$, $\mathbf{W}$	the sets of all candidate nodes and links, respectively
$\mathbf{W}_{q,r}$, a	the set and index of candidate OWC links on route r between OD pair q where $\mathbf{W}_{q,r} \subseteq \mathbf{W}$
$\mathbf{K}_{q,r}$, k	the set and index of candidate nodes for plug-in charging facilities on route r between OD pair q, where $\mathbf{K}_{q,r} \subseteq \mathbf{K}$
N_q	the destination node of the OD pair q, where $N_q \subseteq \mathbf{K}$
N^j	the given number of OWCs, FCSs, and PLs to be deployed for $j \in \{1, 2, 3\}$, respectively
$Y_{q,r}^R$	=1 if the peak traffic flow between OD pair q on route r is captured, 0 otherwise
$Y_{q,r}^N$	=1 if the non-peak traffic flow between OD pair q on route r is captured, 0 otherwise
Y_q^S	=1 if the PEV static charging demand of OD pair q is captured, 0 otherwise
X_a^1	=1 if an OWC is located at candidate link a, 0 otherwise
X_k^2	=1 if an FCS is located at candidate node k, 0 otherwise
X_k^3	=1 if a PL is located at candidate node k, 0 otherwise

each OD pair. The objective function consists of three parts: The first part captures the peak traffic flows by siting the OWCs; The second part captures the non-peak traffic flow by siting the FCSs; The third part captures the PEVs static charging demand by siting the PLs. Constraints (2.9b) and (2.9c) ensure that the flow between an OD pair is captured if each link on the route r is traversable after charging in the OWCs or FCSs along the path. State variables $Y_{q,r}^R$ equal to one if all control variables X_a^1 ($\forall a \in \mathbf{W}_{q,r}$) equal to one. Similarly, state variables $Y_{q,r}^N$ equal to one if all control variables X_k^2 ($\forall k \in \mathbf{K}_{q,r}$) equal to one. These constraints are designed to consider the limited PEV driving range. On route r between OD pairs q, a pre-generated candidate node list $\mathbf{K}_{q,r}$ and candidate link list $\mathbf{W}_{k,r}$ are used to site the charging facilities to ensure that the route is traversable by the limited

range PEVs. The generation of $\mathbf{K}_{q,r}$ and $\mathbf{W}_{q,r}$ is discussed in the following paragraph. Constraint (2.9d) ensures that a PL is sited at the destination node N_q of the OD pair q if the static charging demand of this flow is met. To prevent double-counting, constraint (2.9e) ensures that charging facilities, either OWCs or FCSs, are sited on one route between each OD pair, which can capture the highest possible flow over the time. Only one type of facilities can capture the covered flow. The highest flows during the peak traffic will be covered by OWCs and then the highest flows during non-peak traffic will be covered by FCSs. Also, this constraint ensures that the PEV static charging demand can only be covered if the flows between OD pairs are covered by either OWCs or FCSs, which ensures that PEVs will be able to reach the PL locations. Constraints (2.9f) and (2.9g) ensure that the total number of each type of the deployed charging facilities in the system is less than or equal to a pre-defined number of facilities. Constraint (2.9h) indicates that only one type of plug-in facilities can be deployed at any system node. Constraint (2.9i) forces the binary variables to be either 0 or 1. Although state variables $Y^R_{q,r}$, $Y^N_{q,r}$, and Y^S_q are defined as binary variables, they can be relaxed as continuous variables with upper limit of 1 in constraint (2.9j). This is because the state variables are used in a maximization objective function, which drives the continuous variables to their highest possible values. The ST-FCLM is an mixed-integer linear programming (MILP) problem, in which the number of variables and constraints increase exponentially with an increase of OD pairs and number of routes between each q.

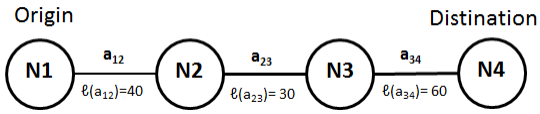

Figure 2.3: Example on generation the set of candidate charging facilities sites.

To consider the PEV limited driving range, more than one charging facility may be allocated between an OD pair in the network if the traveling distance between them is longer than the maximum PEV driving range. For each route that travelers may choose between an OD pair, two sets of candidate sites are generated: 1) Set $\mathbf{K}_{q,r}$ contains all the candidate nodes for plug-in charging facilities (FCSs or PLs) to ensure that all the links on route r are traversable for a round trip between OD pair q; 2) Set $\mathbf{W}_{q,r}$ contains all

candidate links suitable for deploying OWCs. Figure 2.3 illustrates a simple example of a single OD pair connected through three bidirectional RTN links $\{a_{12}, a_{23}, a_{34}\}$ and four RTN nodes $\{N_1, N_2, N_3, N_4\}$. We define $\ell(.)$ as the length of links. In this example, the PEV range is $\mathcal{R} = 90$. The initial PEV battery SoC is assumed equal to $\frac{\mathcal{R}}{2}$. To complete a round trip without running out of battery charge, the first candidate site for plug-in charging facility is N_2 since PEV can travel through a_{12} with the initial battery SoC. If the length of a_{12} exceeds the initial PEV battery SoC, the first candidate site is N_1. In both cases, link a_{12} is a candidate for deploying OWC. PEV battery SoC is equal to $\mathcal{R}$ after recharging at a plug-in facility at N_2 or OWC at a_{12}. Then, the PEV can travel through a_{23} and a_{34}. When the PEV reaches N_4, it must be recharged again in order to return to the origin and complete the round trip via the same route. Hence, another plug-in charging facility should be sited at N_4 or OWC at a_{34}. Therefore, the candidate plug-in charging facility set for this route is $\{N_2, N_4\}$, and the candidate links for OWC is $\{a_{12}, a_{34}\}$. In order to generalize this approach, Algorithm 1 is used to generate the candidate sites for all OD pairs in a network. All the practical routes being chosen by the travelers should be extracted from the DTA model for this algorithm. In this algorithm, $T(.)$ returns the tail node of a link. The set of links between OD pairs q on route r is denoted by $A_{q,r}$, and link i in set $A_{q,r}$ is denoted by $a(i)$, where i is the ordering index.

2.4 Numerical Results

To validate the model and demonstrate its applicability, we select two popular RTNs, which are known as the Nguyen-Dupuis network [49] and the Sioux Falls network [50]. In each case, four steps are taken: 1) The time-varying traffic flows are simulated based on the road traffic simulator SUMO [51]. The simulation tool iteratively computes the travel times on the RTN links, then assigns alternative routes to some vehicles on these routes according to the traveling time; 2) The traffic flow dataset is clustered into distinct categories using the GMM algorithm; 3) The set of candidate charging facilities sites is identified based on Algorithm 1; 4) The ST-FCLM is implemented with Gurobi Optimizer 7.5 under Python environment. The following numerical results are obtained on a laptop computer with a 2.27-GHz Intel(R) Core(TM) i3-M350 CPU and 4 GB of memory.

Algorithm 1 Generating of the candidate site sets

Input: Vehicles range $\mathcal{R}$, Set of links $A_{q,r}$

Output: Candidate nodes set $\mathbf{K}$, Candidate links set $\mathbf{W}$

$\mathbf{K} \leftarrow \emptyset$, $\mathbf{W} \leftarrow \emptyset$.
for each $q \in \mathbf{Q}$ **do**
  for each $r \in \mathbf{R}_q$ **do**
    Set $i = 1$.
    Set $SoC_1 \equiv \frac{\mathcal{R}}{2}$
    for each $a(i) \in A_{qr}$ **do**
      if $\ell(a(i)) \geq SoC_i$ **then**
        $\mathbf{W}_{q,r} \leftarrow \mathbf{W}_{q,r} \cup \{a(i)\}$
        $\mathbf{K}_{q,r} \leftarrow \mathbf{K}_{q,r} \cup \{T(a(i))\}$
        $SoC_{i+1} = \mathcal{R} - \ell(a(i))$
      else
        $SoC_{i+1} = SoC_i - \ell(a(i))$
      end if
    end for
    $\mathbf{K} \leftarrow \mathbf{K} \cup \mathbf{K}_{q,r}$.
    $\mathbf{W} \leftarrow \mathbf{W} \cup \mathbf{W}_{q,r}$.
  end for
end for

2.4.1 Nguyen-Dupuis Network

As shown in Figure 2.4, the Nguyen-Dupuis network contains 13 nodes, 19 links, and 4 OD pairs, which are (1,2), (1,3), (4,2), and (4,3) [49]. The numbers in the circles represent the node indices, and the numbers on the links denote the link indices. The speed limit of the vehicles is 50 km/h, and all links on the network are two-lane one-way roads. Table 2.3 lists the daily travel demand between origins and destinations. The hourly distribution of vehicle trips on a weekday as a percentage of daily traffic versus time of day follows the UK national travel survey [52].

To visualize the traffic simulation output, we plot the time-varying flow volumes between OD pair (1,3) in Figure 2.5. Table 2.4 lists the traffic flows along with the corresponding traveling routes and route lengths for all OD pairs. The results show that f_{11} between OD pair (1,2) travels through a single route which is the route with the shortest distance. This is because no other flows use the links of this route, permitting the flow to

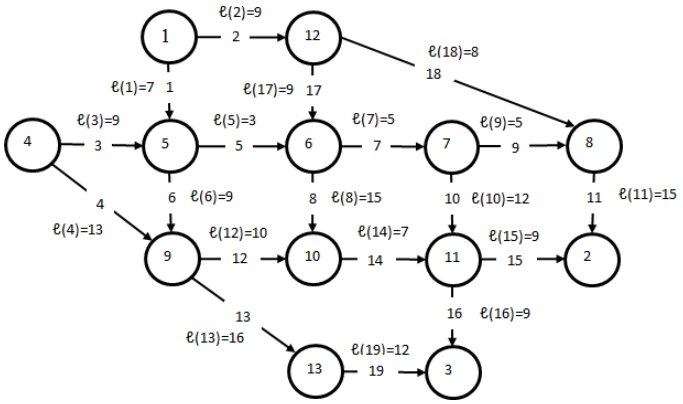

Figure 2.4: The Nguyen-Dupuis network.

Table 2.3: OD matrix of the Nguyen-Dupuis network

OD pair	Daily travel demand
(1,2)	11000
(1,3)	24000
(4,2)	13000
(4,3)	6000

travel without congestion. However, drivers use multiple routes in traveling between all other OD pairs in the network since the links of these routes are shared among multiple flows. Therefore, these links are congested, so travelers choose the routes with minimum traveling time between their OD pairs rather than the routes with the shortest distance. Table 2.4 also shows the cumulative traffic flows (after unity-based normalization) during the peak Φ^R and non-peak Φ^N traffic periods, in addition to the static PEV charging demand Φ^S at the destination nodes. The sets of candidate charging facility sites $\mathbf{K}, \mathbf{W}$ are determined based on Algorithm 1, with assuming that the PEV range is $\mathcal{R} = 24$, which is longer than the longest link in the network.

In formulating the ST-FCLM, the limits on the numbers of OWCs, FCSs, and PLs are set to be less than or equal 3,4,1, respectively. As shown in Figure 2.6, the solution locates OWCs on links $\{4, 14, 17\}$ to cover flows $\{f_{22}, f_{32}\}$, which represent 32.23% of the overall traffic flows in the network. The FCSs are deployed at nodes $\{4, 9, 12, 13\}$ to cover

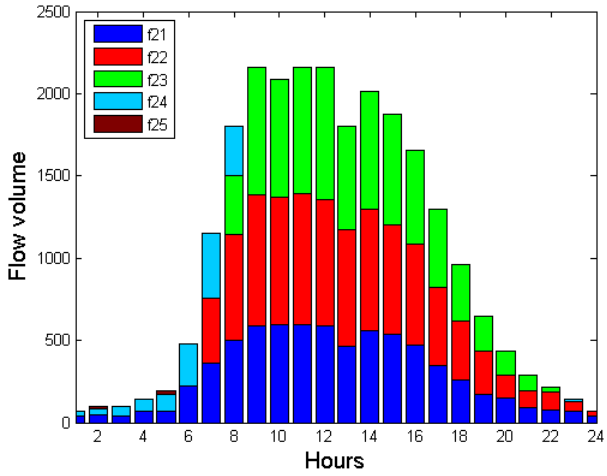

Figure 2.5: The Nguyen-Dupuis network traffic flow between OD pair (1,3).

Table 2.4: Flows routes and candidate sites sets for Nguyen-Dupuis network at $\mathcal{R} = 24$

OD pair	Flow	Route by links	length	Φ^R	Φ^N	Φ^S	**K**	**W**
(1,2)	f_{11}	2-18-11	32	1.000	1.000	20.37%	12	18
(1,3)	f_{21}	1-5-7-10-16	36	0.603	0.714	44.44%	6, 11	7, 16
	f_{22}	2-17-8-14-16	49	0.803	0.669		12, 10	17, 14
	f_{23}	2-17-7-10-16	44	0.740	0.451		12, 7	17, 10
	f_{24}	1-6-13-19	44	0.036	0.334		5, 9, 13	6, 13, 19
	f_{25}	1-5-8-14-16	41	0.000	0.012		6, 11	8, 16
(4,2)	f_{31}	3-5-7-9-11	37	0.340	0.443	24.07%	5, 8	5, 11
	f_{32}	4-12-14-15	39	0.842	0.738		4, 10	4, 14
(4,3)	f_{41}	3-5-7-10-16	38	0.143	0.189	11.11%	5, 11	5, 16
	f_{42}	4-13-19	41	0.402	0.356		4, 9, 13	4, 13, 19

flows $\{f_{11}, f_{42}\}$, which represent 28.32% of the overall traffic flows in the network. Note that f_{22}, f_{32} and f_{42} are not through the shortest distance routes between the OD pairs, but the routes with the highest traffic volumes. A PL is deployed at node $\{2\}$ to cover 55.56% of the overall *static* charging demand. The parentage of overall *en route* charging demand covered by the charging facilities is 60.55%. This percentage is the maximum traffic flows can be covered in this network, because only one route between each OD pair can be covered to prevent double counting of the flows. A higher percentage of traffic flows

can be covered if constraint (2.9e) is relaxed.

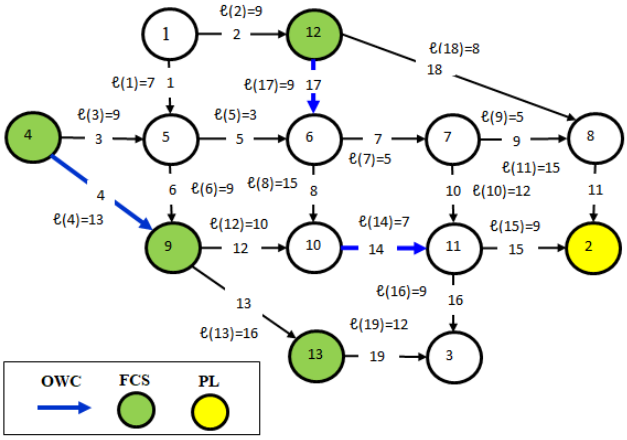

Figure 2.6: ST-FCLM solution for the Nguyen-Dupuis network.

Substantial differences appear when comparing the results of ST-FCLM with those of arc-cover path-cover flow refueling location model (AC-PC FRLM) proposed in [26] for the same network. There are two main differences between ST-FCLM and AC-PC FCLM: 1) In the AC-PC FRLM, drivers are assumed traveling through the shortest distance routes between OD pairs. Then, the siting model is restricted to cover the charging demand on those routes. On the other hand, in the ST-FCLM, drivers are assumed traveling through the routes with minimum travel times to their destinations. Thereby, the ST-FCLM considers all the feasible routes that travelers may choose for each OD pair to minimize their travel time. Both the spatial and temporal distributions of traffic flows are then used in siting of charging facilities in locations that maximize the covered traffic flows; 2) The AC-PC FRLM locates a single type of charging facilities on the transportation network nodes. On the other hand, the ST-FCLM utilizes the clustered traffic flow dataset in siting multiple types of charging facilities.

To compare the ST-FCLM and AC-PC FCLM, we analyze the effect of varying the number of sited facilities on the percentages of covered traffic flows. As shown in Figure 2.7, the ST-FCLM covers either higher or as same traffic flows as AC-PC FRLM. As shown in Figure 2.7, the AC-PC FRLM covers only 12.88% of the overall flows in the network with two charging facilities, although it covers 20.37% with one facility. This is because,

with two charging facilities, this model covers flow f_{21} that has more traveling demand than flow f_{11}, which can be covered by one facility. However, the travelers between OD pair (1,3) choose various routes during their trips and are not restricted to the shortest distance route. On the other hand, the ST-FCLM always covers the routes with the highest traffic volumes. Moreover, the ST-FCLM can cover up to 60.55% by deploying five charging facilities. However, the maximum traffic flows can be covered in the AC-PC FRLM is 43.9%. Consequently, the ST-FCLM outperforms the flow covering model, where traveler route choices are only governed by the distance of routes.

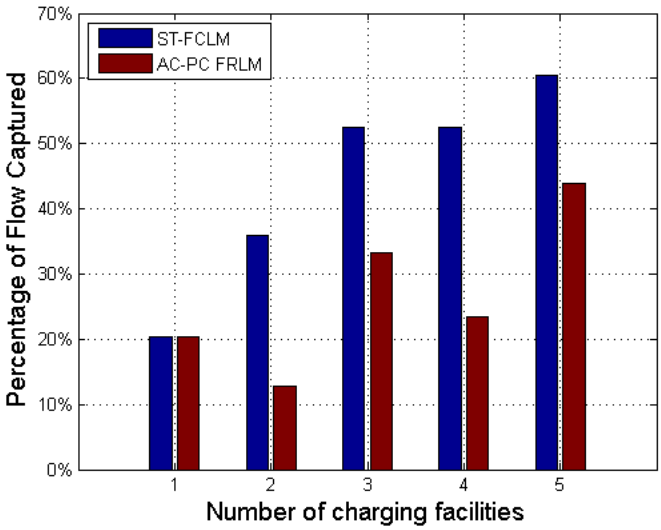

Figure 2.7: Comparison between ST-FCLM and AC-PC FRLM when $\mathcal{R} = 24$.

2.4.2 Sioux Falls Network

To validate our model on a larger network, with more realistic topology and demand properties, we select the well-known transportation network of Sioux Falls, South Dakota, USA. The Sioux Falls network consists of 24 nodes, 76 links, and 576 OD pairs [50]. The topology of the Sioux Falls network is shown in Figure 2.8. Other network attributes, such as OD matrix and link capacity, are reported in [50]. All nodes are candidate sites for FCSs and PLs, and all links are candidate sites for OWCs.

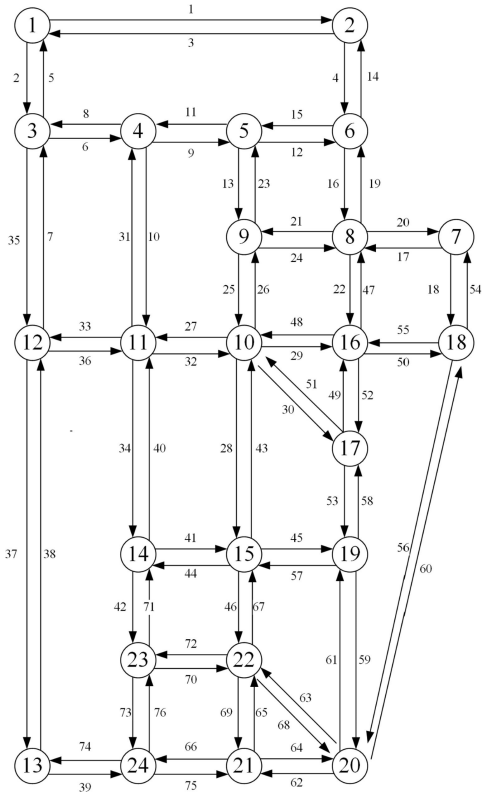

Figure 2.8: The Sioux Falls network.

The DTA simulation for the Sioux Falls network converges to the Wardrop's user equilibrium after three iterations. The number of generated flow vectors between the 576 OD pairs is 1656. Each flow vector has a specific traveling route between the corresponding OD pair. The flow vectors contain the discretized values of traffic volumes on the corresponding traveling routes for 24-time slots over a typical weekday. The traffic flow dataset is partitioned into two categories based on the GMM clustering algorithm. The number of Gaussian components is chosen to be two components, which minimize the BIC score as shown in Figure 2.9. Table 2.5 lists the GMM parameters for the two Gaussian components. The EM algorithm reaches convergence after three iterations.

We implement the ST-FCLM on the Sioux Falls network, with PEV range $\mathcal{R} = 100$ km. Figure 2.10 shows the captured traffic flows and the covered static charging demand as a

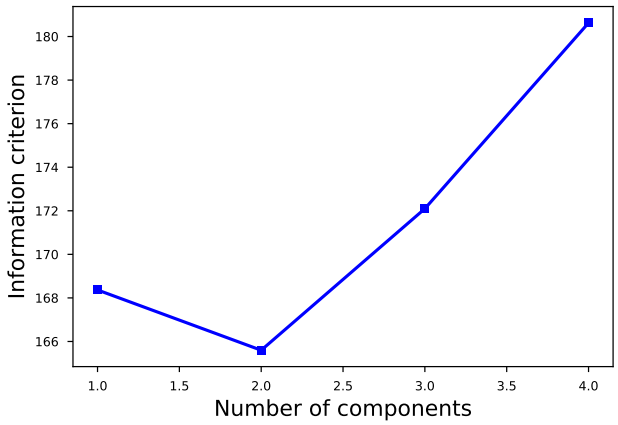

Figure 2.9: BIC score versus the number of GMM components.

Table 2.5: GMM component parameters

i	ω_i	μ_i	Σ_i
1	0.43750854	1.88507101	3.9677486
2	0.56249146	14.59745472	15.14277279

function of the number of charging facilities. The number of deployed facilities is increased gradually until 10 facilities from each type are deployed. It is observed that around 47% and 51% of the *en route* and *static* PEV charging demand, respectively, can be covered by the 10 facilities from each type. The optimized siting plan of multiple types of charging facilities obtained through the ST-FCLM is reported in Table 2.6. In this table, due to space limitations, the number of facilities is limited to five facilities from each type.

Table 2.6: Deployment plan of multiple types of charging facilities

No. of facilities	OWC locations	FCS locations	PL locations
3	32	22	10
6	49,58	11,12	10,17
9	32,36,58	9,16,22	10,17,15
12	25,27,32,36	16,19,22,23	10,17,15,11
15	25,46,49,53,67	11,12,14,19,23	10,17,15,20,22

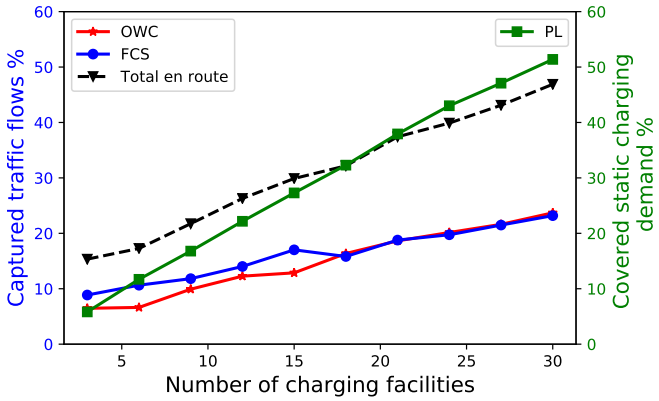

Figure 2.10: Implementing the ST-FCLM on the Sioux Falls network.

2.5 Summary

In this chapter, we propose the spatial-temporal flow capturing location model. This model locates three types of charging facilities based on the spatial-temporal distribution of the traffic flows. A simulation-based DTA model is used to estimate the time-varying traffic flows between all OD pairs in the network. Then, the traffic flow dataset is clustered by the GMM algorithm according to the temporal characteristics to identify the time periods in which the traffic flows are high or low. Our model captures the traffic flows during peak and non-peak traffic periods by OWCs and FCSs, respectively. The ST-FCLM deploys PLs at the destination nodes of the trips to cover the static PEV charging demand. Thus, our model makes use of different characteristics and usage patterns of each charging technology. The simulation results based on the Nguyen-Dupuis and Sioux Falls networks show that the proposed model captures a higher percentage of traffic flows with the same number of facilities when compared with an existing model based only on spatial characteristics of the traffic flows. Additionally, our model can be implemented on a relatively large transportation network with a comparatively high number of OD pairs. Chapter 3 focuses on capacity planning of EVCI, and proposes a framework that sizes charging facilities to fulfill the given QoS targets and minimizes the cost of EVCI integration into PDN.

Chapter 3

QoS-aware Capacity Planning of Networked EVCI

In this chapter, we propose a QoS aware capacity planning of EVCI. The proposed framework accounts for the link between the charging QoS and the PDN capability. As illustrated in Figure 3.1, we firstly optimize charging facility sizes to achieve a targeted QoS level for the entire networked EVCI. PEV charging demand at each facility is estimated for inclusion in the PDN load demand. Then, we minimize the integration cost for the PDN by attaining the most cost-effective allocation of the ESSs and/or upgrading the PDN substation and feeders. Additionally, we capture the correlation between the occupation levels of neighboring charging facilities and the blocked PEV user behaviors. We model the EVCI as a queuing network with finite capacity, and utilize the non-stationary queuing models to study the temporal variability of the PEV charging demand. A network of charging facilities is used to demonstrate the effectiveness of the proposed framework.

3.1 Related Work

Capacity planning of EVCI must ensure not only a satisfactory charging service for PEV users but also a reliable operation of the power grid. Existing capacity planning models of

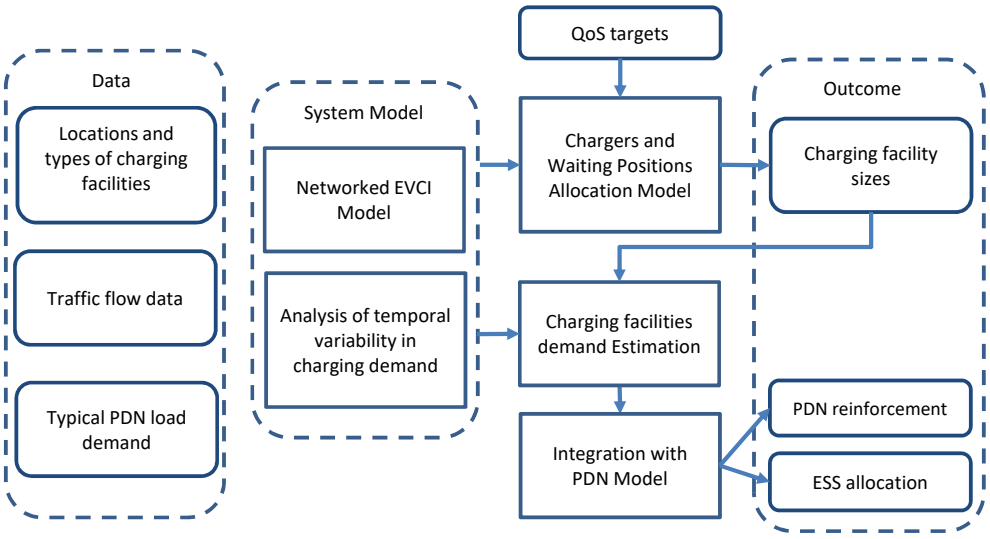

Figure 3.1: EVCI capacity planning framework.

EVCI follow two main approaches [18]. One approach uses stochastic models to size the charging facilities to achieve a targeted QoS level [53–55]. A charging facility is modeled as an isolated stationary queue, while PEVs are modeled as customers in the queue. These PEVs require a charging service from a limited number of identical chargers. Charging facilities are sized based on the expected PEV charging demand at each facility location and evaluated based on statistical metrics, such as blocking probability and waiting time [54]. The $M/M/c$ queuing model can be used to model fast charging stations [5, 42, 54, 56]. This model assumes that all the arrived PEVs will wait for the charging service, which means unlimited waiting positions in the charging facility. In order to consider the limited waiting positions in a charging station, the $M/M/c/K$ queuing model is employed [57, 58]. If all the waiting positions in the facility are occupied, the newly arrived PEV will leave the facility without charging. Based on the expected PEV charging demand, the numbers of chargers and waiting positions in the charging facility can be determined to meet the target QoS set by the planner [54, 57, 58]. Although this approach can ensure a satisfactory charging service with the stochastic PEV demand, it endangers the reliability of the power system. This is because the targeted QoS level is set in isolation from the actual capability of PDN.

The other approach sizes the charging facilities to minimize the negative impacts on

the power grid [19, 22, 59–62]. The sizing objective is to ensure that the charging facility load demand complies with the power system operational constraints by collaboratively planning the EVCI and PDN. For instance, a multi-objective planning model with a coupled distribution and transportation networks is proposed in [11]. The planning model optimizes the locations and sizes of charging facilities to minimize the total energy loss and bus voltage deviation on the distribution network, in addition to maximizing the captured traffic flow of charging facilities. Another model is to optimize the locations and sizes of charging facilities to balance between the PEV charging requirement and power network stability, considering a linearized power network model [63]. This approach ensures that the PDN can safely accommodate the peak load demand of charging facilities; however, PEV user satisfaction is not a focus. This is because the planning models usually re-locate and/or re-size the charging facilities to fulfill power grid requirements.

There are a few published papers that deal with both the charging QoS and the PDN capability in the planning of EVCI. For instance, a siting and sizing model of fast charging stations on coupled transportation and power networks is proposed in [64]. This model utilizes users' waiting time at charging facilities as a service level index. Then, an optimization model is used to size charging stations and determine the required upgrade in the PDN. In [42], a capacitated flow-refueling location model is proposed to optimize the planning of highway fast-charging stations. The proposed model adopts the $M/G/S$ queuing model to size charging facilities based on the upper limit of users' waiting time. This model also introduces capacity constraints in the siting model. Thereby, if PEV charging demand cannot be satisfied in a facility, it is distributed to other facilities in the network.

Even though that capacity planning of EVCI has been extensively studied in the literature, three issues have not yet been well studied: 1) Existing capacity planning models do not capture the inter-relationships among the charging QoS, the capability of existing PDN, and the possibility of allocating ESS in charging facilities. Accounting this relationship in the sizing of charging facility ensures the balance between the requirements of the power system and charging service; 2) Modeling charging facilities as isolated queues with infinite capacity ignores the correlation among the occupation levels of nearby facilities. In practice, if the capacity of a charging facility is less than the demand, the blocked PEV users can spread across the surrounding charging facilities, which can greatly impact the

level of performance in those facilities. Therefore, charging facilities must be modeled as a network with a finite capacity to account for the inter-relationships among nearby facilities, in addition to accounting for the behavior of blocked PEV users by the overloaded facilities; 3) Designing charging facilities using the stationary queuing models do not account the temporal variability of PEV charging demand. Two approaches are used to apply these stationary queuing models to a system with time-varying demand (PEV arrival rate). The first approach uses stationary models with the long-run-average arrival rate to simplify the sizing problem [54]. However, the system can suffer from high congestion (overload) and low QoS at the peak demands [65]. The second approach divides the time horizon into intervals and then uses the peak demand (peak arrival rate) as inputs to the stationary queuing models [22, 53]. This approach aims to fulfill the targeted performance at the peak demand. However, it fails to capture the random time lag between the time of peak demand and the time of peak load on the queuing system. Moreover, this approach does not account for PEVs that are already in the system (either charging or waiting) from the preceding time periods [65].

3.2 System Model

In this section, we present modifications to the system model presented in Chapter 2 to account for the coupling with the PDN, the correlation among the PEV occupancy of neighboring charging facilities, and the temporal variability of the PEV charging demand.

Consider a typical urban area where the RTN is coupled with the PDN according to the geographical information. The PDN consist of a set of buses $\mathcal{B}$ and a set of branches (feeders) $\mathcal{L}$. The PDN is connected to the rest of the power grid through substation(s). Let $\mathcal{H}$ ($\mathcal{H} \subseteq \mathcal{B}$) be the set of buses connected to substations. It is assumed that load forecasting studies are conducted at the PDN to estimate the power demand profile [22]. Furthermore, voltage limits, branch capacity limits, substation capacity limits, and the conductance of all branches are known. Time is partitioned to equal segments, where each time segment duration is chosen to be one hour as an example. This is because energy trading and scheduling are conducted on a one-hour interval basis, according to Ontario's independent

electricity system operator (IESO) [66]. Also, PEV traffic flows are estimated on the same time intervals. The locations of charging facilities are given, as discussed in Chapter 2. FCSs and PLs are allocated on a finite set of RTN nodes, and OWCs are allocated on a finite set of RTN links. AC level 3 chargers and DC fast chargers are deployed in the PLs and FCSs, respectively [6]. Moreover, some PEVs are capable of charging in OWCs via the dedicated wireless charging lanes [53]. The load demand of charging facility equals the aggregated charging demand of all PEVs simultaneously being charged.

3.2.1 Networked EVCI Model

The capacity of any charging facility is always finite. Thereby, a PEV user may be momentarily stopped (rejected) when a charging facility reaches its maximum capacity. This phenomenon is called blocking. Subsequently, the blocked PEV user may move towards one of the neighboring charging facilities, requesting a charging service. Due to the blocking, there is a correlation among the PEV occupancy of neighboring charging facilities, and understanding this correlation helps to explain the propagation of congestion. Consequently, a realistic model of EVCI should address the finite capacity of charging stations, in addition to the behavior of blocked PEV users by the overloaded facilities.

EVCI can be modeled as an open queuing network with finite capacity and blocking. Different from isolated queue models, a finite capacity queuing network can capture the interactions among multiple charging facilities, in addition to the blocked PEV user behaviors. In such a network, EVCI can be represented as a set of interconnected charging facilities (service centers). These service centers are interconnected through a road system. PEV users enter this open network from outside (exogenous arrivals), receive charging services, and eventually leave the network. In order to construct the queuing network, each charging facility is modeled by two types of nodes:

- *Charging facility node (CN)*: A charging facility is represented as a physical node. If the charging facility is an FCS or a PL, CN n ($n \in \mathbf{N}$) can be modelled as a finite queuing system $M/M/c_n/K_n$, which has a Poisson arrival process M [67], exponentially distributed service time M with service rate μ_n [5], c_n chargers (servers), and

maximum number of PEVs, K_n, in the facility including the charging and waiting PEVs. If the charging facility is an OWC, CN node n can be represented as a loss system $M/M/c_n/c_n$, since there is no waiting position on the charging lanes.

- *Decision-making node (DN)*: A DN is a logical (virtual) node associated with each CN. DN n is used to model the behavior of PEV users, who are requesting a charging service from the associated CN. The decision of each PEV user can be either to get a charging service from CN n or move towards another charging facility (DN $\acute{n}$, where $\acute{n} \neq n$). Thus, the arrivals to a DN can be from an external population and/or routed from other DNs. DN n is modeled as a single server queue $M/M/1$ with a very high service rate $\mu_n^d \gg \mu_n$ since a driver usually makes a decision instantaneously without delay.

In the networked EVCI, PEV user behaviors in response to the occupancy level of charging facilities are described through a blocking mechanism, called *repetitive service with random destination (RS-RD)* [68]. When a PEV user chooses charging facility n for a service, the user will first arrive at DN n, then chooses a destination randomly either by attempting to access CN n or routing towards another DN $\acute{n}$ in the network. If CN n at that time is full, the user will be blocked and return to DN n, starting to randomly choose a new destination independent of the previous choice(s). [1] After a PEV is served by a charging facility, it leaves the network with probability 1, under the assumption that the charging demand of a PEV is unsplittable and a PEV will be charged with sufficient energy at the visited facility. An illustrative example of a queuing network composing of two neighboring charging facilities is shown in Figure 3.2.

The routing probability between two charging facilities is denoted by $\alpha_{n\acute{n}}$, where $n \neq \acute{n}$ and $n, \acute{n} \in \mathbf{N}$, while α_{nn} denotes the routing probability between DN n and the associated CN n. The routing probability α_{nn} is larger than any $\alpha_{n\acute{n}}$, for $\acute{n} \neq n$, where $\alpha_{n\acute{n}}$ are assigned to the neighboring DNs depending on the proximity to CN n. That is, a blocked

[1] A deadlock problem may occur in the queuing network if all CNs in the network are full. In this case, a PEV user may be blocked multiple times until space becomes available at a CN. To avoid a network deadlock, it is sufficient that the routing matrix is irreducible and the number of PEVs requesting charging services is less than the total capacity of CNs [69]. In this model, we assumed that the EVCI is a deadlock-free network.

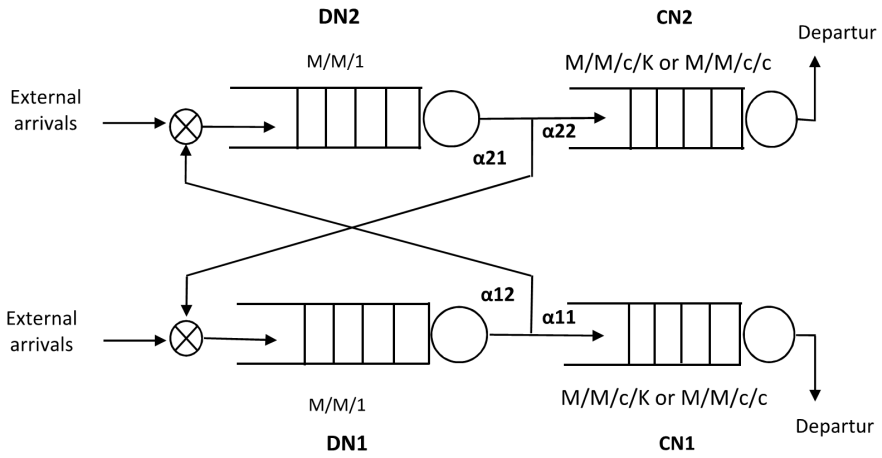

Figure 3.2: Queuing network model of two neighboring facilities.

PEV will be routed to a nearby charging facility with a higher probability than those to farther facilities. This assumption conforms with vehicular traffic modeling [70]. The routing probability can be estimated based on the multinomial logit (MNL) model, which is used to predict driver choice probabilities as a function of a certain utility, such as traveling distance, traveling time, and charging cost [71]. Due to the range anxiety of the blocked PEV users, $\alpha_{n\acute{n}}$ is assumed depending on the distance $d_{n\acute{n}}$ between charging facilities and can be estimated by

$$1 - \alpha_{nn} = \sum_{\substack{\forall i \in N \\ i \neq n}} \alpha_{ni}, \tag{3.1a}$$

$$\alpha_{n\acute{n}} = \frac{(1 - \alpha_{nn}) e^{-d_{n\acute{n}}}}{\sum\limits_{\substack{\forall i \in N \\ i \neq n}} e^{-d_{ni}}}, \quad \forall n \in \mathbf{N}. \tag{3.1b}$$

Analysis of queuing networks with finite capacity and blocking is complex, because the steady-state queue length distributions do not have a product form, except for some special cases [68]. However, the steady-state queue length distribution of the network un-

der investigation can be approximated using the disaggregation-aggregation (DA) iteration method [72]. Based on DA iterations, the underlying Markov chain model of a queuing network is approximated through aggregation. This Markov chain typically has a very large state space and a sparse transition probability matrix. DA iterations exploit the marginal aggregate probabilities instead of the complete state space, in order to approximate a product form solution of the state probabilities. Calculating the state probabilities facilitates the evaluation of the performance indicators of the EVCI. DA iteration algorithm is briefly discussed as used in our application in Appendix A.

3.2.2 Analysis of Temporal Variability in Charging Demand

To incorporate the time-varying demand, a charging facility model can be refined using non-stationary queuing models $M_t/M/c/K$ and $M_t/M/c/c$ (depending on the facility type) with a non-homogeneous Poisson arrival process (NHPP) M_t. The NHPP is a counting process, $\boldsymbol{\mathcal{X}} = \{\mathcal{X}(t) : t \geq 0\}$, having independent and Poisson-distributed increments. The NHPP has a deterministic arrival rate function at time t, $\lambda(t)$, [73].

The analysis of non-stationary queuing models can be approximated by infinite server model $M_t/M/\infty$, which has the same arrival process and service time distribution but with an infinite number of servers [74]. This approximation allows all users to access the service upon arrival without waiting, which simplifies the mathematical model. The PEV number, $\mathcal{X}_t$ at time t, in the finite queuing model is approximated by the number of the busy servers, $\mathcal{X}_t^{\infty}$, in the infinite server model. It is proved, in [74] and the references therein, that $\mathcal{X}_t^{\infty}$ has a Poisson distribution with mean, $m_{\infty}(t)$, which is expressed in terms of the arrival-rate function $\lambda(t)$ as

$$m_{\infty}(t) \equiv \mathbb{E}[\mathcal{X}_t^{\infty}] = \mathbb{E}\left[\int_{t-\mathbb{S}}^{t} \lambda(r)dr\right] = \mathbb{E}[\lambda(t-\mathbb{S}_e)]\mathbb{E}[\mathbb{S}] \tag{3.2}$$

with $\mathbb{S}$ being the service time distribution. In (3.2), random variable $\mathbb{S}_e$ is the stationary-excess distribution, which indicates the distribution of the remaining service time [75]. The time-varying mean in (3.2) is the expected number of busy servers in the system with an infinite number of servers, referred to as *offered load*. This formula is complicated as

there is a random time lag, $\mathbb{S}_e$, in the arrival rate function. The offered load of infinite server model provides insight on both the time-lag and magnitude shift between arrivals and loads of the system.

The offered load approximation in (3.2) is used to derive a new arrival rate function, which is used in evaluating the performance of the non-stationary queuing systems over time. The new arrival rate function is called *modified offered load (MOL)* [65, 75]. Based on the MOL, the instantaneous performance measures for the $M_t/M/c/K$ and $M_t/M/c/c$ systems can be approximated with the steady state performance of the associated stationary models $M/M/c/K$ and $M/M/c/c$, respectively. The MOL arrival rate function, $\lambda^*(t)$, is obtained from the exponentially weighted moving average of the arrival rate for the non-stationary models by [75]

$$\lambda^*(t) = \int_{-\infty}^{t} \mu \, \exp\big[-\mu(t-u)\big] \, \lambda(u) \, du \tag{3.3}$$

where μ is the service rate of the queuing model. The MOL arrival rate accounts for the transient behavior and dependencies among the consecutive intervals. Thereby, the time-dependent system performance can be analyzed accurately [65].

The non-parametric estimation method is used to estimate the MOL arrival rate function over time [73]. The MOL arrival rate function to charging facility n, $\lambda^*_{t,n}$, is assumed piecewise constant on any subinterval $[t-1, t)$, with $t \in \mathbf{T}$, depending on the number of PEVs intercepted at a charging facility, PEV penetration rate, and the facility type. Let $I^n_1, I^n_2, \cdots, I^n_T$ be the numbers of PEVs intercepted at charging facility n, which are collected over T sub-intervals. As discussed in Chapter 2, these numbers are estimated based on the DTA model, which forecasts the time-varying traffic patterns of RTN [53]. Thus, MOL arrival rate function for charging facility n at time slot t can be calculated by

$$\lambda^*_{t,n} = \begin{cases} \mathcal{P}\nu(1-\sigma)(1-\beta) \int\limits_{u=0}^{t} \mu^F \; I^n_u \; \exp\big[-\mu^F(t-u)\big] \; du, & \text{if } n \in \mathbf{F} \\ \mathcal{P}\nu(1-\sigma)\beta \int\limits_{u=0}^{t} \mu^O \; I^n_u \; \exp\big[-\mu^O(t-u)\big] \; du, & \text{if } n \in \mathbf{O} \\ \mathcal{P}\nu\sigma \int\limits_{u=0}^{t} \mu^P \; I^n_u \; \exp\big[-\mu^P(t-u)\big] \; du, & \text{if } n \in \mathbf{P} \end{cases} \tag{3.4}$$

where $\mathcal{P}$ represents the PEV penetration rate; ν is the average charging frequency of a PEV; σ denotes the percentage of PEV drivers who prefer charging in PLs at trip destinations; β denotes the percentage of PEVs that have wireless charging capability; and μ^F, μ^O, μ^P denote service rates of FCS, OWC, and PL, respectively.

3.3 Capacity Planning of EVCI

This planning stage focuses on developing a capacity planning model for EVCI as a resource provisioning problem without considering limits of the PDN. It resolves the issue of sizing the charging facilities efficiently by optimizing the number of chargers and waiting positions required at charging facilities to achieve the targeted QoS level for EVCI.

The allocation of chargers $\mathbf{c} = \{c_n, \forall n \in \mathbf{N}\}$ and waiting positions $\mathbf{B} = \{B_n, \forall n \in \mathbf{N}\}$, where $B_n = K_n - c_n$, in charging facilities affects the overall performance of the charging service and hence customer satisfaction. Obviously, the numbers of chargers and waiting positions allocated to a charging facility lead to differences in the facility's operational capacity, and hence the blocking probability and the expected waiting time. Furthermore, with the propagation of congestion (due to the behaviors of the blocked PEV users), the performance of entire networked EVCI may vary in proportional to the sizes of individual facilities. Thereby, the capacity of each charging facility must be optimized to realize the targeted QoS level for the entire networked EVCI, given that both chargers and waiting positions represent a significant amount of investment during the deployment phase. Two performance metrics are used to measure the QoS at the networked EVCI:

1. The normalized network throughput at time t, Θ_t, measures the percentage of PEV users who can get charging services successfully without being blocked. The more blocked PEVs in a charging facility, the less user satisfaction since the blocked users have to go to another facility to get charging services. The throughput can be obtained by

$$\Theta_t(\mathbf{c}, \mathbf{B}) = \frac{\sum_{\forall n \in \mathbf{N}} \lambda^*_{t,n}(1 - p_{K_{t,n}})}{\sum_{\forall n \in \mathbf{N}} \lambda^*_{t,n}} \tag{3.5}$$

where $p_{K_{t,n}}$ denotes the blocking probability of charging facility n at time t. Note that Θ_t is a function of the time-varying MOL arrival rate to charging facilities, in addition to the numbers of servers and waiting positions of all facilities in the networked EVCI. The lower bound of the normalized network throughput, $\underline{\Theta}$, is defined as

$$\underline{\Theta}(\mathbf{c}, \mathbf{B}) = \min_{\forall t \in \mathbf{T}} \Theta_t * 100\%. \tag{3.6}$$

2. The expected waiting time, $E[W_{t,n}]$, measures the speed of getting a charging service. As PEV users wait longer, their satisfaction level decreases. The expected waiting time at charging facility n at time t can be obtained by

$$\mathbb{E}[W_{t,n}(\mathbf{c}, \mathbf{B})] = \frac{\sum_{i=c_n+1}^{K_n}(i - c_n)p_{i_{t,n}}}{\lambda^*_{t,n}(1 - p_{K_{t,n}})} \tag{3.7}$$

where $p_{i_{t,n}}$ denotes the probability of having i PEVs in charging facility n at time t. On the entire network level, the weighted average at time t over all charging facilities, W_t^{Net}, and the upper bound, $\overline{W^{Net}}$, of the expected waiting time metric are given by

$$W_t^{Net}(\mathbf{c}, \mathbf{B}) = \frac{1}{N} \sum_{\forall n \in \mathbf{N}} \omega'_{t,n} E[W_{t,n}] \tag{3.8a}$$

$$\overline{W^{Net}}(\mathbf{c}, \mathbf{B}) = \max_{\forall t \in \mathbf{T}} W_t^{Net} \tag{3.8b}$$

where $\omega'_{t,n} = \frac{\lambda^*_{t,n}}{\sum_{\forall n \in \mathbf{N}} \lambda^*_{t,n}}$ is a weighting factor that accounts for the differences in charging facility demands. It gives more weight to facilities with a higher demand, and vice versa. Again, W_t^{Net} is a function of the MOL arrival rates and the networked EVCI characteristics.

It assumed that PEV users do not have prior knowledge about the current QoS at the chosen facility. Upon arriving at a charging facility, a PEV user spontaneously attempts to access the charging facility to get a charging service. If the charging facility at that time is full, the user will be blocked and choose a new destination. The investigation of how the QoS and charging price affect the PEV user behaviors is investigated in Chapter 4.

In the sizing problem, both numbers of chargers and waiting positions are minimized to fulfill the given QoS targets for the networked EVCI, which is formulated as

$$\min_{\mathbf{c},\mathbf{B}} \left\{ \sum_{\forall n \in \mathbf{N}} \omega_n c_n + \sum_{\forall n \in \mathbf{N}} (1-\omega_n) B_n \right\} \tag{3.9a}$$

$$s.t.\ \underline{\Theta}(\mathbf{c},\mathbf{B}) \ \geq \ \Theta^{\tau} \tag{3.9b}$$

$$\overline{W^{Net}}(\mathbf{c},\mathbf{B}) \ \leq \ W^{\tau} \tag{3.9c}$$

$$c_n \in \{1,2,\ldots\}, \qquad \forall n \in \mathbf{N} \tag{3.9d}$$

$$B_n = \begin{cases} \{0,1,2,\ldots\}, & \text{if } n \in \{\mathbf{F} \cup \mathbf{P}\} \\ 0, & \text{if } n \in \{\mathbf{O}\}. \end{cases} \tag{3.9e}$$

The objective function (3.9a) minimizes the total number of the allocated chargers and waiting positions in the given queuing network. For each charging facility, a relative cost variable, ω_n, is assigned to the chargers and $(1-\omega_n)$ to the waiting positions. The value of ω_n reflects the relative cost of a charger versus that of a waiting position for each specific charging facility, $n \in \mathbf{N}$. Constraint (3.9b) ensures that $\underline{\Theta}(\mathbf{c},\mathbf{B})$ is not less than predefined targeted network throughput Θ^{τ}. Constraint (3.9c) ensures that $\overline{W^{Net}}(\mathbf{c},\mathbf{B})$ is not larger than predefined maximum expected waiting time threshold W^{τ}. Constraint (3.9d) forces the number of chargers to be a positive integer. Constraint (3.9e) forces the number of waiting positions to be a positive integer if the charging facility is an FCS or PL, and to be 0 if the charging facility is an OWC.

The optimization problem simultaneously determines $\mathbf{c}$ and $\mathbf{B}$ to satisfy the targeted QoS level. However, establishing appropriate QoS thresholds is not a trivial task. These thresholds are determined based on the actual capability of PDN as described in the next section. The sizing problem in (3.9) is a difficult nonlinear integer programming (NIP) problem with black-box constraints. Because the analytical expressions of the two performance metrics (i.e., $\underline{\Theta}(\mathbf{c},\mathbf{B})$ and $\overline{W^{Net}}(\mathbf{c},\mathbf{B})$) of the networked EVCI are unknown, and exact derivatives cannot be provided for those black-box constraints. The values of these functions can be evaluated only through the expensive (time-consuming) DA iteration algorithm.

It is shown that the optimal allocation of the scarce resources in a network is an $\mathcal{NP}$-hard problem [76]. The number of integer variables in the problem is $2N$, and the solution space of the sizing problem grows exponentially with an increase of the number of the networked charging facilities. Additionally, the evaluation time of the black-box constraints grows exponentially with an increase of both the number of nodes in the network and the capacity of the individual nodes.

The mixed-integer sequential quadratic programming (MISQP) algorithm is chosen to solve the optimization problem. The MISQP is a derivative-free heuristic iterative algorithm that searches for a local minimum solution relying on information obtained from the evaluation of several points in the search space [77,78]. This algorithm is used in solving the problems with a relatively small number of variables, in which the integer variables are not relaxable (i.e. the function variables can only evaluated at integer points). The MISQP requires a few number of function evaluations, which is a suitable choice for the expensive black-box constraints in the sizing problem. The MISQP can efficiently compute a feasible solution for the sizing problem; however, the global optimal solution is not guaranteed [79]. To increase the chances of finding the global optimal solution, the solver can be initialized with different random starting solutions.

3.4 EVCI Integration Into Power Grid

So far, the sizes of networked EVCI are optimized to satisfy the targeted QoS metrics, but without accounting for the operational and electrical constraints of the existing PDN. The next step is to integrate charging facilities into PDN, which add a substantial load to the power grid. Originally, the existing system components of the PDN may not be designed to accommodate the power demand of charging facilities [80]. To facilitate the integration of charging facilities, PDN substations and feeders may need to be reinforced, which requires new investments. Alternatively, ESSs can be allocated in charging facilities to alleviate the PDN integration cost if using ESS is more cost-effective. When utilizing an ESS, energy is stored during off-peak times and released when the total system load (i.e., system demand in addition to EVCI demand) is high. The charging service provider will

benefit from covering PEV charging demand in charging facilities, in addition to energy arbitrage profit if the ESS is used on the system demand. This section presents a planning framework that minimizes the integration cost of EVCI into PDN by attaining the most cost-effective ESS allocation and/or PDN reinforcement.

PEV charging demand at each facility is firstly estimated for inclusion in the PDN load demand. This estimation is based on the average number of busy chargers $\mathbb{E}[B_{t,n}^{Ch}]$ at time t in charging facility n, in addition to the charging power, P_n^{Ch}, and the charging efficiency, η_n^{Ch}, of chargers at facility n. [2] The calculation of $\mathbb{E}[B_{t,n}^{Ch}]$ can be done based on the analysis of the networked EVCI [81], as discussed in Subsection 3.2.1. The power demand, $P_{t,n}^{EV}$, of charging facility n at time slot t can be computed by

$$\mathbb{E}[B_{t,n}^{Ch}] = \sum_{i=0}^{c_n} i p_{i_{t,n}} + c_n \sum_{i=c_n+1}^{K_n} p_{i_{t,n}} \tag{3.10a}$$

$$P_{t,n}^{EV} = \eta_n^{Ch} P_n^{Ch} \mathbb{E}[B_{t,n}^{Ch}]. \tag{3.10b}$$

To reduce the charging time, it is recommended that PEV users charge their PEV batteries to about 80% of capacity using constant current charging mode [42]. Based on this assumption and to simplify the calculations, P_n^{Ch} is regarded as constant [63, 80]. Although the charging power is assumed constant, the charging duration of each PEV is assumed to be an independently and exponentially distributed random variable, as discussed in Subsection 3.2.1. This assumption conforms with the PEV battery charging behavior model and reflects the stochastic variability of PEV characteristics and users charging/driving behaviors [5]. After estimating the load demand of charging facilities, EVCI can be integrated into PDN, in which the objective function and constraint sets are described as follows.

[2] To estimate the PEV load demand, each charging facility is assumed to contain a homogeneous type of chargers with the same charging power. Further study is needed to model charging facilities with multiple types of chargers at one location.

3.4.1 Objective Function

The objective function aims to minimize the total capital cost of EVCI integration into PDN, which includes two parts. The first one is the total investment cost, including the cost ESS allocation in charging facilities, in addition to the cost of upgrading the PDN substation(s) and/or feeders. The ESS cost consists of three components [82]: 1) The ESS power cost C^P, which represents the cost of power electronics equipment such as inverters and rectifiers; 2) The ESS energy cost C^E, which is the cost of the storage elements such as the batteries; 3) The ESS annual operational cost C_l^O at year l. The total ESS operational cost is brought to the year of investment by aggregating the annual costs over the ESS lifetime L and multiplied by the present value factor, with annual interest rate $\mathcal{I}$. Let C^{Sb} and C^F denote the costs of substation expanding and feeder upgrade, respectively. The total investment cost can be expressed as

$$C^{Inv} = \sum_{\forall n \in \mathbf{N}} \{C^P P_n^R + C^E E_n^R + \sum_{l=1}^{L} \frac{C_l^O E_n^R}{(1+\mathcal{I})^{l-1}}\} + \sum_{\forall j \in \mathcal{H}} C^{Sb} G_j^R + \sum_{\forall ij \in \mathcal{L}} C^F \ell_{ij} S_{ij}^R. \quad (3.11)$$

The second part of the objective function is the present value of the system daily operational cost during the ESS lifetime. It includes 1) the cost of importing energy from the upstream grid, which is calculated based on the day-ahead hourly energy cost $C_{s,t}^e$ and the power injected to the system through the substation(s), and 2) the benefit from ESS energy arbitrage, which is the profit resulting from ESS charging during the off-peak periods at a low price and ESS discharging at the peak periods at a high price [13]. Let D_s denote the number of days in load scenario s in one year. Including the energy arbitrage in the objective function optimizes the ESS charging/discharging schedule. The total operational cost can be expressed as

$$C^{Opr} = \sum_{l=1}^{L} \frac{1}{(1+\mathcal{I})^{l-1}} \sum_{\forall s \in \mathbf{S}} D_s \{ \sum_{\forall t \in \mathbf{T}} \{ \sum_{\forall j \in \mathcal{H}} C_{s,t}^e P_{s,t,j}^G + \sum_{\forall n \in \mathbf{N}} C_{s,t}^e (P_{s,t,n}^{ES,c} - P_{s,t,n}^{ES,d}) \} \}. \quad (3.12)$$

3.4.2 ESS Operational Constraints

The following constraints regulate the ESS allocation and operation in charging facilities. These constraints should be satisfied for $\forall n \in \mathbf{N}$, $\forall s \in \mathbf{S}$, and $\forall t \in \mathbf{T}$:

$$P_n^R = P^S p_n \leq P_n^{R,\max} \tag{3.13a}$$

$$E_n^R = E^S e_n \leq E_n^{R,\max} \tag{3.13b}$$

$$E_{s,t+1,n} = E_{s,t,n} + (\eta^{ES,c} P_{s,t,n}^{ES,c} - \frac{P_{s,t,n}^{ES,d}}{\eta^{ES,d}})\Delta t \tag{3.13c}$$

$$E_{s,0,n} = E_{s,|T|,n} = E^{In} \tag{3.13d}$$

$$E^{\min} \leq E_{s,t,n} \leq E_n^R \tag{3.13e}$$

$$0 \leq P_{s,t,n}^{ES,c} \leq \delta_{s,t,n}^c P_n^R, \quad \delta_{s,t,n}^c \in \{0,1\} \tag{3.13f}$$

$$0 \leq P_{s,t,n}^{ES,d} \leq \delta_{s,t,n}^d P_n^R, \quad \delta_{s,t,n}^d \in \{0,1\} \tag{3.13g}$$

$$\delta_{s,t,n}^c + \delta_{s,t,n}^d = 1. \tag{3.13h}$$

Constraints (3.13a) and (3.13b) determine the power rating and energy capacity of the allocated ESSs, respectively. Decision variables p_n (≥ 0) and e_n (≥ 0) are chosen to be integers because ESS components are usually available in discrete sizes (modules) [13], where P^S and E^S denote the available module steps for ESS power rating and energy capacity, respectively. The maximum rated power and energy of an ESS in charging facility n are limited to $P_n^{R,\max}$ and $E_n^{R,\max}$, respectively. Constraint (3.13c) models the SoC dynamics of an ESS at any time slot, where $\triangle t$ is time segment duration; and $\eta^{ES,c}$, $\eta^{ES,d}$ denote the charging and discharging efficiency, respectively [83]. Constraint (3.13d) represents the daily initial and final SoC requirements, where E^{In} denotes the daily initial SoC of an ESS. The operator can set the value of E^{In} based on the required reserve of power. This constraint links between consecutive days by ensuring that the stored energy at the end of each day is transferred to the next day [83, 84]. Constraint (3.13e) enforces the SoC upper and lower bound limitations, where $E^{\min}$ denotes the minimum SoC of an ESS. Constraints (3.13f) and (3.13g) limit the injecting/extracting power into/from the ESS [85]. Constraint (3.13h) prevents the simultaneous charging and discharging of ESS.

3.4.3 System Upgrade Constraints

The following constraints regulate the substation(s) and feeders capacity upgrades.[3] These constraints should be satisfied for $\forall j \in \mathcal{H}$, $\forall ij \in \mathcal{L}$, $\forall s \in \mathbf{S}$, and $\forall t \in \mathbf{T}$:

$$G_j^R = G^S g_j \tag{3.14a}$$
$$S_{ij}^R = F^S f_{ij} \tag{3.14b}$$
$$0 \leq P_{s,t,j}^G \leq P_j^{G,\max} + G_j^R \tag{3.14c}$$
$$Q_j^{G,\min} \leq Q_{s,t,j}^G \leq Q_j^{G,\max} \tag{3.14d}$$
$$-(S_{ij}^{\max} + S_{ij}^R) \leq P_{s,t,ij} \leq (S_{ij}^{\max} + S_{ij}^R) \tag{3.14e}$$
$$-(S_{ij}^{\max} + S_{ij}^R) \leq Q_{s,t,ij} \leq (S_{ij}^{\max} + S_{ij}^R) \tag{3.14f}$$
$$-\sqrt{2}(S_{ij}^{\max} + S_{ij}^R) \leq P_{s,t,ij} + Q_{s,t,ij} \leq \sqrt{2}(S_{ij}^{\max} + S_{ij}^R) \tag{3.14g}$$
$$-\sqrt{2}(S_{ij}^{\max} + S_{ij}^R) \leq P_{s,t,ij} - Q_{s,t,ij} \leq \sqrt{2}(S_{ij}^{\max} + S_{ij}^R). \tag{3.14h}$$

Constraints (3.14a) and (3.14b) determine the required reinforcements of the substation(s) and feeders capacities. Decision variables $g_j(\geq 0)$ and $f_{ij}(\geq 0)$ are chosen to be integers because substation and feeder upgrade is assumed to be available in discrete steps, where G^S and F^S denote the available steps for substation and feeder upgrade, respectively. Constraints (3.14c) and (3.14d) limit the active and reactive power supplied by the substation(s), where $P_j^{G,\max}$, $Q_j^{G,\max}$, and $Q_j^{G,\min}$ denote the maximum active power, maximum reactive power, and minimum reactive power of existing substation connected to bus j, repectively. Constraints (3.14e)-(3.14h) represent the linearized branch power capacity limitations [88].

[3]This model makes preliminary decisions on the substation(s) and feeder capacity upgrades. More detailed PDN expansion models that include various types of substation transformers and feeder conductors as well as accounting for any revised impedance resulting from upgrades can be found in [86, 87].

3.4.4 PDN Operational Constraints

A second order cone programming (SOCP) relaxation of the *DistFlow* model [89] is adopted in the power flow analysis of the balanced radial PDN. Different from the standard (non-linear) power flow model, SOCP relaxation of the *DistFlow* model offers a convex relaxation of power flow equations [90]. The following constraints should be satisfied for $\forall ij \in \mathcal{L}$, $\forall j \in \mathcal{B}$, $\forall s \in \mathbf{S}$, and $\forall t \in \mathbf{T}$:

$$\begin{aligned} P_{s,t,ij} = &- P^{G}_{s,t,j} - P^{ES,d}_{s,t,n} + P^{ES,c}_{s,t,n} + P^{EV}_{t,n} + P^{D}_{s,t,j} \\ &+ r_{ij} L_{s,t,ij} + \sum_{m:j\to m} P_{s,t,jm}, \quad \text{if } n \to j \end{aligned} \tag{3.15a}$$

$$Q_{s,t,ij} = -Q^{G}_{s,t,j} + Q^{D}_{s,t,j} + x_{ij} L_{s,t,ij} + \sum_{m:j\to m} Q_{s,t,jm} \tag{3.15b}$$

$$V_{s,t,i} - V_{s,t,j} = -(r^2_{ij} + x^2_{ij}) L_{s,t,ij} + 2(r_{ij} P_{s,t,ij} + x_{ij} Q_{s,t,ij}) \tag{3.15c}$$

$$L_{s,t,ij} V_{s,t,i} \geq P^2_{s,t,ij} + Q^2_{s,t,ij} \tag{3.15d}$$

$$(v_{\min})^2 \leq V_{s,t,i} \leq (v_{\max})^2. \tag{3.15e}$$

Constraints (3.15a) and (3.15b) represent real and reactive power balance at PDN branches, where $n \to j$ and $j \to m$ denote a direct line connection either between charging facility n and bus j or between bus j and another bus m, respectively. Branch resistance and reactance are denoted by r_{ij} and x_{ij}. Bus voltage and current flow constraints are introduced in (3.15c) and (3.15d), respectively. Constraint (3.15d) represents a second-order cone constraint that relaxes the quadratic constraint in the original *DistFlow* model [89]. Finally, constraint (3.15e) enforces the upper and lower bounds on bus voltage magnitude.

Based on the preceding discussion, the integration problem is formulated as a mixed integer SOCP problem given by

$$\begin{aligned} \min_{\mathbf{p},\mathbf{e},\mathbf{g},\mathbf{f}} \; & C^{Opr} + C^{Inv} \; (3.11) - (3.12) \\ s.t. \; & \text{ESS operational constraints } (3.13a) - (3.13f) \\ & \text{System upgrade constraints } (3.14a) - (3.14h) \\ & \text{PDN operational constraints } (3.15a) - (3.15e) \end{aligned} \tag{3.16}$$

where the decision variables for ESS power and energy allocation are denoted by vectors $\mathbf{p} \triangleq \{p_n, \; \forall n \in \mathbf{N}\}$ and $\mathbf{e} \triangleq \{e_n, \; \forall n \in \mathbf{N}\}$, respectively; and the decision variables for substation(s) and feeders upgrade are denoted by vectors $\mathbf{g} \triangleq \{g_j, \; \forall j \in \mathcal{H}\}$ and $\mathbf{f} \triangleq \{f_{ij}, \; \forall ij \in \mathcal{L}\}$, respectively.

3.5 Numerical Results

The performance of the proposed capacity planning framework is evaluated in this section. We consider a small network of three charging facilities, and explore the key relationships among network characteristics. Throughout this case study, we use the Nguyen-Dupuis RTN, which is shown in Figure 3.3a, where the network attributes are given in [53]. The time-varying traffic volumes are simulated based on the DTA model using the traffic simulator SUMO. The PDN under study is a 33-bus radial system, as shown in Figure 3.3b, where buses and branches data are given in [91]. The RTN nodes/links geographically overlap with the PDN buses, which means that each RTN node or link is served by one electric bus of PDN. In the integration with PDN model, we considered four typical daily load scenarios (winter, spring, fall, and summer), which follow the hourly load shape of the IEEE-RTS [92]. Moreover, the energy prices follow the hourly Ontario energy price provided by IESO for different seasons [66]. Each RTN node or link is physically connected to a PDN bus. The sizing problem is solved by nonlinear black-box optimizer Knitro version 12. The EVCI integration into the PDN problem is solved by Gurobi Optimizer version 8.1. Both models are implemented in a Python 3.7 environment. The numerical results are obtained on a laptop computer with a 2.3-GHz Intel(R) Core(TM) i5-8300H CPU and 8 GB of memory.

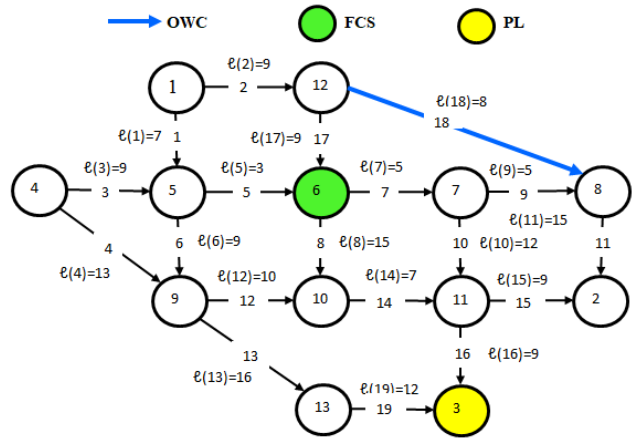

(a) Nguyen-Dupuis RTN [53]

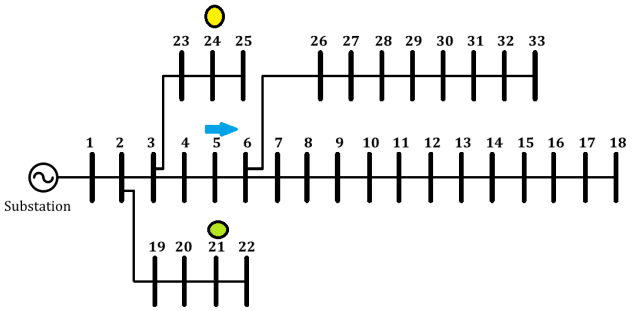

(b) 33-bus radial PDN [91]

Figure 3.3: RTN and PDN systems under study.

We consider EVCI consists of three charging facilities allocated on the Nguyen-Dupuis RTN, which are FCS at node 6, OWC at link 18, and PL at node 3. In this case study, FCS, OWC, and PL are connected to PDN buses 21, 5 and 24, respectively. These charging facilities are serving 1500 PEVs uniformly distributed within origin-destination pairs of the RTN. DC level 2 chargers with 90 kW charging power are assigned in the FCS, and three-phase AC level 3 chargers with 43.5 kW are used in the PL [6]. The charging power of wireless chargers is not standardized yet; however, 22 kW wireless charging panels are assumed for the OWC [10]. An open queuing network with finite capacity and RS-RD blocking is constructed as described in Subsection 3.2.1. The state probabilities of the queuing network nodes are evaluated based on the DA algorithm. The routing probability

between a DN and the associated CN is set at 0.6. The routing probability between any two facilities in the network is calculated based on (3.1).

We firstly examine the performance of the EVCI with stationary arrival rates to explore the relationships among network characteristics. Subsequently, we present the capacity planning of the charging network with more realistic time-varying arrival process and evaluate the time-varying performance metrics. It is shown that the capacity planning framework can achieve targeted performance metrics. Finally, we integrate the EVCI into the PDN, and investigate the relationship between the targeted QoS and the required investment in PDN.

3.5.1 Performance with Stationary Arrivals

This experiment demonstrates the interplay between characteristics of a charging facility on the performance of the other facilities in the network. The blocking probabilities of the three charging facilities are inspected under the alteration of external arrival rate, service rate, number of chargers, and number of waiting positions of the FCS. Number of chargers and waiting positions are set at $\mathbf{c} = \{3, 2, 5\}$ and $\mathbf{B} = \{2, 0, 2\}$ for FCS, OWC, and PL, respectively. The arrival process at OWC and PL are stationary with rate $\lambda_{OWC} = 5$ PEV/h and $\lambda_{PL} = 3$ PEV/h, while the arrival rate at FCS is varied with $\lambda_{FCS} = \{7, 5, 3\}$ PEV/h. As shown in Figure 3.4a, increasing λ_{FCS} leads to a proportional increase in the blocking probabilities of the three facilities, and vice verse. It can be noted also that the variations are higher in the OWC statistics than the PL. This is because the routing probability towards OWC is higher than PL. A similar effect is observed if we alter the service rate, the number of chargers, and the number of waiting positions, as shown in Figures 3.4b, 3.4c, and 3.4d, respectively. This experiment shows that the performance of a charging facility in a network may be highly impacted by the characteristics of the neighboring charging facilities. Consequently, EVCI must be designed as a network to account for the inter-relationships among nearby facilities.

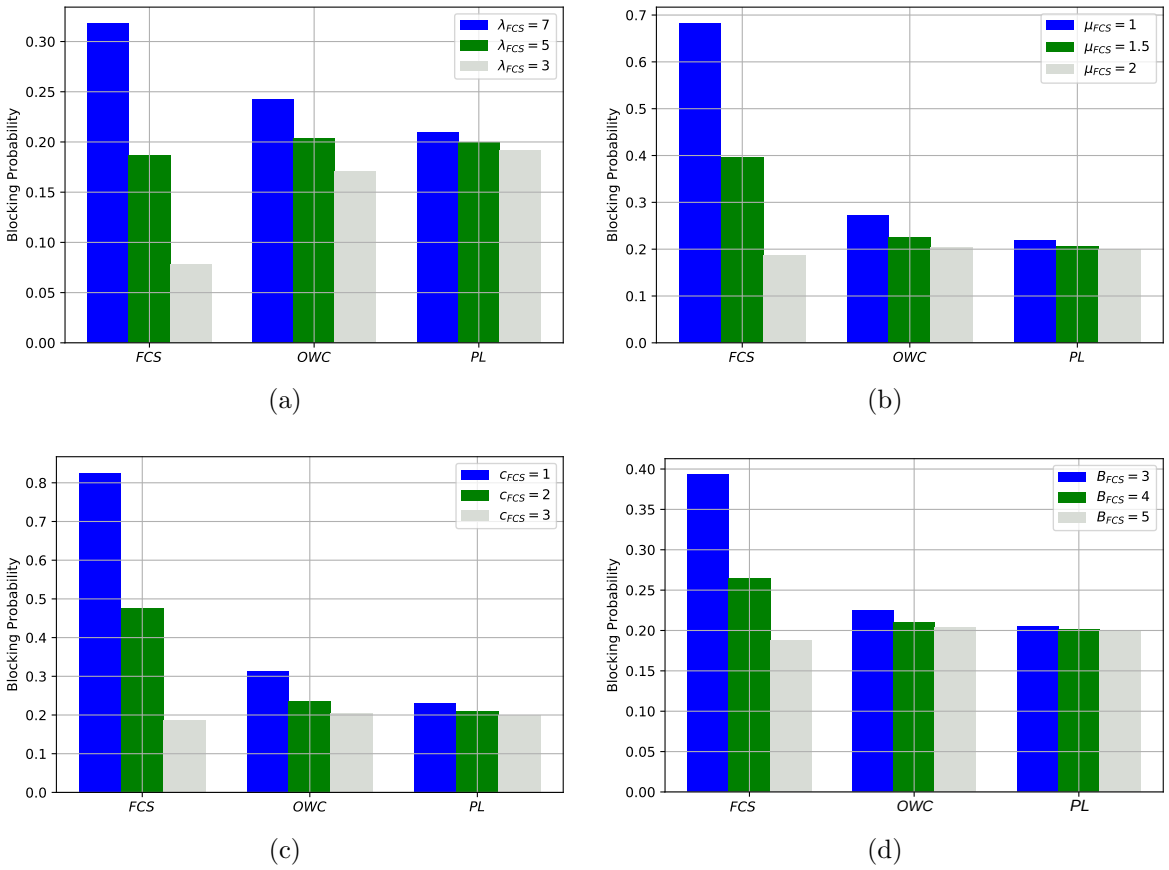

Figure 3.4: Assessment of EVCI blocking probabilities against the variation of FCS characteristics: a) Arrival rate, b) Service rate, c) Number of chargers, d) Number of waiting positions.

3.5.2 Performance with Time-varying Arrivals

We present the capacity planning of the networked EVCI with more realistic time-varying arrival rates. The objective of the experiment is to optimize the charging facility sizes to achieve the predetermined targeted performance metrics for the networked EVCI. These targets are set to be 90% minimum network throughput and 10 minutes maximum expected waiting time.

In order to solve this sizing problem, the MOL arrival rates are firstly estimated based on

Table 3.1: Parameters settings

Parameter	Value	Parameter	Value
ν	0.65 [22]	$\eta^{ES,c}$, $\eta^{ES,d}$	90% [6]
μ^F	2 PEV/h [53]	σ	30%
μ^O	6 PEV/h [53]	β	40%
μ^P	0.3 PEV/h [53]	L	5 years [83]
C^P	175 \$/kW [13]	$\mathcal{I}$	1% [13]
C^E	305 \$/kWh [13]	η^{ES}	95% [93]
C_y^O	15 \$/kWh/year [13]	E^{In}	50% [93]
C^{Sb}	788 \$/kVA [42]	$E^{\min}$	10% [93]
C^F	120 \$/kVA.km [42]	$v_{\min}/v_{\max}$	0.9/1.1 p.u. [59]

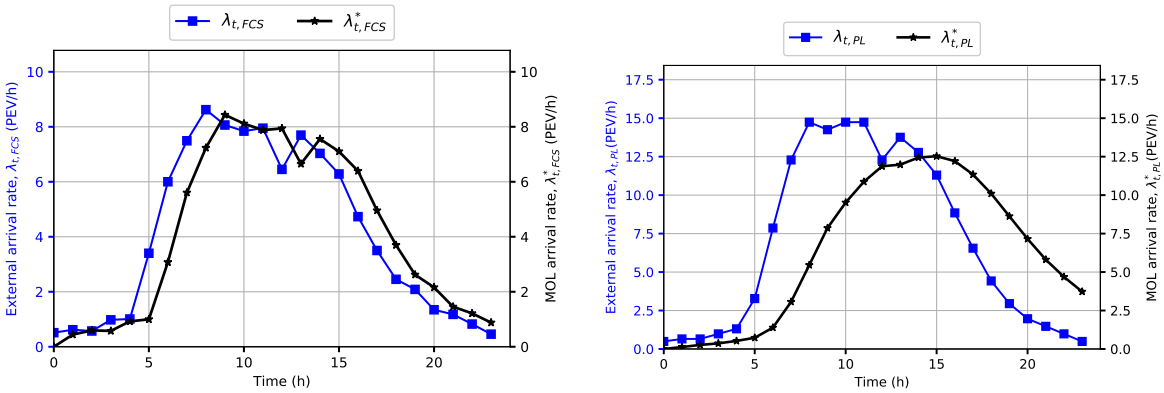

(a) FCS (b) PL

Figure 3.5: External arrival rate versus MOL arrival rate.

(3.4). The time-varying numbers of PEVs intercepted with charging facilities are extracted from traffic simulation. The statistical parameters used in arrival rate estimation are given and summarized in Table 3.1. The listed PEV population parameters are used for illustration purposes. In practice, the system planner should adopt the actual PEV statistical parameters, which can be collected from market surveys.

Figure 3.5 shows the external arrival rate and the MOL arrival rate of both FCS and PL as a function of the time slot index. It can be noted that there are a magnitude difference and a phase shift between λ_t and λ_t^*, which account for time-lag and magnitude difference between the external arrivals and the system loads. This difference is significantly increased

as the service time of the facility increases, as shown in Figure 3.5b. The MOL arrival rate functions are used to analyze the non-stationary queuing models.

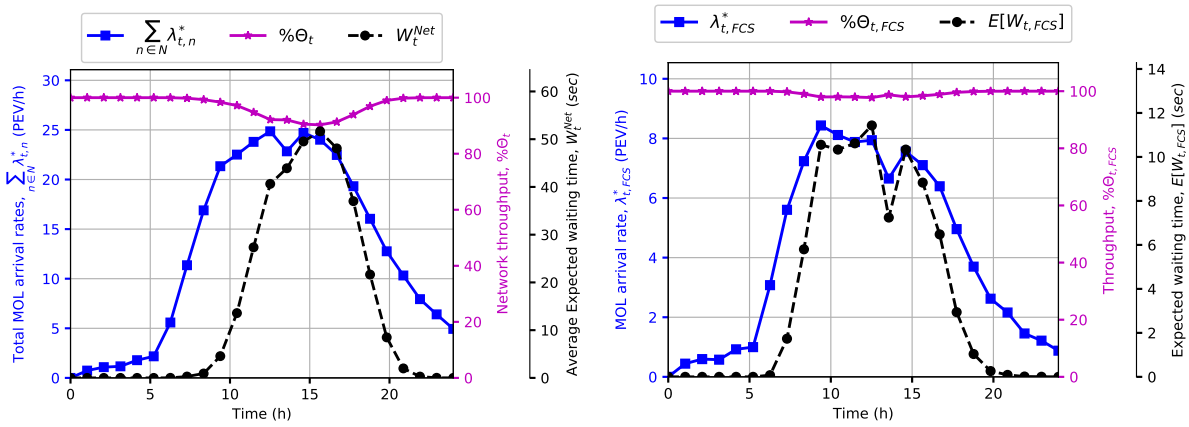

(a) EVCI network (b) FCS

Figure 3.6: Time-varying performance of the EVCI.

The sizing problem, in (3.9), minimizes the total numbers of chargers and waiting positions allocated in charging facilities to achieve the targeted network throughput and average waiting time. Both chargers and waiting positions are assumed to have a similar cost $\omega_n = 0.5, \forall n \in \mathbf{N}$. The objective function has a minimal value at $\mathbf{c} = \{7, 4, 22\}$ and $\mathbf{B} = \{1, 0, 2\}$. Figure 3.6a shows the time-varying performance metrics of the networked EVCI. It is observed that $\underline{\Theta} = 90.13\%$ and $\overline{W^{Net}} = 51.6$ seconds, which achieve the predetermined QoS targets. A similar trend can be observed in the performance of the individual charging facilities, as shown in Figure 3.6b.

The computational time of the sizing problem is highly dependent on the number of charging facilities in the network. For instance, the solution time for the EVCI under investigation is 19 hours. However, the solution time for a network of two charging facilities is around 1 hour.

3.5.3 Integration into PDN

In integrating the EVCI network with the PDN, we aim to investigate the relationship between the targeted QoS level and the required investment in the PDN. The proposed integration model minimizes the total investment and operation cost by allocating ESS in charging facilities and/or upgrading the PDN substation and feeders. The substation capacity is 5 MVA, and the system peak load demand is 3.715 MW (without EVCI loads). The ESSs are available in discrete power and energy capacities with step size of 100 kW and 100 kWh, respectively. The reinforcement of the substation and feeders are available with step size of 500 kVA and 250kVA, respectively. Other financial and technical parameters are summarized in Table 3.1.

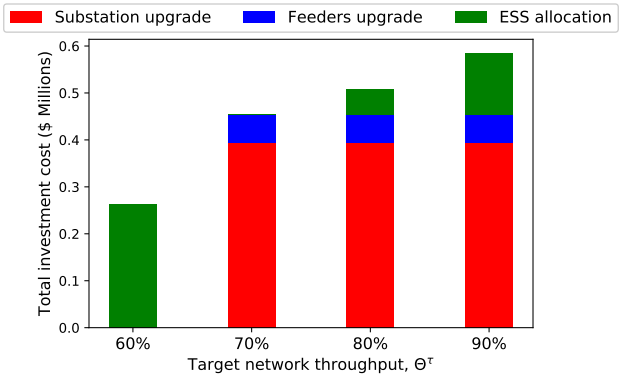

Figure 3.7: QoS targets versus the required PDN investment.

Table 3.2: Detailed integration plans for the EVCI network with the PDN

QoS target		60%	70%	80%	90%
Total capital cost		$\$3.76\times10^6$	$\$4.17\times10^6$	$\$4.24\times10^6$	$\$4.32\times10^6$
Substation	Upgrade	0	0.5 MVA	0.5 MVA	0.5 MVA
	Cost	0	\$394,000	\$394,000	\$394,000
Feeders	Upgrade	0	(0,1): 0.5 MVA	(0,1): 0.5 MVA	(0,1): 0.5 MVA
	Cost	0	\$60,000	\$60,000	\$60,000
ESS	Allocated	(0.1 MW, 0.3 MWh) (0.1 MW, 0.3 MWh)	0	(0.1 MW, 0.1 MWh)	(0.1 MW, 0.3 MWh)
	Cost	\$262,118	0	\$55,353	\$131,059
Energy cost		$\$3.53\times10^6$	$\$3.72\times10^6$	$\$3.74\times10^6$	$\$3.75\times10^6$
Arbitrage profit		\$45,425	0	\$14,174	\$25,357

We analyze the effect of varying network throughput target on the investment cost of the EVCI network integration into the PDN. Figure 3.7 illustrates the total investment cost for each QoS target, and the detailed integration plans are shown in Table 3.2. When the targeted network throughput is set to 60%, ESSs are allocated in the EVCI. On the other hand, when the QoS target is set to 70%, upgrading the PDN substation and feeders is a more cost-efficient solution. In the case of $\Theta^{\tau} = 60\%$, it can be noted that the allocated ESS is higher than the other cases. This is because ESS capacities, as well as feeders and substation reinforcement, are assumed available in discrete steps. Then, the proposed model chooses the lowest cost combination of the allocated ESS and PDN reinforcement to minimize the total capital cost. Hence, in the case of a 60% throughput target, it is cheaper to allocate ESSs than upgrade the feeders and substation. The solution time for the integration into PDN problem under investigation is 8 minutes. Consequently, the required investment in the PDN is highly dependent on the capability of the existing PDN components and the targeted QoS of the EVCI. Also, allocating ESSs in charging facilities can be a cost-effective solution to alleviate the required PDN upgrades if ESS cost is less than the reinforcement cost.

3.5.4 Sensitivity Analysis

Impact of time segment duration

Time segment duration (i.e., $\triangle t$) effect is investigated with $\triangle t = 15$ min and compared with the results with $\triangle t = 1$ hour. As shown in Figure 3.8a, using the shorter time interval scales down the MOL arrival rate at charging facilities. However, the observed EVCI performance is similar for both cases, as shown in Figure 3.8b. This is because the proposed approach utilizes the nonstationary queuing models, which account for PEVs that are already in the system (either charging or waiting) from the preceding time periods.

Impact of the routing probability value between a DN and the associated CN

A slight shift in the performance occurs at the overloaded charging facility with an increase of the routing probability value between a DN and the associated CN (i.e., α_{nn}), as shown

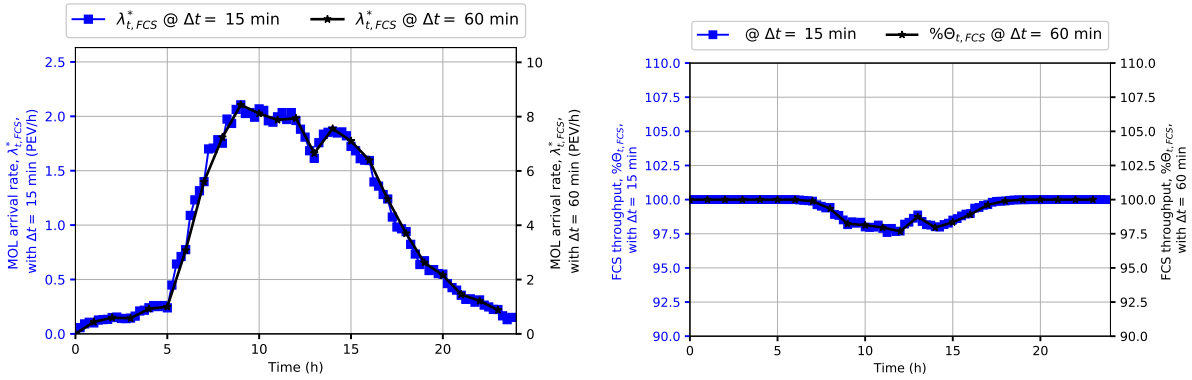

(a) MOL arrival rate

(b) FCS throughput

Figure 3.8: EVCI performance with different time intervals.

in Figure 3.9. This is because, in the networked EVCI model, only a small percentage of the blocked PEVs are choosing the same charging facility instead of routing to another facility. In practice, a PEV user will choose another facility after being blocked at one facility. Since this shift in the performance is observed only at the overloaded charging facilities, it may not affect the capacity planning problem with acceptable QoS targets.

Impact of the variations of the mean charging time

We have examined the EVCI performance with different PEV charging power capability. For instance, if most of the PEVs in the system can only charge with 50 kW DC fast chargers at FCS and 7.4 kW AC level 2 chargers at PL, the PEV charging time at these facilities increases. In this case, for the commonly available PEVs with 60-70 kWh battery capacity, the service time is 1 hour ($\mu^F = 1$) in FCS and 5 hours ($\mu^P = 0.2$) in PL [2]. As shown in Figure 3.10, the EVCI throughput decreases with the increasing of the mean service time, as charging facilities will be occupied for a longer time. Thereby, the capacity planning of EVCI must account for the charging characteristic of PEVs in the system to achieve the targeted performance.

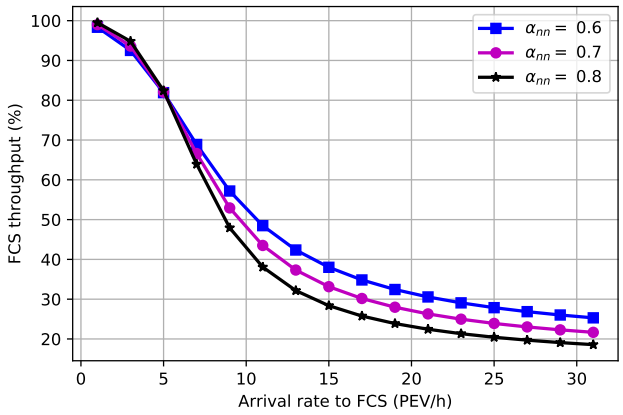

Figure 3.9: FCS throughput versus arrival rate with various routing probabilities.

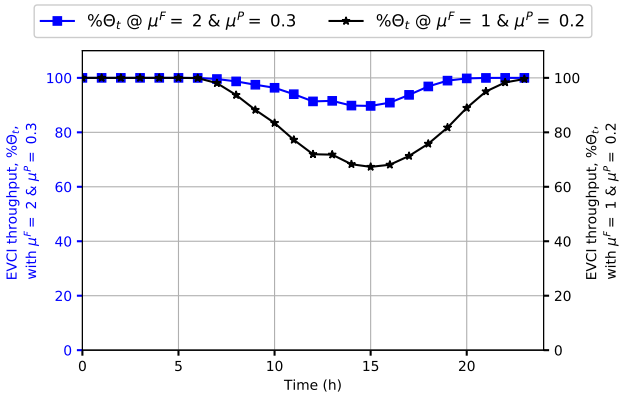

Figure 3.10: Influence of mean charging time on EVCI throughput.

3.6 Summary

In this chapter, we study capacity planning of EVCI and propose a framework that sizes charging facilities to fulfill the given QoS targets. The proposed framework minimizes the cost of EVCI integration into PDN by either allocating ESSs in charging facilities and/or reinforcing the PDN. The link between the targeted QoS level and the PDN capability offers insights into how to make a trade-off between the PEV user satisfaction and the required investment in PDN. Our framework captures the correlation among the occupancy

of neighboring charging facilities, which ensures that the targeted QoS level is achieved for the entire networked EVCI. Furthermore, the proposed framework accounts for the temporal variability of PEV charging demand by addressing the time-lag and magnitude shift between arrivals and loads of the system. The numerical results demonstrates that the inter-relationship between the targeted QoS level and the required investment in the PDN plays a vital role in capacity planning of EVCI. Chapter 4 shows how to leverage dynamic pricing mechanisms in coordinating the PEVs charging process and influencing the behaviors of PEV users.

Chapter 4

Dynamic Pricing for Differentiated PEV Charging Services Using Deep Reinforcement Learning

In this chapter, we propose a differentiated pricing mechanism for a multiservice PEV charging infrastructure. The proposed framework motivates PEV users to avoid over-utilization of particular service classes. Currently, most of dynamic pricing schemes require full knowledge of the customer-side information. Since such information is stochastic, non-stationary, and expensive to collect at scale, the obtained pricing mechanism can lead to suboptimal solutions. Our proposed pricing mechanism utilizes model-free deep reinforcement learning to learn and improve automatically without an explicit model of the environment. We formulate our framework to adopt the twin delayed deep deterministic policy gradient algorithm. Simulation results for the EVCI environment demonstrate effectiveness of the proposed framework.

4.1 Related work

This section provides an overview of the research areas relevant to this study, which is divided into two parts. The first part discusses dynamic pricing mechanisms for PEV charging demand coordination, while the second part presents a survey of adopting RL algorithms in optimizing the dynamic pricing policies.

4.1.1 Dynamic Pricing for PEV Charging Demand Coordination

Dynamic pricing is a decentralized coordination and load management method for the PEV charging demand. In literature, significant efforts have been devoted to the coordination of PEV charging demand through dynamic pricing. Deriving the dynamic pricing signals for PEV charging coordination follows three main categories, namely, game theoretic approaches, stochastic optimization methods, and queuing network based models.

Game theory based dynamic pricing is widely employed to map the relation among multiple entities, where each entity maximizes its own profit [17, 94–96]. For instance, the relation between charging station operator and PEV users can be modeled as a single-leader-multi-follower Stackelberg game [17]. The station operator is modeled as a leader whose main interest is to optimize the service price to maximize its profit with the same amount of energy resources. The PEV users are modeled as followers who maximize their own level of satisfaction by selecting a nearby charging station with low charging cost. Game theory is then used to derive a dynamic pricing scheme that balances the PEV load demand among the adjacent charging stations. In order to account for the randomness of PEV charging demand, a repeated inverse Stackelberg game along with a Markov decision process is proposed in [94]. In this model, the randomness of PEV arrivals, departures and charging demands is integrated into a stochastic game. Real-time prices that minimize the losses on the power distribution system are determined based on the Nash equilibrium solution and power flow analysis. The energy trading between the smart grid and a number of PEV groups can also be modeled as a noncooperative Stackelberg game [95]. The smart grid is to maximize its revenue, while PEV groups are to balance the tradeoff between battery charging and associated cost. The relation among the competitive charging stations

and the PEV users can be modeled as a multi-leader-multi-follower Stackelberg game [96]. In the framework, each charging station optimizes its price with an objective of maximizing its profit based on the expected PEV charging demand and the prices of other stations. Furthermore, PEV users select the charging stations that maximize their satisfaction considering the charging price, waiting time, and traveling distance.

Optimization models can be used to determine the dynamic pricing of the PEV charging service [97, 98]. For instance, stochastic dynamic programming can be used to determine charging prices [97]. This model considers multiple uncertainties, such as in PEV charging demand, the intermittency of renewable energy sources, and the electricity price fluctuation. The optimal incentives offered by the local distribution company (LDC) to the PEV users in order to participate in the smart charging program are investigated in [98]. The study aims to address the relationships among the incentives offered by LDC, the share of PEV fleet participation in smart charging, and the expected investment deferral in the distribution system.

Queuing models can be used to estimate the PEV charging demand and then derive a dynamic pricing expression to coordinate the PEV charging service [7, 99, 100]. For instance, the impact of wireless charging load demand and PEV mobility on the location marginal price (LMP) of electricity is investigated in [7]. The BCMP queuing network model is used to estimate the charging demand of PEVs, considering the PEVs mobility. Then, a dynamic pricing scheme is optimized to adjust the retails price of wireless charging.

Based on the preceding discussion, the existing works study various aspects of the dynamic pricing of charging services. The existing pricing schemes treated all types of charging facilities equally. In practice, however, a PEV charging infrastructure includes various types of facilities such as on-road wireless chargers, fast charging stations, and slow chargers at parking lots. Each charging service has a distinct QoS level that matches the user expectations. The charging service demand is interdependent, which means the demand for one service is often affected by the prices of others. In order to provide differential QoS, a differential pricing is needed to discourage the over-utilization of a certain type of charging service. Thus, a differential pricing mechanism should be developed to set the price for each charging service, which offers the necessary incentives for PEV users to choose the charging service that matches their requirements. Consequently, the

QoS levels of charging faculties are maintained.

4.1.2 Reinforcement Learning for Dynamic Pricing

Despite the previous efforts, there exist several challenges facing the implementation of dynamic pricing mechanisms. One challenge is the lack of complete customer-side information. CSP needs to have full knowledge of future PEV charging demand in addition to impacts of pricing signals on customers' behaviors. Usually, such information is stochastic and difficult to estimate. Another challenge is caused by the temporal variability of system variables. Typically, PEV charging demand is a dynamically changing environment that is influenced by the non-stationary user behaviors. To overcome the limitations, RL can be leveraged to adaptively decide a pricing policy for PEV charging demand coordination. RL is an area of machine learning, which deals with goal-directed learning based on the interaction between an active decision-making agent and its unknown environment, while the agent seeks to maximize a numerical reward signal [101]. Using deep RL algorithms, neural networks are trained off-line in a simulated environment. Then, the neural networks can be exploited on-line in the practical system.

Recently, there has been a collection of research works studying how to optimize dynamic pricing policies using reinforcement learning. For example, dynamic pricing of interdependent perishable products can be optimized using Q-learning [102]. Given an initial inventory for the products, this approach is to maximize the revenue by dynamically adjusting the pricing policy over a finite sale horizon when the demand function is stochastic and unknown. Also, RL algorithms can be used in the context of demand response [103–105]. For instant, Q-learning can help to reduce supply-demand mismatches by dynamically deciding the retail electricity price, considering both the service provider profit and customers' cost [103]. In [104], deep Q-learning and deep policy gradient are used for on-line optimization of building energy consumption, where the objective is either to minimize the energy cost or to flatten the net energy profile.

In this work, inspired by the recent research outcomes, we present a dynamic pricing algorithm for differentiated PEV charging services using deep RL.

4.2 System Model

In this section, we present modifications to the system model presented in Chapter 2 and Chapter 3 to account for the presence of a price-based coordination mechanism for PEV charging demand.

Consider an EVCI with M classes of charging services managed by a CSP. Let set $\mathbf{M} = \{1, 2, \ldots, M\}$ denote the available service class in the system, where $i < j$ indicates i is a higher service class than j with more strict QoS requirements. Each service class is specified by a minimum QoS level that is to be maintained all the time. Each service class is offered by a number of charging facilities, where $n \rightarrow m$ indicates that charging facility n provides charging service of class m. Charging facility n ($n \in \mathbf{N}$) with service class m ($m \in \mathbf{M}$) provides a charging service with minimum QoS $q_m \in [0, 1]$ and associated with normalized charging price $p_{n,t} \in [0, 1]$ for all $t \in \mathbf{T}$. The CSP announces one-time (stationary) minimum QoS level of each service class at the beginning of the planning horizon, $\mathbf{q} = (q_1, \ldots, q_M)$. To maintain these QoS classes, the CSP adjusts the pricing policy of charging services periodically at the beginning of each time slot. Thereby, at time slot t, the CSP adopts a pricing policy represented in the price vector $\mathbf{p}_t = (p_{1,t}, \ldots, p_{N,t})$.

PEV users compare prices, QoS, and other service attributes (e.g., location of the charging facility, type of charging technology) of all services and choose a charging service at one charging facility offering the particular service class. The offered charging services are substitutable because the demand for one service class not only depends on its own price but also depends on the prices of other services in the EVCI. Also, the charging service classes are vertically differentiated, which means that customers always prefer a higher service class if the charging prices are the same among different classes [106]. Thereby, any change in the price of one service can impact the demand for other services in the system.

4.2.1 PEV Charging Demand Model

PEV demand for charging services is assumed sensitive to both the charging service price and the QoS guarantees. This assumption is only used in the simulated environment for RL agent training. However, the proposed RL approach is adaptive and able to learn the

actual PEV user behaviors based on the interactions with the environment. To represent the PEV charging demand at each charging facility, we use the linear demand model [107]. Based on this model, the time-varying charging demand (arrival rate), $\lambda_{n,t}$, at charging facility n in time slot t is a linear function of all prices and service levels of charging facilities, given by

$$\lambda_{n,t}(\mathbf{p},\mathbf{q}) = \Lambda_{n,t} - \beta_n p_{n,t} + \sum_{\hat{n}\neq n} \beta_{n,\hat{n}} p_{\hat{n},t} + \gamma_m q_{m,t} - \sum_{\hat{m}\neq m} \gamma_{m,\hat{m}} q_{\hat{m},t}, \quad n \to m,\ \forall n,\hat{n} \in \mathbf{N},\ \forall m,\hat{m} \in \mathbf{M} \tag{4.1}$$

where $\Lambda_{n,t}$ (> 0) denotes PEV arrival rate to charging facilities facility n at time slot t at the base price, which is accepted by all users. This arrival rate can be estimated based on the traffic volume intercepted at the charging facility [53]; β_n and γ_m are positive parameters denoting self-elasticity, which indicate the relative change in the demand for a charging service that would result from a change in the service price and quality, respectively; $\beta_{n,\hat{n}}$ and $\gamma_{m,\hat{m}}$ are positive parameters representing cross-elasticity, which reflect the change in the service demand as a result of the change in the prices and service levels of other charging facilities, respectively. The demand for charging service at facility n should be more sensitive to its own price changes than those for the other services. Thus, the elasticity parameters have the relation $\beta_n > \sum_{\hat{n}\neq n} \beta_{n,\hat{n}}$. The demand function is assumed to satisfy the monotonicity properties [108], as follows

$$\frac{\partial \lambda_{n,t}(\mathbf{p},\mathbf{q})}{\partial p_{n,t}} \leq 0,\ \frac{\partial \lambda_{n,t}(\mathbf{p},\mathbf{q})}{\partial p_{\hat{n},t}} \geq 0, \frac{\partial \lambda_{n,t}(\mathbf{p},\mathbf{q})}{\partial q_{m,t}} \geq 0, \frac{\partial \lambda_{n,t}(\mathbf{p},\mathbf{q})}{\partial q_{\hat{m},t}} \leq 0, \quad \forall n,\hat{n} \in \mathbf{N}. \tag{4.2}$$

The assumption means that, if the CSP increases $p_{n,t}$ (or decreases q_m), the demand for charging service at facility n decreases; however, if the CSP increases $p_{\hat{n},t}$ (or decreases $q_{\hat{m},t}$), the the demand at charging facility n increases. Note that PEV users' demand at facility n for service class m is assumed depending on the announced QoS level of service class q_m rather than its actual service level in the facility.

4.2.2 Charging Station Model

The capacity of any charging facility in the EVCI is finite. Thereby, charging facilities can be modeled as a finite queuing system [81], where arriving PEV users are rejected (blocked) at times when the charging facility is full. Also, PEV users may wait until service becomes available if all chargers are busy and there is waiting space available. PEVs arrivals to a charging facility follow a non-homogeneous Poisson arrival process, which is a non-stationary counting process with a deterministic arrival rate $\lambda_{n,t}$. As discussed in Subsection 4.2.1, this arrival rate depends on various factors such as traffic volume and users' response to changes in $\mathbf{p}$ and $\mathbf{q}$. The charging time of PEVs at a charging facility is assumed independently and exponentially distributed, with service rate μ that depends on the chargers' power capability at the charging facility [53]. Each charging facility has c_n independent and identical chargers (servers) that serve PEV users according to the first-come-first-served rule. The maximum number of PEVs that can be admitted to charging facility n is denoted by K_n.

Let $\mathcal{X}_{t,n}$ denotes the number of admitted PEVs to charging facility n ($n \in \mathbf{N}$) at time t, where $\mathcal{X}_{t,n}$ is a random variable that reflects the utilization of charging facility n. The number of admitted PEVs can be expressed as

$$0 \leq \mathcal{X}_{t,n} \leq K_n. \tag{4.3}$$

Due to the finite capacity of charging facilities, high congestion (overload) may occur at a facility if the number of admitted PEVs approaches the maximum facility capacity. Then, the newly arrived PEVs may suffer from a low QoS level in terms of long waiting time or service rejection (blocking). Thereby, we define QoS metric $\mathcal{Q}_{n,t} \in [0, 1]$ to measure the service performance at charging facility n at time t, which is related to the weighted sum of the blocking and delay rates. We define the QoS metric as

$$\mathcal{Q}_{t,n} = 1 - \alpha \mathbb{P}_{K_{t,n}} - \beta \mathbb{P}\{W_{t,n} > 0\} \tag{4.4}$$

where α and β are weighting factors to reflect the impact of service blocking and service delay respectively on the satisfaction level of PEV users, with $\alpha + \beta = 1$; $\mathbb{P}_{K_{t,n}}$ and

$\mathbb{P}\{W_{t,n} > 0\}$ denote the blocking and delay probabilities of the charging facility, respectively. Both $\mathcal{X}_{t,n}$ and $\mathcal{Q}_{n,t}$ represent the state of the charging facility in terms of the facility utilization and service quality.

4.3 Dynamic Pricing for Differentiated PEV Charging Services

Price-based coordination mechanisms can be leveraged to dynamically meet the QoS requirements of charging facilities, while maximizing social welfare which is the sum of utilities over all users and service providers. In a multiservice charging infrastructure, a differentiated pricing scheme is required to provide different QoS classes. Thus, a PEV user has incentives to use a charging service that matches their needs. The differentiated pricing scheme can enhance the performance of charging facilities in meeting the expectation of PEV users by discouraging the over-utilization of some charging services.

Our objective in this research is to develop a differentiated dynamic pricing scheme that accounts for the interactions between two players, which are the CSP and the non-cooperative PEV users. On one hand, PEV users want to choose the charging service that maximizes their utilities, when making the charging decisions. The utilities depend on various random variables, including the current SoC of PEV battery, the charging price, and the user's value of time, which indicates how much a user appreciates time-saving during the charging process. On the other hand, the CSP wants to dynamically adjust the service prices for all charging facilities based on the current and anticipated demand patterns. The pricing policy should maximize revenue while achieving the targeted QoS. Thereby, differentiated pricing should dynamically provide incentives for PEV users to behave in ways that improve the overall utilization and performance of the charging infrastructure.

Choosing the *right* price for a PEV charging service is challenging. Determining a pricing policy requires information not only about how much the current PEV user values each charging service but also about what the future demand will be. In order to develop the differentiated pricing scheme, some assumptions are necessary: 1) The PEV charging infrastructure includes a limited set of service classes, and each service is offered by a

set of charging facilities as discussed in our system model; 2) There is no competition between charging facilities with different QoS classes; 3) PEV charging demand is elastic and price-responsive; 4) PEV users are informed about the real-time charging service prices at all charging facilities in the system, which can be facilitated by web applications offered to PEV users; 5) The targeted minimum QoS level of each class of charging services is predetermined based on user preferences, which can be collected from market surveys.

The differentiated pricing policy can be represented as a social welfare maximization problem, where the objective is to maximize the demand for charging services in all charging facilities, while maintaining the minimum targeted QoS in all service classes. The differentiated pricing problem can be formulated as

$$\max_{\mathbf{p}} \sum_{t=1}^{T} \sum_{n=1}^{N} \lambda_{n,t}(\mathbf{p}, \mathbf{q}) \tag{4.5a}$$

$$s.t.\ \mathcal{Q}_{t,n} \ \leq \ q_m, \quad n \rightarrow m, \forall n \in \mathbf{N},\ \forall m \in \mathbf{M},\ \forall t \in \mathbf{T}. \tag{4.5b}$$

Optimizing this pricing policy must explicitly incorporate the stochasticity and nonstationarity of the PEV charging demand. Also, the pricing policy must be forward-looking by setting the price signals in anticipation of future demand patterns. Thereby, the generated charging price in a time slot is based on the previously observed charging demand and the expected future charging requests. However, due to the lack of complete information and the variability of system variables, conventional abstract models cannot guarantee optimality of the pricing policy. Thereby, we propose a reinforcement learning approach to determine this pricing mechanism. Based on the proposed approach, the CSP can adjust the pricing signals in real-time, considering the anticipated future charging demand and potential service congestion.

4.4 RL Approach for Differentiated Pricing

Determining a differentiated pricing policy is a real-time decision-making problem in an unknown environment. Here, we present an RL approach to decide the pricing policy based on learning while interacting with the environment. Towards this goal, the differentiated pricing problem is firstly formulated as a discrete finite-horizon Markov decision process (MDP) [101]. Then, the twin delayed deep deterministic policy gradient (TD3) algorithm is used to train neural networks that generate the pricing policy, without requiring the full knowledge of system dynamics and uncertainties. Finally, we present the implementation details of the TD3 algorithm along with the associated hyperparameter, neural network architectures, and the reward function design.

4.4.1 Markov Decision Process

As shown in Figure 4.1, MDP for the differentiated pricing problem is a formalization of the interaction between an agent and the environment [101]. The agent is the learner and decision-maker that selects actions. The environment responds to the agent's actions, presents new situations to the agent, and gives a numerical value to the agent as a reward to evaluate the agent's actions. The MDP is defined by the following key components:

- A set of states, $\mathcal{S}$, that reflects the current state of the EVCI. At each discrete time step t, system state $s_t \in \mathcal{S}$ is denoted as $s_t = (t, \mathcal{X}_{t,1}, \mathcal{Q}_{t,1}, \ldots, \mathcal{X}_{t,N}, \mathcal{Q}_{t,N})$. As discussed in Subsection 4.2.2, the system state represents the utilization and QoS of all charging facilities in the EVCI;

- A set of actions, $\mathcal{A}$, that is selected by the agent based on the current system state and the anticipated future PEV charging demand. The selected actions affect the charging demand on the next time slot. At discrete time t, the agent selects an action, $a_t \in \mathcal{A}$, based on its policy $\pi : \mathcal{S} \mapsto \mathcal{A}$. This action is a vector of length equal to N with elements normalized to the range $[-1, 1]$. The CSP maps this action into pricing vector $\mathbf{p}_{t+1}$ that sets the charging price (money value) for all facilities at time slot $t + 1$;

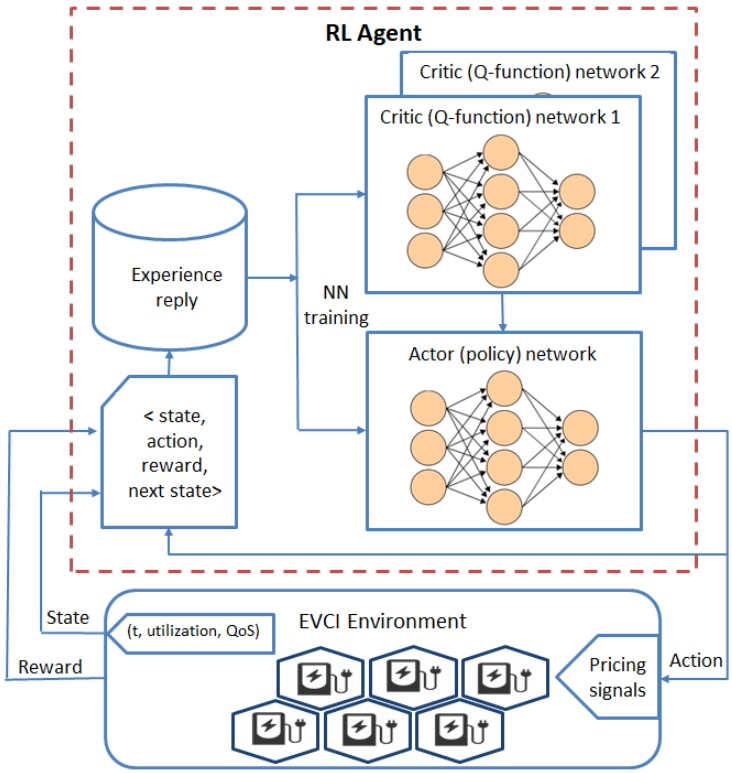

Figure 4.1: MDP framework for differentiated pricing.

- State-transition probabilities $p : \mathcal{S} \times \mathcal{S} \times \mathcal{A} \mapsto [0, 1]$, where $p(s_{t+1}|s_t, a_t)$ indicates the likelihood that action a_t results in the transition from state s_t to next state s_{t+1};
- Reward function $r : \mathcal{S} \times \mathcal{A} \mapsto \mathbb{R}$, where $r(s_t, a_t)$ computes an immediate reward signal for executing action a_t when the system is at state s_t. The agent's goal is to maximize not only the immediate reward but also the cumulative discounted future rewards $R_t = \sum_{i=t}^{T} \gamma^{i-t} r(s_i, a_i)$, where $\gamma \in [0, 1)$ is a discount factor indicating the priority of short-term rewards.

One episode of the MDP forms a finite sequence or a trajectory in the form

$$(s_1, a_1, r_1, \ldots, s_{T-1}, a_{T-1}, r_{T-1}, s_T).$$

Determining optimal policy π^* can be done using the action-value function $Q^\pi \in \mathbb{R}^{|\mathcal{S}|\times|\mathcal{A}|}$, which is defined as the discounted expected total reward when taking action a_t at state s_t and thereafter following policy π [101]. The Q-function can be formulated as

$$Q^\pi(s,a) = \mathbb{E}^\pi\left[\sum_{t=0}^{\infty} \gamma^t r(s_t,a_t)|s_0 = s, a_0 = a\right]. \tag{4.6}$$

The optimal Q-function for each state-action pair is $Q^*(s,a) = \max_\pi Q^\pi(s,a)$, and the optimal policy that returns the highest valued action can be obtained by [109]

$$\pi^*(s) = \arg\max_{a\in\mathcal{A}} Q^*(s,a). \tag{4.7}$$

4.4.2 Adopting TD3 Algorithm for Differentiated Pricing

Optimizing a policy based on the MDP can be done using either policy iteration or value iteration if system transition dynamics (probabilities) are known [105]. However, system dynamics are unknown and need to be estimated through interactions with the environment. RL can adopt the model-free approach, in which the RL agent learns to optimize an action for each state without requiring a complete and perfect model of the environment. One of the most common model-free algorithms in RL is Q-learning, which uses a table to store and update Q values while exploring the environment. However, Q-learning is only applicable when the action space is finite and discrete [110]. In the context of differentiated pricing for charging services, both the state and action spaces are continuous, and discretization of the states and actions introduces a dimensionality problem [105]. Instead, here we resort to the TD3 algorithm [111], which is a model-free off-policy actor-critic algorithm. The TD3 algorithm builds on the deterministic policy gradient (DPG) algorithm, along with deep neural network function approximators. It can learn policies in a high-dimensional continuous action space.

Actor-critic methods directly optimize policy $\pi(s)$ in addition to learning Q-function $Q^\pi(s,a)$. Policy optimization, known as the actor, directly maps the states to actions. The Q-function, known as the critic, assigns a value that evaluates the policy's action given

the system state and the selected action. Different from Q-learning, Q-table is replaced by deep neural networks (NN) that act as a function estimator, which achieves better generalization for continuous state and action spaces via deriving unknown correlations from previous experience.

As shown in Figure 2, the TD3 architecture consists of two critic (Q-value) networks and one actor (policy) network. Each NN is characterized by a set of parameters that consist of the NN weights and biases. The parameters of the critic networks are denoted by ϕ_1 and ϕ_2, and the parameters of the actor network are denoted by vector θ. Since learning of NN can be unstable, target networks are needed to slowly keep track of the updates in the (online) critic and actor networks. Thereby, TD3 uses two target critic networks with parameters $\grave{\phi}_1$ and $\grave{\phi}_2$, and a target actor network with parameters $\grave{\theta}$. During learning, a set of transitions need to be collected and stored in experience replay buffer $\mathcal{R}$. Each transition has the form of 4-tuple $(s, a, r, \grave{s})$, which denote state, action, reward, and next state, respectively. Then, a mini-batch is uniformly sampled at each step to train the actor and critic networks. Training NN using mini-batches ensures that the selected samples are independently and identically distributed, which in turn facilities an efficient optimization of NN parameters.

The TD3 concurrently updates two critic networks, Q_{ϕ_1} and Q_{ϕ_2}, using the recursive Bellman equation

$$Q^{\pi}(s_t, a_t) = r(s_t, a_t) + \gamma Q^{\pi}(s_{t+1}, \pi(s_{t+1})). \tag{4.8}$$

To approximate the optimal Q-function, the mean-squared Bellman error function is utilized to indicate how closely Q_{ϕ_1} and Q_{ϕ_2} satisfy the Bellman equation, as follow

$$L(\phi_i, \mathcal{R}) = \mathbb{E}_{(s,a,r,\grave{s})\backsim\mathcal{R}}\Big[\big(Q_{\phi_i}(s, a) - y(r, \grave{s})\big)^2\Big], \; i = 1, 2 \tag{4.9a}$$

$$y(r, \grave{s}) = r(s, a) + \gamma \min_{i=1,2} Q_{\grave{\phi}_i}(\grave{s}, \pi_{\grave{\theta}}(\grave{s}) + \epsilon). \tag{4.9b}$$

Note that, in (4.9b), the TD3 uses the smallest of the two Q-values to form the targets in the Bellman error loss functions. This practice helps in reducing the overestimation bias problem of Q-values [111]. Also, the target policy is smoothed by adding a small Gaussian noise component, ϵ, to the target action, which prevents over-fitting on the narrow peaks

of Q-values. Optimizing the policy can be done by training the actor network to give the action that maximizes the expected Q-function as

$$\max_{\theta} = \mathbb{E}_{s \backsim \mathcal{R}} \Big[Q_{\phi_1}(s, \pi_\theta(s)) \Big]. \tag{4.10}$$

The parameters of the actor network are updated through the gradient ascent of the expected return $\nabla_\theta J(\theta)$ with respect to actor parameters only, as given by [112]

$$\nabla_\theta J(\theta) = \mathbb{E}_{s \backsim \mathcal{R}} \Big[\nabla_a Q_{\phi_1}(s, a)|_{a=\pi(s)} \nabla_\theta \pi_\theta(s) \Big]. \tag{4.11}$$

To improve training stability and reduce the accumulation of errors resulting from temporal difference learning, the actor network is updated once every two updates of the critic networks [111]. The stability of NN learning is also improved by adopting soft target update [110], in which the parameters of the target networks is slowly updated to track the changes in the online actor and critic networks by some portion τ, as follows

$$\grave{\phi}_i \leftarrow \tau \phi_i + (1 - \tau)\grave{\phi}_i, \quad i = 1, 2 \tag{4.12a}$$

$$\grave{\theta} \leftarrow \tau \theta + (1 - \tau)\grave{\theta}. \tag{4.12b}$$

To remove the dependence on the randomly initialized parameters of NN, actions are sampled uniformly from the action space (pure exploratory policy) for limited time steps at the beginning of the training process. Subsequently, the TD3 starts exploiting what NN learned and exploring the environment by adding an uncorrelated mean-zero Gaussian noise to the selected action. The added noise is clipped to conforms with the action space bounds. The TD3, as adopted in our application, is summarized in Algorithm 2.

Algorithm 2 TD3 for differentiated pricing

Randomly initialize critic networks parameters ϕ_1,ϕ_2, and actor network parameters θ
Set the target NN parameters equal the online NN parameters
$\grave{\phi}_1 \leftarrow \phi_1$, $\grave{\phi}_2 \leftarrow \phi_2$, $\grave{\theta} \leftarrow \theta$
Initialize empty replay buffer $\mathcal{R}$ with size 100k
for Episode $= 1, 15k$ **do**
  Receive initial observation state s
  for $t = 1, T$ **do**
    if Episode $\leq$ 1k **then**
      Randomly select actions $a = \mathcal{U}(-1, 1)$
    else
      Select actions according to the current policy and add exploration noise $a \leftarrow \pi_\theta(s) + \epsilon$, where $\epsilon \sim \mathcal{N}(0, 0.1)$
    end if
    Execute action a, observe reward r and next state $\grave{s}$
    Store transition tuple $(s, a, r, \grave{s})$ in $\mathcal{R}$
    Randomly sample a mini-batch of N transitions from $\mathcal{R}$
    Compute greedy actions for next states using target actor network and add clipped Gaussian noise
    $\grave{a} \leftarrow \pi_{\grave{\theta}}(\grave{s}) + \epsilon$, where $\epsilon \sim \texttt{clip}(\mathcal{N}(0, 0.2), -0.5, 0.5)$
    Compute targets $y \leftarrow r(s, a) + \gamma \min_{i=1,2} Q_{\grave{\phi}_i}(\grave{s}, \grave{a}))$
    Update critic networks parameters using gradient descent
    $\phi_i \leftarrow \arg\min_{\phi_i} \frac{1}{N} \sum_{(s,a,r,\grave{s}) \backsim N} (y - Q_{\phi_i}(s, a))^2$, $i = 1, 2$
    if Episode mod $2 = 0$ **then**
      Update actor network parameters using gradient ascent
      $\nabla_\theta J(\theta) = \frac{1}{N} \sum_{s \backsim N} \Big[\nabla_a Q_{\phi_1}(s, a)|_{a=\pi(s)} \nabla_\theta \pi_\theta(s) \Big]$.
      Update target networks
      $\grave{\phi}_i \leftarrow \tau\phi_i + (1 - \tau)\grave{\phi}_i, \quad i = 1, 2$
      $\grave{\theta} \leftarrow \tau\theta + (1 - \tau)\grave{\theta}$
    end if
  end for
end for

4.4.3 Implementation Details

States and actions

As described in Section 4.2 and Subsection 4.4.1, the system state (observation space) is a combination of state variables that include time-of-day t, and the utilization and current QoS of each charging facility in the EVCI. The agent's action represents continuous control of the charging service prices in all charging facilities. At each time slot t, the RL agent generates a pricing action, a_t, based on the current state of the EVCI, s_t, and the expected future charging demand. The selected pricing action, a_t, influences the behaviors of PEV users in the next time slot $t+1$. The length of the state tuple is $2N+1$, and all elements in the state tuple are normalized to range $[0, 1]$. The action space is a tuple of size N, and all elements in the tuple are normalized to range $[-1, 1]$. Normalization of action and observation spaces facilitates the convergence of the TD3 algorithm.

Network architecture and hyper-parameters

The TD3 has a pair of critic networks along with a single actor network. Each neural network consists of two fully-connected hidden layers with 400 and 300 units, respectively. Rectified linear (`ReLU`) activation units are used for all hidden units. For the critic networks, the size of input layers is equal to the sum of the observation space size and the action space size. Critic network outputs consist of a single linear unit per network, representing the Q-value. For the actor network, the input layer size is equal to the observation space size, and the output layer size is equal to the action space size. Actor network output consists of `tanh` activation units.

Adam optimizer [113] is used to optimize the parameters of actor and critic networks, with a learning rate of 10^{-4} and 10^{-3} for actor and critic networks, respectively. The mini-batch size is chosen to be 64, and the experience replay memory can hold up to 10^5 state transitions. We use a discount factor of $\gamma = 0.99$, and a soft target update factor of $\tau = 0.005$. For policy exploration, we use uncorrelated additive Gaussian action space noise $\mathcal{N}(0, 0.1)$ with zero mean and 0.1 standard deviation. Target policy is smoothed by

adding Gaussian noise $\mathcal{N}(0, 0.2)$, clipped to $(-0.5, 0.5)$, to the selected action from the target network. The selected hyper-parameters are summerized in Table 4.1.

Table 4.1: TD3 hyper-parameters settings

Hyper-parameter	**Value**	**Hyper-parameter**	**Value**
Episodes	15k	Discount Factor	0.99
Batch Size	64	Optimizer	Adam
Learning Rate Actor	10^{-4}	Target Update Rate	0.005
Learning Rate Critic	10^{-3}	Exploration Policy	$\mathcal{N}(0, 0.1)$
Actor NN units (L1/L2)	400/300	Normalized Observations	True
Critic NN units (L1/L2)	400/300	Reply Memory	10^5

Reward function

The performance of RL algorithms is highly impacted by the reward function. To achieved the desired behavior, a reward function must be designed in a way to guide the agent towards the goal. Reward functions can be designed to follow two main forms: sparse reward and shaped reward [114]. In sparse reward functions, the agent is given a positive reward if it achieves the desired goal and zero rewards otherwise. Although sparse reward functions are easy to design for most of the tasks, it does not motivate the RL agent to learn and may need a lot of training to converge to an acceptable policy. To motivate the agent's learning, reward shaping is usually used to give more rewards to the agent in the states that are closer to the target state. Shaped reward functions are difficult to design. This is because a shaped reward function can bias learning towards undesirable behaviors if it is not carefully designed. To achieve the proposed objective in (4.5), we design the following reward function

$$r_t(s_t, a_t) = \frac{1}{N} \sum_{n=1}^{N} \mathcal{X}_{t,n}^2 \prod_{n=1}^{N} \mathcal{C}_{t,n} \tag{4.13a}$$

$$\mathcal{C}_{t,n} = \begin{cases} \exp\left[-300(q_m + \zeta - \mathcal{Q}_{t,n})^2\right] & \text{, if } q_m + \zeta < \mathcal{Q}_{t,n} \\ 1 & \text{, otherwise.} \end{cases} \tag{4.13b}$$

The reward function consists of two parts representing the differentiated pricing problem in (4.5). The first part imitates the objective function in (4.5a) and incentivizes the RL agent to increase facility utilization. As $\mathcal{X}_{t,n}$ increases, the RL agent receives more rewards. The second part mimics constraint (4.5b), where $\mathcal{C}_{t,n}$ penalizes the reward signal if the current QoS at a charging facility is less than the targeted QoS. To encourage learning of a pricing policy that guarantees the targeted QoS all the time, a safeguard constant ζ in the range of $[2\%, 5\%]$ is added to the targeted QoS.

Training and validation processes

The training proceeds episodically for 15×10^3 episodes. Each episode represents one business day that is simulated from an initial state at time $t = 1$ until the end of the daily time horizon at $t = T$. To prevent overfitting and to achieve good generalization, neural networks are trained on simulated environments that vary in each training run. Each simulated environment differs in the random seeds that is sampled uniformly from 50 random seeds. The performance of the training process is evaluated using daily cumulative rewards, which is the total rewards that the RL agent receives over a day. As expected, the cumulative reward rapidly increases at the beginning of training, then increases at a much slower rate as the training goes on. During training, the pricing policy is evaluated periodically without exploration noise. Different from the training process, the validation process always uses an environment with the same random seed, which is different from the training seeds. The neural network that achieves the best performance (maximum cumulative reward) in the evaluation process is selected to form the final pricing policy.

4.5 Numerical Results

In this section, we evaluate our proposed differentiated pricing framework and demonstrate the applicability of the TD3 algorithm in determining dynamic pricing policies. Firstly, we present a numerical example that highlights the relationship among the pricing signals, charging facility utilization, facility QoS. Then, we demonstrate the scalability of our proposed framework on a relatively larger EVCI, with more realistic architecture and

demand properties. In both examples, the daily time horizon is divided into 24 time-slots each of which lasts for one hour. Also, the CSP determines a dynamic pricing policy for each charging facility to maximize the utilization of charging facilities, while maintaining the targeted QoS. The CSP does not make any assumptions regarding the PEV charging demand or the impact of pricing signals on PEV user behaviors (beyond the assumptions made in Section 4.3). Instead, neural networks are trained to optimize the pricing decisions based on the interaction with the environment. The simulations are implemented under Python 3.7 environment on a laptop computer with a 2.3-GHz Intel(R) Core(TM) i5-8300H CPU, 8 GB of memory, and NVIDIA GeForce GTX 1050 Ti GPU unit.

4.5.1 Example 1: Two Charging Facilities

In this example, the CSP finds a pricing policy for two charging facilities. For clarity of illustration, PEV charging demands in these facilities are assumed sensitive only to the pricing signals. The numbers of chargers and waiting positions in both charging facilities are the same, with five chargers and three waiting-positions. The service rate in both charging facilities equals to 3 PEV/h. As discussed in Subsection 4.2.2, PEV arrivals to charging facilities are modeled as nonhomogeneous Poisson process, and the arrival rates are given by $\Lambda_{1,t} = 21 + 10\sin(2\pi t/24)$ and $\Lambda_{2,t} = 21 + 10\cos(2\pi t/24)$. For the two facilities, the charging price is normalized to range $[0, 1]$, where zero represents the base price and one is the maximum allowable charging price. The CSP objective is to decide a differentiated pricing policy that maintains two QoS classes, with PEV charging service completion targets at 80% and 90% for the first and second charging facilities, respectively.

We first consider an independent demand scenario, where PEV charging demand in a facility is only dependent on the charging price at that facility. In this scenario, self-elasticity and cross-elasticity parameters are set to $\beta_1 = \beta_2 = 20$ and $\beta_{1,2} = \beta_{2,1} = 0$, respectively. The simulated environment is represented by two finite queuing systems, as described in Section 4.2. For each charging facility, a QoS index is calculated based on (4.4), with parameters $\alpha = 0.75$ and $\beta = 0.25$. The reward function is given in (4.13), with $\zeta = 0.02$. As shown in Figures 4.2a and 4.2b, the RL agent decides pricing policies that anticipate the stochastic and non-stationary charging demand. The charging prices

increase as the expected PEV charging demand increases, and the prices decrease to the base price when the charging demand is less than the maximum facility capacities. The impact of these pricing policies on the performance of charging facilities is evaluated in Figures 4.2c and 4.2d, where the resulting facility utilization and QoS are shown. It can be noted that the resulting pricing policy preserves the targeted QoS in both facilities. Furthermore, facility 1 has a higher utilization than facility 2, because the targeted QoS in facility 1 is less than in facility 2. Figure 4.3 shows the convergence of the TD3 algorithm. The RL agent explores the environment at the beginning of the training. Then, as the iteration goes by, the cumulative reward increases because the RL agent learns from the interaction with the environment and, finally, the algorithm converges to the maximum value.

Another scenario is considered, where PEV charging demand in the charging facilities are interdependent. Thereby, the charging demand at one facility not only depends on its price but also on the charging price in the other facility. Self-elasticity and cross-elasticity parameters are set to $\beta_1 = \beta_2 = 20$ and $\beta_{1,2} = \beta_{2,1} = 10$, respectively. As shown in Figures 4.4a and 4.4b, the pricing policies are adapted to address the interdependence in charging demand between the two facilities. It can be noted in Figure 4.4b that the charging price of facility 2 is higher than that in Figure 4.2b in response to the increasing demand in facility 1. Also, the pricing policy is capable of maximizing the facility utilization while maintaining the targeted QoS levels, as shown in Figures 4.4c and 4.4d. The RL approach automatically adjusts the pricing policies according to the changes in customer behaviors without any preliminary settings.

This example demonstrates that the RL approach can learn and optimize the dynamic pricing strategies, while interacting with an unknown environment. Based on the proposed approach, deep neural networks are trained to receive the current state of the EVCI and generate pricing signals that coordinate the future PEV charging demand.

4.5.2 Example 2: Large-Scale Scenario

To validate our approach on a relatively larger EVCI, with more realistic charging demand properties, we select the well-known Nguyen-Dupuis RTN [49]. The topology and traffic

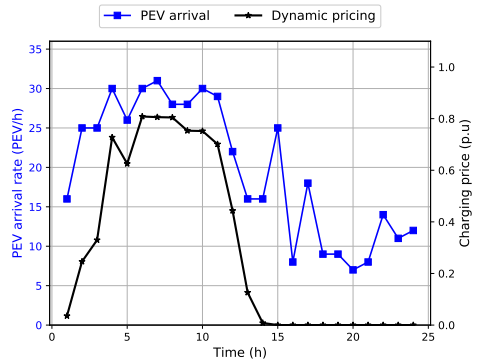

(a) PEV arrivals and pricing for facility 1

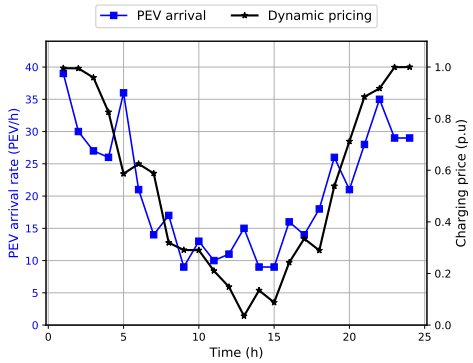

(b) PEV arrivals and pricing for facility 2

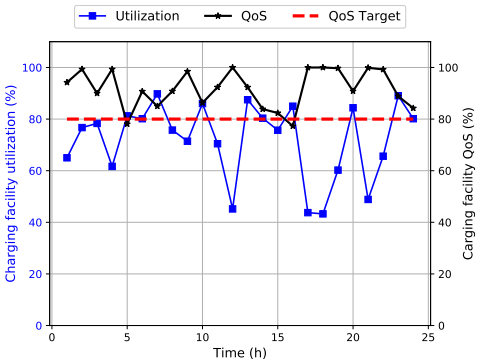

(c) Facility 1 utilization and QoS

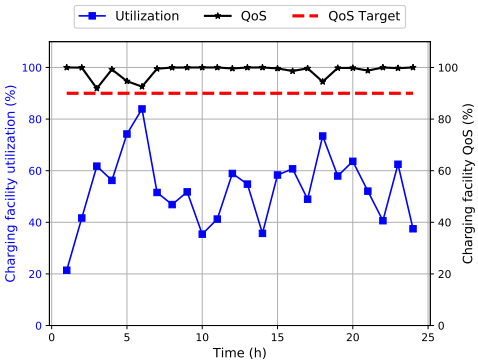

(d) Facility 2 utilization and QoS

Figure 4.2: Pricing policy for independent demand scenario

demand attributes of the Nguyen-Dupuis network are introduced in Subsection 2.4.1. We consider EVCI that consists of three service classes:

- The first service class is offered by two OWCs, called OWC-1 and OWC-2, which are located at links 5 and 16, respectively. The targeted QoS for the first class is 95%, and 4 chargers are allocated in each OWC. The mean charging time in OWCs is set to 15 minutes. Usually, charging service price is set as an hourly rate, which is billed by the minute based on the usage time and the type of charging service [115]. The charging price for the first class service is set to range [20, 40] \$/h, with self-elasticity parameter setting to 0.15;

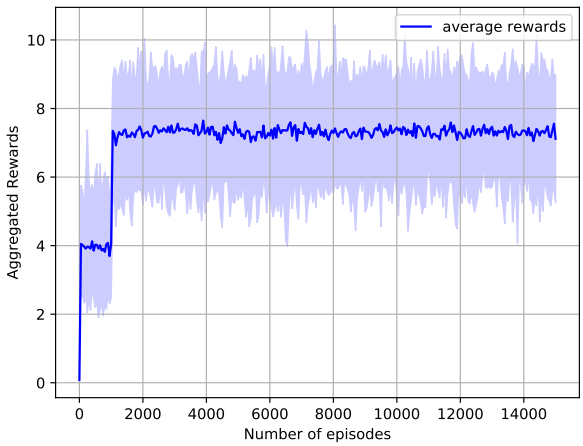

Figure 4.3: Convergence process of TD3 algorithm

- The second service class is offered by two FCSs, with targeted QoS levels are set at 90%. One FCS, called FCS-1, is placed at node 10, and contains 5 chargers and 2 waiting positions. The second FCS, called FCS-2, is located at node 12, and contains 11 chargers and 2 waiting positions. The mean charging time in FCSs is set to 30 minutes. The charging price for the second class service is set to range [17, 35] \$/h, with self-elasticity parameter is set to 0.6;

- The third service class is offered by one PL, located at node 3. The targeted QoS for PL is 85%. The PL contains 30 chargers and 10 waiting positions. The mean charging time in PL is set to 3 hours. Charging price for the third class service is set to range [13, 25] \$/h, with self-elasticity parameter is set to 2.5.

Service quality elasticity parameters, γ_m and $\gamma_{m,\hat{m}}$, for all service classes are set to 3 and 1, respectively. We implement our RL approach to determine the charging prices for each facility in the EVCI. For compactness, we utilize box-plots to visualize the variability in the pricing policy, i.e., the distribution of the EVCI prices and performance over a day are visualized instead of the time-varying visualization. Box-plots provide a simplified approach for ease of performance comparison among multiple charging facilities. Figure 4.5a shows the PEV arrival distributions to charging facilities, which represent the demand

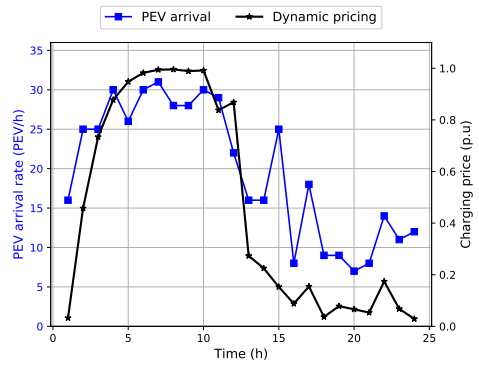

(a) PEV arrivals and pricing for facility 1

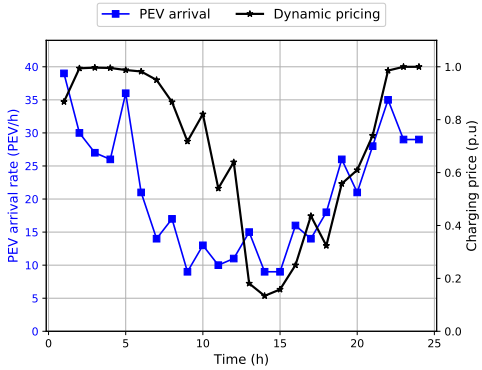

(b) PEV arrivals and pricing for facility 2

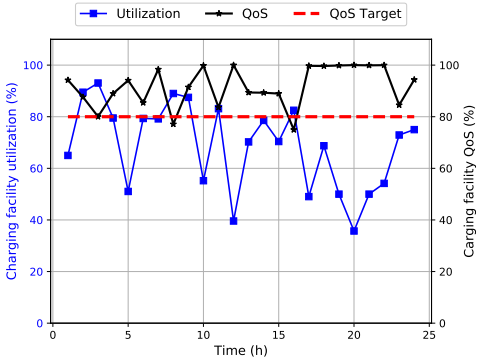

(c) Facility 1 utilization and QoS

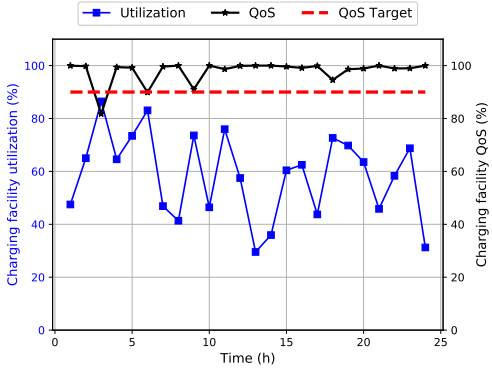

(d) Facility 2 utilization and QoS

Figure 4.4: Pricing policy for interdependent demand scenario

for the charging services. Figure 4.5b shows the pricing signal distribution for each charging facility. It can be noted that charging prices change in the whole specified price range, and the median prices (shown in dashed line) for OWCs are higher than that in FCSs and PL. As shown in Figure 4.5c, the pricing policy achieves a 100% QoS level for all service classes most of the time, except for a few outliers of low QoS (shown in + sign). However, for each charging facility, the lowest achieved QoS level is higher than the specified service completion target. Figure 4.5d shows that the utilization at OWCs is less than that of both FCSs and PL because the targeted QoS at OWCs is higher than that in FCSs and PL.

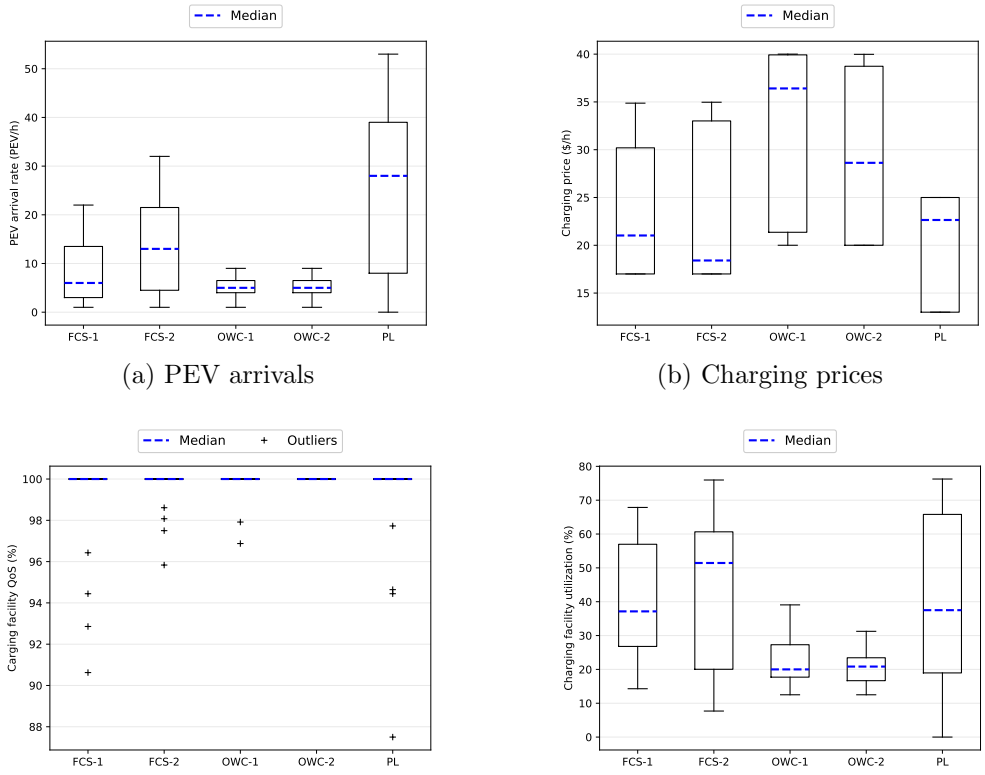

(a) PEV arrivals (b) Charging prices

(c) EVCI QoS (d) EVCI utilization

Figure 4.5: Pricing policy for EVCI

4.6 Summary

In this chapter, we study decentralized coordination of PEV charging demand and propose a differentiated pricing mechanism for a multiservice EVCI. The objective of the proposed pricing mechanism is to maximize the utilization of charging facilities, while preserving the targeted QoS level for each service class. A deep RL approach is utilized to determine the pricing policy without requiring an explicit model for PEV charging demand. The decision-making problem is solved based on the interaction with the environment. Firstly, the differentiated pricing problem is formulated as a finite-discrete MDP. Then, TD3 algorithm, which is a model-free RL algorithm based on the actor-critic approach, is employed to train neural networks to encode the current EVCI state into pricing signals. The pricing signals

regulate the future PEV charging demand to achieve the problem objectives. The numerical results show that the generated pricing policy anticipates future service congestion and adjusts the pricing signals accordingly.

Chapter 5

Conclusions and Future Work

5.1 Conclusions

Transportation electrification through the adoption of PEVs is gaining more popularity due to the increased awareness of its environmental and economic benefits. Along with the growing number of PEVs, public EVCI becomes indispensable to accommodate the increasing PEV charging demand. The objective of this PhD research is to develop solutions for integrating the EVCI into the smart grid, considering both the PEV user requirements and the service provider's utility. From the PEV user perspective, planning and operation of EVCI should achieve the following objectives: 1) to site suitable types of charging facilities at locations that are accessible by the users, considering the limited driving range of PEVs and the unique usage patterns of each facility type; 2) to plan appropriate sizes for charging facilities, which prevent service congestion and fulfill the stochastic and time-varying charging demand; 3) to coordinate the operation of the EVCI efficiently by preserving the expected QoS at charging facilities all the time and preventing the over-usage of particular service classes. From the service provider perspective, planning and operation of EVCI should achieve the following objectives: 1) to ensure high utilization and profitability of the chosen facility locations by siting the EVCI based on an accurate location estimation of the potential PEV charging demand; 2) to minimize the investment cost associated with charging facility construction and integration with the PDN by optimizing the numbers of

chargers and waiting positions allocated at each charging facility, and attaining the most cost-effective ESS allocation and/or PDN reinforcement; 3) to maximize the revenue from the EVCI by maximizing the demand for charging service and adaptively deciding a pricing policy that maximizes facility utilization. To achieve these objectives, this thesis presents a spatial-temporal flow capturing location model, a QoS aware capacity planning framework, and a dynamic pricing mechanism for a multiservice EVCI.

In the spatial-temporal flow capturing location model, three types of charging facilities are located on the transportation network based on the spatial-temporal distribution of the traffic flows. The proposed model accounts for not only the transportation network dynamics and congestion but also the different characteristics and usage patterns of each charging facility type. A simulation-based DTA model is used to estimate the time-varying traffic flows between all OD pairs in the network. Then, the traffic flow dataset is clustered by the GMM algorithm according to the temporal characteristics to identify the time periods in which the traffic flows are high or low. Our model captures the traffic flows during peak and non-peak traffic periods by OWCs and FCSs, respectively. Also, PLs are deployed at the destination nodes of the trips to cover the static PEV charging demand. Simulation results demonstrate that the proposed model captures a higher percentage of traffic flows with the same number of facilities when compared with an existing model based only on spatial characteristics of the traffic flows.

The proposed QoS aware capacity planning framework sizes charging facilities to fulfill the targeted QoS level, while minimizing the integration cost for the PDN. The proposed framework consists of two models that are solved sequentially: Firstly, the capacity planning of EVCI model is used to optimize the numbers of chargers and waiting positions allocated at each charging facility to realize the targeted QoS level for the entire networked EVCI. After that, the integration with the PDN model is used to minimize the integration cost of EVCI with PDN by attaining the most cost-effective ESS allocation and/or PDN reinforcement. The link between the targeted QoS level and the PDN capability offers insights into how to make a trade-off between the PEV user satisfaction and the required investment in PDN. The numerical results show that the inter-relationship between the targeted QoS level and the required investment in the PDN plays a vital role in capacity planning of EVCI.

We further develop a differentiated dynamic pricing mechanism for multiservice EVCI, which motivates PEV users to avoid over-allocation of particular service classes, and learns and improves automatically without an explicit model of the environment. The pricing problem is formulated as a social welfare maximization problem, where the objective is to maximize the demand for charging services while maintaining the targeted QoS in all service classes. Then, a deep RL approach, called the TD3 algorithm, is utilized to determine the pricing policy without requiring an explicit model for PEV charging demand. The adopted RL approach trains neural networks to encode the current EVCI state into pricing signals that anticipate future PEV charging demand and potential service congestion.

5.2 Future Research Directions

This PhD research can be extended in several directions by investigating open issues. These issues can be summarized as follows:

- The proposed ST-FCLM, in Chapter 2, can be extended by optimizing the number of charging facilities of various types to maximize user satisfaction within a budget limit. This extension would address the trade-off between establishing user preferred but expensive charging facilities and deploying more inexpensive facilities to maximize the captured traffic flow. More research is required to derive a user satisfaction index, and to develop a siting model that counterbalance the percentage of covered charging demand and user satisfaction.

- The proposed QoS aware capacity planning framework, in Chapter 3, can be extended by optimizing the QoS targets to maximize user satisfaction within a budget limit. In this case, both the EVCI capacity planning model and integration with the PDN model can be simultaneously solved. This extension is to address the trade-off between the targeted QoS level of EVCI and the required investment in both EVCI and PDN.

- EVCI planning involves the optimization of both siting and sizing of charging facilities. In this PhD research, we divide the planning problem into two sequentially

solved sub-problems, where a piece-wise optimal solution of the siting problem (Chapter 2) is used as input for the sizing problem (Chapter 3). However, our approach does not guarantee the global optimal solution to the EVCI planning problem. Therefore, more research is required to develop a joint optimization of both the siting and sizing of charging facilities.

- The proposed differentiated dynamic pricing mechanism, in Chapter 4, can be extended to minimize the negative impacts on the power grid. Various charging services may impact the power system differently. This is because each charging service class has a unique charging rate, thereby the load demand of the facilities varies according to the facility type. To minimize the negative impacts on the power system, differentiated pricing should motivate the PEV users to follow the valley-filling strategy. Consequently, PEV users are encouraged to shift the request of charging services to the time periods and the service classes, which can be safely accommodated by the power grid.

Appendix A

Disaggregation-aggregation Iteration Method

The networked EVCI is modeled as a finite capacity queuing network with RS-RD blocking. The performance metrics of the network can be approximated using the DA iteration method [72]. The queuing network consists of V nodes, where each node can be either CN or DN. To simplify the notations, in this algorithm, each node v ($v \in \{1, 2, \ldots, V\}$) has μ_v service rate, λ_v arrival rate, c_v number of servers, and K_v number of buffer spaces. The transfer probability among nodes is denoted by $t_{v,l}$, where $v, l \in \{1, 2, \ldots, V\}$. A PEV may leave the network after getting service in node v with transfer probability $t_{v,0}$. The transfer probability matrix of the network is generated based on the routing probabilities among charging facilities as described in the networked EVCI model, where $\boldsymbol{\alpha} \mapsto \boldsymbol{t}$. The state of the network can be represented as V-tuple $\mathbf{z} = (z_1, z_2, \ldots, z_V)$, where z_v indicates the number of PEVs in queue v. The state space of the network is represented as follows

$$\mathcal{Z} = S_1 \times S_2 \times \ldots \times S_V$$

where $S_v = [0 : K_v]$ is the node's state space, and $\times$ represents the Cartesian product. In queuing networks modeling, continuous-time Markov chains are used to model system states [116]. Instead, DA algorithm uses discrete-time Markov chain ($Z(t),\ t \in \mathbb{N}$), with

state space $\mathcal{Z}$, underlying the queuing network model. This discrete-time Markov chain has transition probability matrix $P = Q\Delta + I$, where Q denotes the generator (transition rate) matrix and $\Delta = 0.99/\max_x |q_{x,x}|$ denotes the randomization constant. The discrete-time Markov chain has the same steady-state distribution as the continuous-time Markov chain. The state probabilities of the Markov chain are denoted by $p(\mathbf{z}) \triangleq \mathbb{P}\{Z(t) = \mathbf{z}\},\ \mathbf{z} \in \mathcal{Z}$. These probabilities are collected in vector $\mathbf{p}$.

The state probabilities of the Markov chain model can be approximated based on canonical aggregation. Aggregates is a set of system states. A canonical aggregate can uniquely define the whole system's (network) state based on the states of all subsystems (nodes). Aggregate is denoted by $\mathcal{Z}_{v,j}$, which is the set of all system states where node v is in state j irrespective to the states of other nodes, as follows:

$$\mathcal{Z}_{v,j} = \{\mathbf{z} \in \mathcal{Z} \mid z_v = j\},\ j \in S_v,\ \forall v.$$

Each aggregate $\mathcal{Z}_{v,j}$ defines a marginal probability, which is called the aggregate probability, as follows:

$$r_v(j) \triangleq \mathbb{P}\{Z(t) \in \mathcal{Z}_{v,j}\} = \sum_{\mathbf{z} \in \mathcal{Z}_{v,j}} p(\mathbf{z}),\ j \in S_v,\ \forall v. \tag{A.1}$$

Aggregate probabilities are collected in tuples $\mathbf{r}_v \triangleq (r_v(0), \ldots, r_v(K_v)),\ \forall v$. Then, these tuples are collected again into $R \triangleq (\mathbf{r}_1, \ldots, \mathbf{r}_V)$. Thus, an aggregation function is defined as $R = \mathcal{A}(\mathbf{p})$. This function calculates the aggregate probabilities given the state probabilities. For this particular Markov chain, the aggregate transition probabilities $\pi_v(j,l) \triangleq \mathbb{P}\{\mathcal{Z}_v^{t+1} = l \mid \mathcal{Z}_v^t = j\}$ can be calculated as follows:

$$\pi_v(j,l) = \begin{cases} \gamma_v & \text{if } l = j-1 \geqslant 0, \\ 1-\delta_v & \text{if } l = j = 0, \\ 1-\gamma_v-\delta_v & \text{if } 0 < l = j < K_v, \\ 1-\gamma_v & \text{if } l = j = K_v, \\ \delta_v & \text{if } l = j+1 \leqslant K_v, \\ 0 & \text{Otherwise} \end{cases} \quad j,l \in S_v,\ \forall v \tag{A.2}$$

where

$$\gamma_v = n(j)\mu_v \Delta t_{v,0} + \sum_{\substack{s=1 \\ s\neq v}}^{V} n(j)\mu_v \Delta t_{v,s}(1 - r_s(K_s)),$$

$$\delta_v = \lambda_v \Delta + \sum_{\substack{s=1 \\ s\neq v}}^{V} \mu_v \Delta t_{s,v}(1 - r_s(0)),$$

$$n(j) = \begin{cases} j, & \text{if } j < c_v, \\ c_v, & \text{if } j \geq c_v. \end{cases}$$

The algorithm also uses a disaggregation function $\boldsymbol{\pi} = \mathcal{D}(R)$, where a maximum entropy distribution (MED) $\boldsymbol{\pi}$ is uniquely determined from a given aggregate probabilities R. The MED has a product form solution and is completely determined by MED parameters $\rho_{v,j}$, which are collected in tuple $\boldsymbol{\rho}$, as follows:

$$r_v(j) = \frac{1}{G} \sum_{\substack{\mathbf{z}\in\mathcal{Z} \\ z_v = j}} \prod_{i=1}^{V} \rho_{i,z_i}, \quad j \in S_v, \ \forall v, \tag{A.3}$$

$$G = \sum_{\mathbf{z}\in\mathcal{Z}} \prod_{v=1}^{V} \rho_{v,z_v}. \tag{A.4}$$

The state probabilities vector can then approximated using $\mathbf{p} = \mathcal{D}(R)$, where $R = \mathcal{A}(\mathcal{D}(R)P)$. The algorithm begins, at the first iteration i, with an initial MED parameters $\boldsymbol{\rho}$ and iteratively computes the aggregate probabilities R and the transition probability matrix P until convergence. The algorithm converges when $\max_{v,j} |r_v(j)^{(i+1)} - r_v(j)^{(i)}|$ is less than a threshold value ε. It is shown that the algorithm always converges to accurate results. Algorithm 3 describes DA iteration method, as used in the analysis of the networked charging infrastructure.

Algorithm 3 DA iteration method algorithm

Input: $V, \varepsilon, \lambda_v, \mu_v, c_v, K_v, \{t_{v,l}\}, \{t_{v,0}\},\ v, l = 1, \ldots, V$;

Output: Aggregate probabilities R;

Set the iteration index $i \leftarrow 1$, and the convergence index Conv $\leftarrow$ False;

Initialize MED parameters $\boldsymbol{\rho}^{(1)}$ by setting $\rho_{v,j}^{(1)} \leftarrow \frac{1}{K_v}$;

Calculate $G^{(1)}$ based on (A.4), and $R^{(1)}$ based on (A.3);

while Conv = False **do**

  Calculate the aggregate transition probabilities $\pi_v(j,l),\ \forall j, l \in S_v,\ \forall v$ based on Eq.A.2;

  Calculate the new aggregate probabilities $R^{(i+1)}$ based on the following equation:

$$r_v(l)^{(i+1)} = \sum_{j=0}^{K_v} \pi_v(j,l) r_v(j)^{(i)},\ l \in S_v,\ \forall v;$$

  Approximate new MED parameters $\boldsymbol{\rho}^{(i+1)}$ based on the following equation:

$$\rho_{v,j}^{(i+1)} = \frac{r_v(j)^{(i+1)}}{r_v(j)^{(I)}} \rho_{v,j}^{(i)};$$

  From $\boldsymbol{\rho}^{(i+1)}$, calculate $G^{(i+1)}$ based on (A.4), and $R^{(i+1)}$ based on (A.3);

  if $\max_{v,j} |r_v(j)^{(i+1)} - r_v(j)^{(i)}| > \varepsilon$ **then**

    $i \leftarrow i + 1$;

  else

    Conv $\leftarrow$ True;

  end if

end while

Extracted Publications

1. Ahmed Abdalrahman and Weihua Zhuang. QoS-aware capacity planning of networked PEV charging infrastructure. IEEE Open Journal of Vehicular Technology, 2020.
2. Ahmed Abdalrahman and Weihua Zhuang. PEV charging infrastructure siting based on spatial-temporal traffic flow distribution. IEEE Trans. Smart Grid, 10(6):6115–6125, 2019.
3. Ahmed Abdalrahman and Weihua Zhuang. A survey on PEV charging infrastructure: Impact assessment and planning. Energies, 10(10):1650, 2017.
4. Ahmed Abdalrahman and Weihua Zhuang. Impact assessment of PEV charging demand on smart grid. IEEE Smart Grid Newsletter, March 2017.

References

[1] Xi Fang, Satyajayant Misra, Guoliang Xue, and Dejun Yang. Smart grid—the new and improved power grid: A survey. *IEEE Commun. Surv. Tutor.*, 14(4):944–980, 2012.

[2] The International Energy Agency (IEA). Global EV outlook 2019, scaling-up the transition to electric mobility. 2019.

[3] Antti Rautiainen, Sami Repo, P Jarventausta, Antti Mutanen, K Vuorilehto, and K Jalkanen. Statistical charging load modeling of PHEVs in electricity distribution networks using national travel survey data. *IEEE Trans. Smart Grid*, 3(4):1650–1659, 2012.

[4] Difei Tang and Peng Wang. Probabilistic modeling of nodal charging demand based on spatial-temporal dynamics of moving electric vehicles. *IEEE Trans. Smart Grid*, 7(2):627–636, 2016.

[5] Omar Hafez and Kankar Bhattacharya. Queuing analysis based PEV load modeling considering battery charging behavior and their impact on distribution system operation. *IEEE Trans. Smart Grid*, 9(1):261–273, 2018.

[6] Alireza Khaligh and Michael D'Antonio. Global trends in high-power on-board chargers for electric vehicles. *IEEE Trans. Veh. Technol.*, 68(4):3306–3324, 2019.

[7] Chia-Ho Ou, Hao Liang, and Weihua Zhuang. Investigating wireless charging and mobility of electric vehicles on electricity market. *IEEE Trans. Ind. Electron.*, 62(5):3123–3133, 2015.

[8] Seungmin Jeong, Young Jae Jang, and Dongsuk Kum. Economic analysis of the dynamic charging electric vehicle. *IEEE Trans. Power Electron.*, 30(11):6368–6377, 2015.

[9] Zicheng Bi, Tianze Kan, Chunting Chris Mi, Yiming Zhang, Zhengming Zhao, and Gregory A Keoleian. A review of wireless power transfer for electric vehicles: Prospects to enhance sustainable mobility. *Appl. Energ.*, 179:413–425, 2016.

[10] Su Y Choi, Seog Y Jeong, Beom W Gu, Gyu C Lim, and Chun T Rim. Ultraslim s-type power supply rails for roadway-powered electric vehicles. *IEEE Trans. Power Electron.*, 30(11):6456–6468, 2015.

[11] Guibin Wang, Zhao Xu, Fushuan Wen, and Kit Po Wong. Traffic-constrained multiobjective planning of electric-vehicle charging stations. *IEEE Trans. Power Del.*, 28(4):2363–2372, 2013.

[12] Albert Lam, Yiu-Wing Leung, and Xiaowen Chu. Electric vehicle charging station placement: Formulation, complexity, and solutions. *IEEE Trans. Smart Grid*, 5(6):2846–2856, 2014.

[13] Ahmed SA Awad, Tarek HM EL-Fouly, and Magdy MA Salama. Optimal ESS allocation for benefit maximization in distribution networks. *IEEE Trans. Smart Grid*, 8(4):1668–1678, 2015.

[14] Danilo Sbordone, I Bertini, B Di Pietra, Maria Carmen Falvo, A Genovese, and Luigi Martirano. EV fast charging stations and energy storage technologies: A real implementation in the smart micro grid paradigm. *Electr. Pow. Syst. Res.*, 120:96–108, 2015.

[15] Soodeh Negarestani, Mahmud Fotuhi-Firuzabad, Mohammad Rastegar, and Abbas Rajabi-Ghahnavieh. Optimal sizing of storage system in a fast charging station for plug-in hybrid electric vehicles. *IEEE Trans. Transport. Electrific.*, 2(4):443–453, 2016.

[16] Qinglong Wang, Xue Liu, Jian Du, and Fanxin Kong. Smart charging for electric vehicles: A survey from the algorithmic perspective. *IEEE Commun. Surv. Tutor.*, 18(2):1500–1517, 2016.

[17] Islam Safak Bayram, George Michailidis, and Michael Devetsikiotis. Unsplittable load balancing in a network of charging stations under qos guarantees. *IEEE Trans. Smart Grid*, 6(3):1292–1302, 2015.

[18] Ahmed Abdalrahman and Weihua Zhuang. A survey on PEV charging infrastructure: Impact assessment and planning. *Energies*, 10(10):1650, 2017.

[19] Weifeng Yao, Junhua Zhao, Fushuan Wen, Zhaoyang Dong, Yusheng Xue, Yan Xu, and Ke Meng. A multi-objective collaborative planning strategy for integrated power distribution and electric vehicle charging systems. *IEEE Trans. Power Syst.*, 29(4):1811–1821, 2014.

[20] Fouad Baouche, Romain Billot, Rochdi Trigui, and Nour-Eddin El Faouzi. Efficient allocation of electric vehicles charging stations: Optimization model and application to a dense urban network. *IEEE Intell. Transp. Syst. Mag.*, 6(3):33–43, 2014.

[21] Wei Tu, Qingquan Li, Zhixiang Fang, Shih-lung Shaw, Baoding Zhou, and Xiaomeng Chang. Optimizing the locations of electric taxi charging stations: A spatial–temporal demand coverage approach. *Transport. Res. C-Emer.*, 65:172–189, 2016.

[22] Yue Xiang, Junyong Liu, Ran Li, Furong Li, Chenghong Gu, and Shuoya Tang. Economic planning of electric vehicle charging stations considering traffic constraints and load profile templates. *Appl. Energ.*, 178:647–659, 2016.

[23] Michael Kuby and Seow Lim. The flow-refueling location problem for alternative-fuel vehicles. *Socioecon. Plann. Sci.*, 39(2):125–145, 2005.

[24] Joonho Ko, Tae-Hyoung Tommy Gim, and Randall Guensler. Locating refuelling stations for alternative fuel vehicles: a review on models and applications. *Transport Rev.*, 37(5):551–570, 2017.

[25] M John Hodgson. A flow-capturing location-allocation model. *Geogr. Anal.*, 22(3):270–279, 1990.

[26] Ismail Capar, Michael Kuby, V Jorge Leon, and Yu-Jiun Tsai. An arc cover–path-cover formulation and strategic analysis of alternative-fuel station locations. *Eur. J. Oper. Res.*, 227(1):142–151, 2013.

[27] Yongxi Huang, Shengyin Li, and Zhen Sean Qian. Optimal deployment of alternative fueling stations on transportation networks considering deviation paths. *Netw. Spat. Econ.*, 15(1):183–204, 2015.

[28] Barış Yıldız, Okan Arslan, and Oya Ekin Karaşan. A branch and price approach for routing and refueling station location model. *Eur. J. Oper. Res.*, 248(3):815–826, 2016.

[29] Fei Wu and Ramteen Sioshansi. A stochastic flow-capturing model to optimize the location of fast-charging stations with uncertain electric vehicle flows. *Transp. Res. D Transp. Environ.*, 53:354–376, 2017.

[30] Raffaela Riemann, David ZW Wang, and Fritz Busch. Optimal location of wireless charging facilities for electric vehicles: flow-capturing location model with stochastic user equilibrium. *Transport. Res. C-Emer.*, 58:1–12, 2015.

[31] Ying-Wei Wang and Chuah-Chih Lin. Locating multiple types of recharging stations for battery-powered electric vehicle transport. *Transport. Res. E-Log.*, 58:76–87, 2013.

[32] Zhibin Chen, Wei Liu, and Yafeng Yin. Deployment of stationary and dynamic charging infrastructure for electric vehicles along traffic corridors. *Transport. Res. C-Emer.*, 77:185–206, 2017.

[33] Chao Luo, Yih-Fang Huang, and Vijay Gupta. Placement of EV charging stations — balancing benefits among multiple entities. *IEEE Trans. Smart Grid*, 8(2):759–768, 2017.

[34] Colin JR Sheppard, Andrew Harris, and Anand R Gopal. Cost-effective siting of electric vehicle charging infrastructure with agent-based modeling. *IEEE Trans. Transport. Electrific.*, 2(2):174–189, 2016.

[35] Hongcai Zhang, Zechun Hu, Zhiwei Xu, and Yonghua Song. An integrated planning framework for different types of PEV charging facilities in urban area. *IEEE Trans. Smart Grid*, 7(5):2273–2284, 2016.

[36] Yi-Chang Chiu, Jon Bottom, Michael Mahut, Alex Paz, Ramachandran Balakrishna, Travis Waller, and Jim Hicks. Dynamic traffic assignment: A primer. *Transportation Research E-Circular*, (E-C153), 2011.

[37] Christian Gawron. *Simulation-based traffic assignment: Computing user equilibria in large street networks*. PhD thesis, Universität zu Köln, 1999.

[38] Pushkin Kachroo and Neveen Shlayan. Dynamic traffic assignment: A survey of mathematical models and techniques. In *Advances in Dynamic Network Modeling in Complex Transportation Systems*, pages 1–25. Springer, 2013.

[39] David Boyce, Der-Horng Lee, and Bin Ran. Analytical models of the dynamic traffic assignment problem. *Netw. Spat. Econ.*, 1(3):377–390, 2001.

[40] Francesco Calabrese, Giusy Di Lorenzo, Liang Liu, and Carlo Ratti. Estimating origin-destination flows using opportunistically collected mobile phone location data from one million users in boston metropolitan area. *IEEE Pervas. Comput.*, 10(4):36–44, 2011.

[41] Soora Rasouli and Harry Timmermans. Uncertainty in travel demand forecasting models: literature review and research agenda. *Transp. lett.*, 4(1):55–73, 2012.

[42] Hongcai Zhang, Scott J Moura, Zechun Hu, and Yonghua Song. PEV fast-charging station siting and sizing on coupled transportation and power networks. *IEEE Trans. Smart Grid*, 9(4):2595–2605, 2018.

[43] Bassant Selim, Omar Alhussein, Sami Muhaidat, George K Karagiannidis, and Jie Liang. Modeling and analysis of wireless channels via the mixture of Gaussian distribution. *IEEE Trans. Veh. Technol.*, 65(10):8309–8321, 2016.

[44] Xinyu Yang, Peng Zhao, Xialei Zhang, Jie Lin, and Wei Yu. Toward a gaussian-mixture model-based detection scheme against data integrity attacks in the smart grid. *IEEE Internet Things J.*, 4(1):147–161, 2017.

[45] Anil K Jain. Data clustering: 50 years beyond k-means. *Pattern Recogn. Lett.*, 31(8):651–666, 2010.

[46] Douglas Reynolds. Gaussian mixture models. *Encyclopedia of biometrics*, pages 827–832, 2015.

[47] Paul D McNicholas. *Mixture model-based classification*. CRC Press, 2016.

[48] Chris Fraley and Adrian E Raftery. How many clusters? which clustering method? answers via model-based cluster analysis. *Comput. J.*, 41(8):578–588, 1998.

[49] Sang Nguyen and Clermont Dupuis. An efficient method for computing traffic equilibria in networks with asymmetric transportation costs. *Transport. Sci.*, 18(2):185–202, 1984.

[50] Transportation Networks for Research Core Team. Transportation Networks for Research. Sioux falls transportation network. https://github.com/bstabler/TransportationNetworks. Accessed: May 12, 2018.

[51] Daniel Krajzewicz, Jakob Erdmann, Michael Behrisch, and Laura Bieker. Recent development and applications of SUMO - Simulation of Urban MObility. *International Journal On Advances in Systems and Measurements*, 5(3&4):128–138, December 2012.

[52] U.K National Travel Survey: 2010. When people travel. https://www.gov.uk/government/statistics/national-travel-survey-2010. Accessed: Jan 5, 2018.

[53] Ahmed Abdalrahman and Weihua Zhuang. PEV charging infrastructure siting based on spatial-temporal traffic flow distribution. *IEEE Trans. Smart Grid*, 10(6):6115–6125, 2019.

[54] Cuiyu Kong, Raka Jovanovic, Islam Safak Bayram, and Michael Devetsikiotis. A hierarchical optimization model for a network of electric vehicle charging stations. *Energies*, 10(5):675, 2017.

[55] Islam Safak Bayram, Ali Tajer, Mohamed Abdallah, and Khalid Qaraqe. Capacity planning frameworks for electric vehicle charging stations with multiclass customers. *IEEE Trans. Smart Grid*, 6(4):1934–1943, 2015.

[56] Sungwoo Bae and Alexis Kwasinski. Spatial and temporal model of electric vehicle charging demand. *IEEE Trans. Smart Grid*, 3(1):394–403, 2012.

[57] Muhammad Ismail, I Safak Bayram, Mohamed Abdallah, Erchin Serpedin, and Khalid Qaraqe. Optimal planning of fast PEV charging facilities. In *Proc. IEEE SGRE'15*, pages 1–6, 2015.

[58] I Safak Bayram, George Michailidis, Michael Devetsikiotis, and Fabrizio Granelli. Electric power allocation in a network of fast charging stations. *IEEE J. Sel. Area. Comm.*, 31(7):1235–1246, 2013.

[59] Mostafa F Shaaban, Sayed Mohamed, Muhammad Ismail, Khalid Qaraqe, and Erchin Serpedin. Joint planning of smart EV charging stations and DGs in eco-friendly remote hybrid microgrids. *IEEE Trans. Smart Grid*, 10(5):5819–5830, 2019.

[60] Walied Alharbi and Kankar Bhattacharya. Electric vehicle charging facility as a smart energy microhub. *IEEE Trans. Sustain. Energy*, 8(2):616–628, 2017.

[61] Wei Wei, Shengwei Mei, Lei Wu, Mohammad Shahidehpour, and Yujuan Fang. Optimal traffic-power flow in urban electrified transportation networks. *IEEE Trans. Smart Grid*, 8(1):84–95, 2017.

[62] Zhipeng Liu, Fushuan Wen, and Gerard Ledwich. Optimal planning of electric-vehicle charging stations in distribution systems. *IEEE Trans. Power Del.*, 28(1):102–110, 2013.

[63] Zhonghao Sun, Xingshe Zhou, Jian Du, and Xue Liu. When traffic flow meets power flow: On charging station deployment with budget constraints. *IEEE Trans. Veh. Technol.*, 66(4):2915–2926, 2017.

[64] Hongcai Zhang, Scott J Moura, Zechun Hu, Wei Qi, and Yonghua Song. A second-order cone programming model for planning PEV fast-charging stations. *IEEE Trans. Power Syst.*, 33(3):2763–2777, 2017.

[65] Justus Arne Schwarz, Gregor Selinka, and Raik Stolletz. Performance analysis of time-dependent queueing systems: Survey and classification. *Omega*, 63:170–189, 2016.

[66] Independent Electricity System Operator (IESO). Hourly Ontario Energy Price (HOEP). http://www.ieso.ca/Power-Data/Price-Overview/Hourly-Ontario-Energy-Price. Accessed: May 14, 2019.

[67] Nawaporn Wisitpongphan, Fan Bai, Priyantha Mudalige, Varsha Sadekar, and Ozan Tonguz. Routing in sparse vehicular Ad Hoc wireless networks. *IEEE J. Sel. Area. Comm.*, 25(8):1538–1556, 2007.

[68] Simonetta Balsamo. Queueing networks with blocking: Analysis, solution algorithms and properties. In *Network performance engineering*, pages 233–257. Springer, 2011.

[69] Simonetta Balsamo, Vittoria De Nitto Personè, and Paola Inverardi. A review on queueing network models with finite capacity queues for software architectures performance prediction. *Perform. Eval.*, 51(2-4):269–288, 2003.

[70] G Hosein Mohimani, Farid Ashtiani, Adel Javanmard, and Maziyar Hamdi. Mobility modeling, spatial traffic distribution, and probability of connectivity for sparse and dense vehicular ad hoc networks. *IEEE Trans. Veh. Technol.*, 58(4):1998–2007, 2008.

[71] Michiel CJ Bliemer and Piet HL Bovy. Impact of route choice set on route choice probabilities. *Transp. Res. Rec.*, 2076(1):10–19, 2008.

[72] Johann Christoph Strelen, Berthold Bärk, Jürgen Becker, and Volker Jonas. Analysis of queueing networks with blocking using a new aggregation technique. *Ann. Oper. Res.*, 79:121–142, 1998.

[73] Lawrence M Leemis. Nonparametric estimation and variate generation for a nonhomogeneous poisson process from event count data. *IIE Transactions*, 36(12):1155–1160, 2004.

[74] Zohar Feldman, Avishai Mandelbaum, William A Massey, and Ward Whitt. Staffing of time-varying queues to achieve time-stable performance. *Manage. Sci.*, 54(2):324–338, 2008.

[75] Linda V Green, Peter J Kolesar, and Ward Whitt. Coping with time-varying demand when setting staffing requirements for a service system. *POM*, 16(1):13–39, 2007.

[76] Tom Van Woensel, R Andriansyah, Frederico RB Cruz, J MacGregor Smith, and Laoucine Kerbache. Buffer and server allocation in general multi-server queueing networks. *Int. T. Oper RES.*, 17(2):257–286, 2010.

[77] Oliver Exler and Klaus Schittkowski. A trust region SQP algorithm for mixed-integer nonlinear programming. *Optim. Lett.*, 1(3):269–280, 2007.

[78] Richard H Byrd, Jorge Nocedal, and Richard A Waltz. Knitro: An integrated package for nonlinear optimization. In *Large-scale nonlinear optimization*, pages 35–59. Springer, 2006.

[79] Oliver Exler, Thomas Lehmann, and Klaus Schittkowski. A comparative study of sqp-type algorithms for nonlinear and nonconvex mixed-integer optimization. *Math. Program. Comput.*, 4(4):383–412, 2012.

[80] Jia Ying Yong, Vigna K Ramachandaramurthy, Kang Miao Tan, and N Mithulananthan. A review on the state-of-the-art technologies of electric vehicle, its impacts and prospects. *Renew. Sust. Energ. Rev.*, 49:365–385, 2015.

[81] Peter Köchel. Finite queueing systems—structural investigations and optimal design. *Int. J. Prod. Econ.*, 88(2):157–171, 2004.

[82] Piyasak Poonpun and Ward T Jewell. Analysis of the cost per kilowatt hour to store electricity. *IEEE Trans. Energy Convers.*, 23(2):529–534, 2008.

[83] Haijun Xing, Haozhong Cheng, Yi Zhang, and Pingliang Zeng. Active distribution network expansion planning integrating dispersed energy storage systems. *IET Gener. Transm. Dis.*, 10(3):638–644, 2016.

[84] Xinwei Shen, Mohammad Shahidehpour, Yingduo Han, Shouzhen Zhu, and Jinghong Zheng. Expansion planning of active distribution networks with centralized and distributed energy storage systems. *IEEE Trans. Sustain. Energy*, 8(1):126–134, Jan 2017.

[85] Hossein Farzin, Mahmud Fotuhi-Firuzabad, and Moein Moeini-Aghtaie. A stochastic multi-objective framework for optimal scheduling of energy storage systems in microgrids. *IEEE Trans. Smart Grid*, 8(1):117–127, 2017.

[86] Simon Wong, Kankar Bhattacharya, and J David Fuller. Electric power distribution system design and planning in a deregulated environment. *IET Gener. Transm. Distrib.*, 3(12):1061–1078, 2009.

[87] Pilar Meneses de Quevedo, Gregorio Muñoz-Delgado, and Javier Contreras. Impact of electric vehicles on the expansion planning of distribution systems considering renewable energy, storage, and charging stations. *IEEE Trans. Smart Grid*, 10(1):794–804, 2017.

[88] Xin Chen, Wenchuan Wu, and Boming Zhang. Robust restoration method for active distribution networks. *IEEE Trans. Power Syst.*, 31(5):4005–4015, 2016.

[89] Daniel K Molzahn, Florian Dörfler, Henrik Sandberg, Steven H Low, Sambuddha Chakrabarti, Ross Baldick, and Javad Lavaei. A survey of distributed optimization and control algorithms for electric power systems. *IEEE Trans. Smart Grid*, 8(6):2941–2962, 2017.

[90] Steven H. Low. Convex relaxation of optimal power flow—part i: Formulations and equivalence. *IEEE Control Netw. Syst.*, 1(1):15–27, 2014.

[91] Mesut E Baran and Felix F Wu. Network reconfiguration in distribution systems for loss reduction and load balancing. *IEEE Trans. Power Del.*, 4(2):1401–1407, 1989.

[92] Cliff Grigg. The IEEE reliability test system-1996. a report prepared by the reliability test system task force of the application of probability methods subcommittee. *IEEE Trans. Power Syst.*, 14(3):1010–1020, 1999.

[93] Shuhan Yao, Peng Wang, and Tianyang Zhao. Transportable energy storage for more resilient distribution systems with multiple microgrids. *IEEE Trans. Smart Grid*, 10(3):3331–3341, 2018.

[94] Yuan Liu, Ruilong Deng, and Hao Liang. A stochastic game approach for PEV charging station operation in smart grid. *IEEE Trans. Ind. Informat.*, 14(3):969–979, 2018.

[95] Wayes Tushar, Walid Saad, H Vincent Poor, and David B Smith. Economics of electric vehicle charging: A game theoretic approach. *IEEE Trans. Smart Grid*, 3(4):1767–1778, 2012.

[96] Wei Yuan, Jianwei Huang, and Ying Jun Angela Zhang. Competitive charging station pricing for plug-in electric vehicles. *IEEE Trans. Smart Grid*, 8(2):627–639, 2017.

[97] Chao Luo, Yih-Fang Huang, and Vijay Gupta. Stochastic dynamic pricing for EV charging stations with renewable integration and energy storage. *IEEE Trans. Smart Grid*, 9(2):1494–1505, 2018.

[98] Abdullah S Bin Humayd and Kankar Bhattacharya. Design of optimal incentives for smart charging considering utility-customer interactions and distribution systems impact. *IEEE Trans. Smart Grid*, 10(2):1521–1531, 2017.

[99] Yongmin Zhang, Pengcheng You, and Lin Cai. Optimal charging scheduling by pricing for EV charging station with dual charging modes. *IEEE Trans. Intell. Transp. Syst.*, 20(9):3386–3396, 2018.

[100] Hao Liang, Isha Sharma, Weihua Zhuang, and Kankar Bhattacharya. Plug-in electric vehicle charging demand estimation based on queueing network analysis. In *Proc. IEEE PES Gen. Meet.*, pages 1–5, Jul. 2014.

[101] Richard S Sutton and Andrew G Barto. *Reinforcement learning: An introduction*. MIT press, 2018.

[102] Rupal Rana and Fernando S Oliveira. Dynamic pricing policies for interdependent perishable products or services using reinforcement learning. *Expert Syst. Appl.*, 42(1):426–436, 2015.

[103] Renzhi Lu, Seung Ho Hong, and Xiongfeng Zhang. A dynamic pricing demand response algorithm for smart grid: reinforcement learning approach. *Appl. Energy*, 220:220–230, 2018.

[104] Elena Mocanu, Decebal Constantin Mocanu, Phuong H Nguyen, Antonio Liotta, Michael E Webber, Madeleine Gibescu, and Johannes G Slootweg. On-line building energy optimization using deep reinforcement learning. *IEEE Trans. Smart Grid*, 10(4):3698–3708, 2019.

[105] José R Vázquez-Canteli and Zoltán Nagy. Reinforcement learning for demand response: A review of algorithms and modeling techniques. *Appl. Energy*, 235:1072–1089, 2019.

[106] Ming Chen and Zhi-Long Chen. Recent developments in dynamic pricing research: multiple products, competition, and limited demand information. *Prod. Oper. Manag.*, 24(5):704–731, 2015.

[107] Fernando Bernstein and Awi Federgruen. A general equilibrium model for industries with price and service competition. *Oper. Res.*, 52(6):868–886, 2004.

[108] Jian Huang, Mingming Leng, and Mahmut Parlar. Demand functions in decision modeling: A comprehensive survey and research directions. *Decision Sciences*, 44(3):557–609, 2013.

[109] Jianyu Chen, Bodi Yuan, and Masayoshi Tomizuka. Model-free deep reinforcement learning for urban autonomous driving. In *Proc. IEEE ITSC'09*, pages 2765–2771, 2019.

[110] Timothy P Lillicrap, Jonathan J Hunt, Alexander Pritzel, Nicolas Heess, Tom Erez, Yuval Tassa, David Silver, and Daan Wierstra. Continuous control with deep reinforcement learning. *arXiv preprint arXiv:1509.02971*, 2015.

[111] Scott Fujimoto, Herke van Hoof, and David Meger. Addressing function approximation error in actor-critic methods. *arXiv preprint arXiv:1802.09477*, 2018.

[112] David Silver, Guy Lever, Nicolas Heess, Thomas Degris, Daan Wierstra, and Martin Riedmiller. Deterministic policy gradient algorithms. In *Proc. ICML'F14*, 2014.

[113] Diederik P Kingma and Jimmy Ba. Adam: A method for stochastic optimization. *arXiv preprint arXiv:1412.6980*, 2014.

[114] Alex Irpan. Deep reinforcement learning doesn't work yet. https://www.alexirpan.com/2018/02/14/rl-hard.html, 2018.

[115] Electric Circuit Canada. Charging stations and prices. https://lecircuitelectrique.com/charging-stations-and-rates. Accessed: Mar 11, 2020.

[116] János Sztrik. Basic queueing theory. *University of Debrecen, Faculty of Informatics*, 193, 2012.